ATMOSPHERIC TRANSPORT OF HYDROGEN SULFIDE

FROM PROPOSED GEOTHERMAL POWER PLANT (UNIT 18)

Predictions by Physical Modeling
in a Wind Tunnel

by

J. E. Cermak* and R. L. Petersen**

Prepared for

Pacific Gas and Electric Company
San Francisco, California

Fluid Dynamics and Diffusion Laboratory
Fluid Mechanics and Wind Engineering Program
Colorado State University
Fort Collins, Colorado 80523

September 1977   CER77-78JEC-RLP3

*Director, Fluid Dynamics and Diffusion Laboratory
**Graduate Research Assistant, Department of Civil Engineering

ABSTRACT

Tests were conducted in the Colorado State University environmental wind tunnel facility of the transport and dispersion of the H_2S plume emanating from a cooling tower (Unit 18) positioned at two locations near Anderson Springs, California. The wind tunnel tests were conducted with a cooling tower and terrain modeled to a scale of 1:1920. The effects of wind direction and wind speed upon the ground-level H_2S concentrations in the vicinity of Anderson Springs were established. Data obtained include photographs and motion pictures of smoke plume trajectories and ground-level tracer gas concentrations downwind of the cooling tower.

i

ACKNOWLEDGMENTS

TABLE OF CONTENTS

LIST OF TABLES

LIST OF FIGURES

LIST OF FIGURES (continued)

LIST OF SYMBOLS

Symbol	Definition	Dimensions
D	Stack diameter	(L)
E	Gas chromatograph response	(mvs)
Fr	Froude number $\dfrac{V^2}{g(\frac{\Delta\rho}{\rho_a})D}$	(-)
g	Gravitational constant	(L/T^2)
h	Cooling tower height	(L)
H	Height of terrain above cooling tower elevation	
k	von Karman constant	(-)
K	Concentration isopleth	(-)
L_o	Distance from beginning of wind tunnel	(L)
Q_s	Source strength	(M/T)
R	Exhaust velocity ratio V_s/V_a	(-)
Re_{L_o}	Reynolds number $\dfrac{VL_o}{\nu}$	(-)
U_*	Friction velocity	(L/T)
V	Mean velocity	(L/T)
x;y	General coordinates--downwind, lateral	(L)
z_o	Surface roughness parameter	(L)

Symbol	Definition	Dimensions
(Greek Symbols)		
χ	Local concentration	$(M/L^3$ or ppm)
τ	Sampling time	(T)
θ	Azimuth angle of upwind direction measured from plant north	$(-)$
σ	Standard deviation of either plume dispersion or wind angle fluctuations	(L) $(-)$
ν	Kinematic viscosity	(L^2/T)
δ	Boundary layer thickness	(L)
γ	Specific weight	$(M/T^2 L^2)$
ρ	Density	(M/L^3)
Ω	Angular velocity	$(1/L)$
μ	Dynamic viscosity	$M/(TL)$
Λ	Volume flow rate	(L^3/T)
(Subscripts)		
a	Meteorological tower	
s	Stack	
m	Model	
p	Prototype	
max	Maximum	
g	Geostrophic or gradient wind	
rms	Root mean square	
∞	Reference value	
FS	Free stream	

CONVERSION TABLE

(English to Metric Units)

Multiply Units	by	To Obtain
inches	2.540	centimeters
square inches	6.452	square centimeters
cubic inches	16.39	cubic centimeters
feet	0.3048	meters
square feet	0.0929	square meters
cubic feet	0.02832	cubic meters
feet/second	0.3048	meters/second
miles/hour	0.4470	meters/second
cubic feet/minute	0.02832	cubic meters/minute
cubic feet/minute	0.00047	cubic meters/second

1.0 <u>INTRODUCTION</u>

The purpose of this study was to determine the transport characteristics of hydrogen sulfide released in plumes emanating from the cooling tower of a proposed new geothermal power plant (Unit 18) in the Geysers Geothermal Area. Using a 1:1920 scale model of the cooling tower and surrounding topography in a wind tunnel capable of simulating the appropriate meteorological conditions, two possible locations for the power plant were studied (referred to as Site C and Site X). These locations are shown in Figure 1.1 in relation to Anderson Springs and Whispering Pines.

Downwind ground-level H_2S concentrations were determined by sampling concentrations of a tracer gas (propane) released from the model cooling tower. Overall plume geometry was obtained by photo-graphing the plumes made visible by releasing smoke (titanium tetrachloride) from the model cooling tower.

The primary focus of this study was on the H_2S concentrations in the vicinity of Anderson Springs for neutral thermal stratification. Accordingly, studies of the upper-level winds were confined to three directions: 210°, 230°, and 250° azimuth. Figure 1.2 shows the wind rose which was obtained from a meteorological tower (Site 6) in the vicinity of Sites C and X which is considered representative of ridge-line flow. Information from the meteorological station indicated that winds in the sector 210° to 250° occur approximately 40 per cent of the time. Wind speeds of 3.1, 4.5, 8.9 and 11.6 m/s at the meteorological station were modeled to obtain representative concen-trations under beneficial and adverse plume rise conditions.

Another objective was to relate wind speed at the proposed Unit 18 sites to that at the meteorological station in the area and the upper-level (ambient) wind speed in the wind tunnel.

Included in this report are a brief description of the similarity requirements for atmospheric motion, an explanation of test methodology and procedures, results of plume visualization and concentration measurements, and results of wind flow measurements.

This report is supplemented by a motion picture (in color) which shows plume behavior for the various wind speed and wind direction test scenarios. Black and white photographs as well as slides of each plume visualization further illustrate the material presented.

2.0 SIMULATION OF ATMOSPHERIC MOTION

The use of wind tunnels for model tests of gas diffusion by the
atmosphere is based upon the concept that nondimensional concentra-
tion coefficients will be the same at corresponding points in the model
and the prototype and will not be a function of the length scale ratio.
Concentration coefficients will only be independent of scale if the
wind tunnel boundary layer is made similar to the atmospheric boundary
layer by satisfying certain similarity criteria. These criteria are
obtained by inspectional analysis of physical statements for conser-
vation of mass, momentum, and energy. Detailed discussions have been
given by Halitsky (1963), Martin (1965), and Cermak, et al. (1966).
Basically, the model laws may be divided into requirements for geometric,
dynamic, thermic, and kinematic similarity. In addition, similarity
of upwind flow characteristics and ground boundary conditions must be
achieved.

For this study, geometric similarity is satisfied by an undistorted
model of length ratio 1:1920. This scale was chosen to facilitate
ease of measurements and to provide a representative upwind fetch.

When interest is focused on the vertical motion of plumes of
heated gases emitted from stacks into a thermally neutral atmosphere,
the following variables are of primary significance:

ρ_a = density of ambient air

$\Delta\gamma$ = $(\rho_a - \rho_s)g$--difference in specific weight of ambient air
and cooling tower gas

Ω = local angular velocity component of earth

μ_a = dynamic viscosity of ambient air

V_a = speed of ambient wind at meteorological tower

V_s = speed of cooling tower gas emission

h = cooling tower height

H = local difference in elevation of topography

D = cooling tower diameter

δ_a = thickness of planetary boundary layer

z_o = roughness heights for upwind surface

Grouping the independent variables into dimensionless parameters with ρ_a, V_a and H as reference variables yields the following parameters upon which the dependent quantities of interest must depend:

$$\frac{V_a}{H\Omega} \ , \ \frac{\delta_a}{H} \ , \ \frac{z_o}{H} \ , \ \frac{D}{H} \ , \ \frac{V_a \rho_a H}{\mu_a} \ , \ \frac{V_s}{V_a} \ , \ \frac{\rho_a V_a^{\ 2}}{\Delta\gamma D} \ , \ \frac{\Delta\gamma}{g\rho}$$

Tables 2.1 and 2.2 summarize the pertinent dimensional and dimensionless parameters relevant to this study.

The laboratory boundary-layer thickness $\frac{\delta_a}{H}$ was estimated to be nearly equal for model and prototype. Near equality (within a factor of two) of the surface parameter $\frac{z_o}{H}$ for model and prototype was achieved through geometrical scaling of the cooling towers and upwind roughness. The cooling tower parameter $\frac{D}{H}$ was equal for model and prototype.

The magnitude of the roughness parameter, z_o, for the model was calculated by using the logarithmic wind equation

$$\frac{V}{U_*} = \frac{1}{k} \ \ell n \left(\frac{z}{z_o}\right)$$

The wind speeds at heights 0.97 cm and 2.24 cm above the location of the meteorological tower in the model were substituted into the equation. With the resulting two equations, z_o (and U_*) was calculated.

The magnitude of z_o for the prototype was estimated by reference to a plot of z_o versus terrain type presented in Cermak (1975).

Dynamic similarity is achieved in a strict sense if the Reynolds number, $\dfrac{\rho_a V_a L_o}{\mu_a}$, and Rossby number, $\dfrac{V_a}{H\Omega}$, for the model are equal to their counterparts in the atmosphere. The model Rossby number cannot be made equal to the atmospheric value. However, over the short distances considered (up to 5000 m), the Coriolis acceleration has little influence upon the flow. Accordingly, the standard practice is to relax the requirement of equal Rossby numbers (Cermak, 1971).

Kinematic similarity requires the scaled equivalence of streamline movement of the air over prototype and model. It has been shown in Halitsky, et al. (1963) that flow around geometrically similar sharp-edged buildings at ambient temperatures in a neutrally stratified atmosphere should be dynamically and kinematically similar. This approach depends upon producing flows in which the flow characteristics become independent of Reynolds number if a lower limit of the Reynolds number is exceeded. For example, the resistance coefficient for flow in a sufficiently rough pipe, as shown in Schlichting (1960, p. 521), is constant for a Reynolds number larger than 2×10^4. This implies that surface or drag forces are directly proportional to the mean flow speed squared. In turn, this condition is the necessary condition for mean turbulence statistics such as root-mean-square value and correlation coefficient of the turbulence velocity components to be equal for the model and the prototype flow.

Equality of the parameter $\dfrac{\rho_a V_a{}^2}{\Delta\gamma D}$ for model and prototype in

essence determines the relationship between the atmospheric wind

speed and the model wind speed once the geometric scale has been

selected (1:1920 in this case). Often this criteria results in $(V_a)_m$

being too small to satisfy the minimum Reynolds number requirements.

When this happens, the specific weight difference for the model

$(\Delta\gamma)_m$ can be made larger than $(\Delta\gamma)_p$ to compensate for the effect of

small geometric scale. However, this relaxes the equality of the

density difference ratio for model and prototype. This equality

ensures that the initial plume behavior where acceleration of the tower

gases is maximum will be modeled correctly. However, since the

measured concentrations for this study are not in the building vicinity,

relaxation of this requirement is justified. More important is attain-

ment of equal Froude numbers and equal values of the velocity ratio

V_s/V_a for model and prototype.

Using a wind speed of $(V_a)_p$ of 3.1 m/s, a scale of 1:1920, and a

specific weight ratio $\dfrac{(\Delta\gamma)_m}{(\Delta\gamma)_p} = 7.2$, the Froude number equality gives

$$\frac{(V_a)^2{}_m}{(V_a)^2{}_p} = \frac{1}{1920}\,\frac{(\Delta\gamma)_m}{(\Delta\gamma)_p} \quad \text{or}$$

$$(V_a)_m = \left(\frac{1}{43.8}\right)(7.2)\,(3.1) = 0.19 \text{ m/s} .$$

The corresponding representative model velocity at a height of

1.0 m (1920 m prototype) is 0.45 m/s. Using this velocity as the

freestream velocity and a distance of 13.6 m from the beginning of

the wind tunnel to the test site, the Reynolds number becomes

$$Re_{L_o} = \frac{0.45 \times 13.6}{15 \times 10^{-6}} = 4.1 \times 10^5.$$

Referring to Figure 2.1 from Cermak (1975) it can be seen that for a Reynolds number of 4.1×10^5 the ratio of surface length to roughness length L_o/K_s must be less than 300 for the flow to be independent of Reynolds number. Thus K_s, the roughness length, must be greater than $\frac{13.6}{300}$ or 0.045 m. Taking the ridge height above the cooling tower elevation as the roughness height, K_s, results in $K_s = 0.06$ m, which is greater than the critical value of 0.054. Consequently, the flow over the test section is Reynolds number independent.

The method used to increase the Reynolds number such that the flow was independent of Re was to increase the specific weight difference between model and prototype. Since $\frac{(\Delta\gamma)_m}{(\Delta\gamma)_p} = 7.2$ represented the maximum specific weight difference practically attainable, the greatest increase in the local Reynolds number was achieved using this difference. Since the minimum Reynolds number for the cases studied was 4.1×10^5, similarity of concentration distributions over the topographic surface can be assured for all wind speeds studied.

To summarize, the following scaling criteria were applied for the neutral boundary layer situation:

1. $Fr = \dfrac{\rho_a V_a^2}{\Delta\gamma D}$; $(Fr)_m = (Fr)_p$,

2. $R = \dfrac{V_s}{V_a}$; $R_m = R_p$,

3. $L_o/K_s > 300$ (implies Reynolds number independence),

4. $(z_o)_m = (z_o)_p$,

5. Similar geometric dimensions, and

6. Similar velocity and turbulence profiles upwind.

3.0 TEST APPARATUS

3.1 Wind Tunnels

The environmental wind tunnel (EWT) shown in Figure 3.1 was used for this neutral flow study. This wind tunnel, especially designed to study atmospheric flow phenomena, incorporates special features such as adjustable ceiling, rotating turntables, transparent boundary walls, and a long test section to permit adequate reproduction of micro-meteorological behavior. Mean wind speeds of 0.06 to 37 m/s (0.14 to 80 miles/hour) in the EWT can be obtained. In the EWT, boundary layers four feet thick over the downstream 12.2 meters can be obtained with the use of vortex generators at the test section entrance. The flexible test section roof on the EWT is adjustable in height to permit the longitudinal pressure gradient to be set at zero.

3.2 Model

The model cooling tower was modeled at a scale of 1:1920. The relevant building dimensions are given in Table 2.1 and a photograph of the model is shown in Figure 3.2-1.

Topography was modeled to the same scale by cutting styrofoam sheets of 0.6 cm and 1.27 cm thicknesses to match contour lines of a topographic map enlarged to the 1:1920 scale. The topography for the 210° wind direction is shown mounted in the wind tunnel in Figure 3.2-2. The model terrain was not smoothed so as to increase the surface roughness and thereby prevent the formation of a laminar sublayer. This increased roughness also contributed toward achieving Reynolds number independence of flow over the test section.

Sections of modeled topography for the three wind directions were constructed for regions upwind and downwind of the topography mounted on the 3.66 m diameter turntable. In this way, rectangular regions could be fitted into the wind-tunnel test section.

An array of sampling tubes was inserted into the model terrain to give a minimum of 34 representative sampling locations for each wind direction. The sampling locations for each wind direction are shown in Figure 4.2-4, 4.2-5, and 4.2-6 and enumerated in Table 4.2-4.

Metered quantities of gas were allowed to flow from the cooling tower to simulate the exit velocity. Helium, compressed air, and propane (the tracer) were mixed to give the highest practical specific weight. Fischer-Porter flow meter settings were adjusted for pressure, temperature, and molecular weight effects as necessary. When a visible plume was required, the gas was bubbled through titanium tetrachloride before emission.

3.3 Flow Visualization Techniques

Smoke was used to define plume behavior from the geothermal power plant complex. The smoke was produced by passing the air mixture through a container of titanium tetrachloride located outside the wind tunnel and transported through the tunnel wall by means of a tygon tube terminating at the cooling tower inlet. A schematic of the process is shown in Figure 3.3-1.

The plume was illuminated with arc-lamp beams and a visible record was obtained by means of pictures taken with a Speed Graphic camera. Additional still pictures were obtained with a Hasselblad camera. Stills were taken with a camera speed of one second to identify mean

plume boundaries. A series of 16 mm color motion pictures was also taken with a Bolex motion picture camera.

3.4 Gas Tracer Technique

After the desired tunnel speed was obtained, a mixture of propane, helium, and air of predetermined concentration was released from the cooling tower at the required rate to simulate prototype plume rise. Samples of gas were withdrawn from the sample points and analyzed. The flow rate of propane mixture was controlled by a pressure regulator at the supply cylinder outlet and monitored by a Fischer-Porter precision flow meter. The sampling system is shown in Figure 3.4-1.

-Analysis of Data-

Propane is an excellent tracer gas in wind-tunnel dispersion studies. It is a gas that is readily obtainable and of which concentration measurements are easily obtained using gas chromatography techniques.

The procedure for analyzing the samples was as follows:

1. A sample volume drawn from the wind tunnel of 2 cc was introduced into the Flame Ionization Detector.

2. The output from the electrometer (in millivolt seconds) was integrated and then the readings were recorded for each sample.

3. These readings were transformed into propane concentrations values by the following steps:

$$\chi(ppm) = C(ppm/mvs)E(mvs)$$

where C was determined from a calibration gas of known concentration

$$C = (ppm/mvs)_{\text{calibration gas}}.$$

The values of the concentration parameter initially determined
apply to the model and it is desirable to express these values in
terms of the field. At the present time, there is no set procedure
for accomplishing this transformation. The simplest and most straight-
forward procedure is to make this transformation using the scaling
factor of the model. Since

$$1m\big|_m = 1920m\big|_p \quad ,$$

one can write

$$\frac{\chi V}{Q_s}\bigg|_p (m^{-2}) = \frac{1}{1920^2} \frac{\chi V}{Q_s}\bigg|_m (m^{-2})$$

The sample scaling of the concentration parameter from model to
field appears to give reasonable results. All data reported herein
are in terms of the dimensionless value, $K = \dfrac{\chi V_a D^2}{Q_s}$.

-Errors in Concentration Measurement-

Each sample as it passes through the flame ionization detector is
separated from its neighbors by a period during which nitrogen flows.
During this time, the detector is at its baseline, or zero level. When
the sample passes through the detector, the output rises to a value
equal to the baseline plus a level proportional to the amount of tracer
gas flowing through the detector. The baseline signal is set to zero
and monitored for drift. Since the chromatograph used in this study
features a temperature control on the flame and electrometer, there is
very low drift. The integrator circuit is designed for linear
response over the range considered.

A total system error can be evaluated by considering the standard deviation found for a set of measurements where a pre-calibrated gas mixture is monitored. For a gas of ~ 100 ppm propane ± 1 ppm, the average standard deviation from the electrometer was two per cent. Since the source gas was premixed to the appropriate molecular weight and repetitive measurements were made of its source strength, the confidence in source strength concentration is similar. The flow rate of the source gas was monitored by Fischer-Porter flow meters which are accurate to two per cent, including calibration and scale fraction error. The wind-tunnel velocity was constant to ± 10 per cent at such low settings. Hence, the cumulative confidence in the measured values of the dilution factor $(\frac{\chi V}{Q})_s$ will be a standard deviation of about ± 11 per cent, whereas the worst cumulative scenario suggests an error of no more than ± 20 per cent.

The lower limit of measurement is imposed by the instrument sensitivity and the background concentrations of hydrocarbons in the air within the wind tunnel. Background concentrations were measured and subtracted from all measurements quoted herein; however, a lower limit of one to two ppm of propane is available as a result of background methane levels plus previous propane releases. An upper limit for propane with the instrument used is 10 per cent propane by volume. A recent report on the flame ionization detector for sampling gases in atmospheric wind tunnels prepared by Dear and Robins (1974) arrives at similar figures.

-Test Results: Concentration Measurements-

Since the conventional point-source diffusion equations cannot be used for predicting diffusion near objects which cause the wind to be

nonuniform and nonhomogeneous in velocity and turbulence, it is necessary to calculate gaseous concentrations on the basis of experimental data. It is convenient to report dilution results in terms of a nondimensional factor independent of model to prototype scale.

In Cermak, et al. (1966) and Halitsky (1963), the problem of similarity for diffusing plumes is discussed in detail. Considering this, the concentration measurements were transformed to K-isopleths by the formula

$$K = \frac{\chi V_a D^2}{Q_s}$$

where

χ = sample volume concentration,

D = cell diameter,

V_a = mean wind velocity at meteorological tower,

Q_s = gas source release rate (mass per unit time).

When interpreting model concentration measurements, it is important to remember that there can be considerable difference between the instantaneous concentration in a plume and the average concentration due to horizontal meandering. In the wind tunnel, a plume does not generally meander due to the absence of large-scale eddies. Thus, it is found that field measurements of peak concentrations which effectively eliminate horizontal meandering should correlate with the wind tunnel data (Hino, 1968). In order to compare downwind measurements of dispersion to predict average field concentrations, it is necessary to use data on peak-to-mean concentration ratios as gathered by Singer, et al. (1953, 1963). Their data is correlated in terms of the gustiness categories suggested by Pasquill for a variety of terrain

conditions. It is possible to determine the frequency of different gustiness categories for a specific site. Direct use of wind tunnel data at points removed from the building cavity region may underestimate the dilution capacity of a site by a factor of four unless these adjustments are considered (Martin, 1965). This dilution factor has not been included in the scaling relationships.

To estimate the equivalent prototype samply time, another dimensionless variable was derived by including time as one of the pertinent parameters. The relation then exists

$$\left(\frac{\tau V_a}{L_o}\right)_m = \left(\frac{\tau V_a}{L_o}\right)_p \quad \text{or,}$$

$$\tau_p = \tau_m \left(\frac{L_p}{L_m}\right)\left(\frac{V_{am}}{V_{ap}}\right).$$

Since the model sampling time was approximately 30 s, then

$$\tau_p = \left(\frac{30}{60}\right)\left(\frac{1920}{1}\right)\left(\frac{7.2}{1920}\right)^{1/2} = 59 \text{ min.}$$

Since the prototype sampling time of interest is one hour, the data presented herein have not been corrected for sampling time.

3.5 Wind Profile Measurements

The following instruments were used during the course of this study to measure velocity:

1) Pitot tube (velocities higher than 4 m/s)--used for freestream velocity and upper level velocity profile measurements.

2) Data metrics model 800 LV Linear Flow Meter (for velocities from 0.5 to 4.5 m/s)--used for freestream velocity and upper level velocity profile measurements.

3) Thermo System (TSI model 1050) constant temperature hot-film anemometer (for velocities from 0.20 - 1.9 m/s)--used for low speed measurements close to surface of model.

The use of a pitot tube for velocity measurements* entails measuring the difference between total and static pressure. The velocity is calculated by the relationship

$$V = K' \sqrt{\frac{T}{P_{AT}} \Delta P}$$

V   - velocity

K' - proportionality coefficient

T   - absolute air temperature

P_{AT} - barometric pressure

ΔP - the difference between total and static pressure

The pressure difference was measured with a MKS Baratron Type 77. The Linear Flow Meter was calibrated against a pitot tube in the free stream of the wind tunnel. The calibration curve is shown in Figure 3.5-1.

Calibration of the TSI hot-film anemometer was carried out with a TSI calibrator. The calibration measurements were correlated to King's law and put in the following form:

$$\frac{E^2}{R_h (R_h - R_c)} = A + BV^n$$

*Detailed discussion on pitot tube and hot-wire anemometry can be found in textbooks. Only those concepts that are essential to our measurements are presented here.

where

R$_h$ = hot resistance of the wire

R$_c$ = cold resistance of the wire

E = the output signal of the wire (mv)

V = the velocity sensed (m/s)

n, A and B = the constants of King's law

The coefficients A, B, and n for the velocity range of 0.25 -
1.9 m/s were found to be

A = 3.55

B = 5.30

n = 0.55

King's law fit to the calibration of the hot film is shown in Figure 3.5-2.

To obtain the velocity profiles a calibrated carriage was used
together with a digital voltmeter. In this manner, the location of the
anemometer over the terrain could be adjusted from outside the tunnel.

Mean velocities were obtained by integrating the instantaneous
velocities over 60 s.

4.0 TEST PROGRAM RESULTS - SITE X

4.1 Plume Visualization

The test results consist of photographs and movies showing Site X
plume behavior for different wind directions and speeds. Of parti-
cular interest is the plume transport and dispersion in the vicinity
of Anderson Springs.

The sequence of photographs in Figures 4.1-1, 4.1-2, and 4.1-3
shows plume behavior for the 210°, 230°, and 250° wind directions and
wind speeds at meteorological tower height (10 m, AGL) of 3.1, 4.5,
8.9, and 11.6 m/s for each direction. The plume behavior for each
direction is generally the same. For the light wind speed cases
(3.1 m/s) the plume tends to rise over Anderson Springs. However,
as the wind speed increases, the plume altitude decreases, and for
the high wind speed cases, the plume tends to follow along the terrain
confluences.

For a wind direction of 210°, 230° and 250° and wind speeds of
4.5 m/s or greater the plume emanating from the cooling tower appears
to flow along the terrain at a relatively low effective plume altitude.
Plume transport toward Whispering Pines was observed for the 210° wind
direction.

Complete sets of still photographs supplement this report. Color
motion pictures have been arranged into titled sequences and the sets
available are given by run number in Table 4.1-1.

4.2 Concentration Measurements

The diffusion of gaseous effluent emitted from a model cooling
tower located at Site X was studied for three wind directions (210°,
230°, and 250° azimuth) and four wind speeds for each direction

(3.1, 4.5, 8.9 and 11.6 m/s). Propane concentrations at ground level were measured at distances from 2500 to 4500 m downwind.

For each wind direction studied, thirty-four gas samples were collected at ground level. The sampling arrays for the three wind directions are shown in Figures 4.2-4, 4.2-5 and 4.2-6. The prototype locations for all sampling points are summarized in Table 4.2-4 with north and east as positive directions. The zero coordinate is the center of the terrain which was mounted on the turntable. This point is represented by the base of the wind direction arrow in all figures.

All concentration data have been reported in dimensionless form as explained in Section 3.4. To convert from a dimensionless concentration coefficient, K, to a prototype H_2S concentration, refer to the procedure outlined in Appendix A.

The results for the wind directions and speeds studied are presented in Tables 4.2-1, 4.2-2, and 4.2-3. Sample locations in the tables are defined in Table 4.2-4, and Figures 4.2-10, 4.2-11, and 4.2-12.

In order to visually and quantitatively assess the effect of wind direction and wind speed on ground level concentration patterns, Figures 4.2-1 through 4.2-3 were prepared. These figures show isopleths for the dimensionless concentration coefficient, K, for the wind directions and speeds studied. For a fixed wind direction the figures show a similar isopleth pattern for speeds of 4.5 m/s or greater. The maximum nondimensional concentration generally occurs with a 4.5 or 8.9 m/s wind speed depending upon wind direction.

The highest K-value near Anderson Springs of 3.4 was observed to occur with a 250° wind direction at 4.5 m/s. Figure 4.2-2 shows the isopleth pattern for this case. At this speed and direction, it is evident that the plume is mixed rapidly to the ground after emission and follows the terrain confluences down through Anderson Springs. This same pattern is evident for the other high wind speed cases except the plume transport is not as close to Anderson Springs. The highest K-value near Whispering Pines of 1.0 was observed with a wind speed of 4.5 m/s and a 210° wind direction.

The K-isopleths for the 3.1 m/s cases are usually close to the background value and consequently the absolute values have a larger error than for the higher wind speed cases. Regardless, the values for the light wind cases are low and near zero.

5.0 TEST PROGRAM RESULTS - SITE C

5.1 Plume Visualization

The test results consist of photographs and movies showing Site C plume behavior for different wind directions and speeds. Of particular interest is the plume transport and dispersion in the vicinity of Anderson Springs.

The sequence of photographs in Figure 5.1-1, 5.1-2, and 5.1-3 shows plume behavior for the 210°, 230°, and 250° wind directions and speeds at meteorological tower height (10 m, AGL) of 3.1, 4.5, 8.9 and 11.6 m/s for each direction. The plume behavior for each direction is generally the same. For the light wind speed cases, (3.1 m/s), the plume tends to rise over Anderson Springs, However, as the wind speed increases, the plume altitude decreases and for the high wind speed cases tends to follow along the terrain confluences.

For a wind direction of 250° and wind speeds of 4.5 m/s or greater the plume emanating from the cooling tower appears to flow over Anderson Springs at a relatively low effective plume altitude. Plume transport toward Whispering Pines was observed for the 210° wind direction.

Complete sets of still photographs supplement this report. Color motion pictures have been arranged into titled sequences and the sets available are summarized by run number in Table 5.1-1.

5.2 Concentration Measurements

The diffusion of gaseous effluent emitted from a model cooling tower located at Site C was studied for three wind directions (210°, 230°, and 250° azimuth) and three wind speeds for each direction

(3.1, 4.5, 8.9 and 11.6 m/s). Propane concentrations at ground level were measured at distances from 2500 to 4500 meters downwind.

For each wind direction studied, thirty-four gas samples were collected at ground level. The sampling arrays for the three wind directions are shown in Figures 4.2-4, 4.2-5, and 4.2-6. The prototype locations for all sampling points are summarized in Table 4.2-4 with north and east as positive directions. The zero coordinate is the center of the terrain which was mounted on the turn-table. This point is represented by the base of the north arrow in all figures.

All concentration data have been reported in dimensionless form as explained in Section 3.4. To convert from a dimensionless concentration coefficient, K, to a prototype H_2S concentration, refer to the procedure outlined in Appendix A.

The results for the wind directions and speeds studied are presented in Tables 5.2-1, 5.2-2, and 5.2-3. Sample locations in the tables are defined in Table 4.2-4 and Figures 4.2-4, 4.2-5, and 4.2-6.

In order to visually and quantitatively assess the effect of wind direction and wind speed on ground level concentration patterns, Figures 5.2-1 through 5.2-3 were prepared. These figures show isopleths of the dimensionless concentration coefficient, K, for the wind directions and speeds studied. The isopleth patterns are similar to those for Site X which is to be expected due to the close proximity of the two sites.

The highest K-value near Anderson Springs of 3.5 was observed to occur with a 250° wind direction at 8.9 m/s. Figure 5.2-3 shows the isopleth pattern for this case. At this speed and direction, it is evident that the plume is mixed rapidly to the ground after emission and follows the terrain confluences down through Anderson Springs. This same pattern is evident for the other high wind speed case except the plume transport is not as close to Anderson Springs. The highest K-value near Whispering Pines of 1.0 occurred with a wind speed of 4.5 m/s and a wind direction of 210°.

Most of the K-values for the 3.1 m/s cases are all near the background value and consequently the absolute values have a larger error than for the higher wind speeds studied. Regardless, the values for the light-wind cases are low and near zero.

6.0   TEST RESULTS - VELOCITY MEASUREMENTS

This section discusses the results of the velocity measurements. Techniques for data collection are described in Section 3.5.   Velocity measurements were obtained to meet the following objectives.

- Provide a relation between the freestream velocity and the velocity at the meteorological tower (Site 6).

- Present velocity profiles above Sites 6 and C.

Figures 6.1, 6.2, and 6.3 show the curves of freestream velocity versus the wind speed at the meteorological tower height for the three directions studied.   These curves were used to set the tunnel conditions for each run.

Figure 6.4 shows the velocity profile at Site C and Figure 6.5 the profiles at Site 6, respectively.   Further information on the velocity measurements is given in Cermak and Petersen (1977).

REFERENCES

Cermak, J. E. and J. Peterka, "Simulation of Wind Fields Over Point Arguello, California, by Wind-Tunnel Flow Over a Topographical Model," Final Report, U.S. Navy Contract N126(61756)34361 A(PMR), Colorado State University, CER65JEC-JAP64, December 1966.

Cermak, J. E., "Laboratory Simulation of the Atmospheric Boundary Layer," AIAA Jl., Vol. 9, No. 9, pp. 1746-1754, September, 1971.

Cermak, J. E., V. A. Sandborn, E. J. Plate, G. J. Binder, H. Chuang, R. N. Meroney, and S. Ito, "Simulation of Atmospheric Motion by Wind-Tunnel Flows," Colorado State University, CER66JEC-VAS-EJP-HC-RNM-SI17.

Cermak, J. E., "Applications of Fluid Mechanics to Wind Engineering," 1974 Freeman Scholar Lecture, ASME Journal of Fluids Engineering, Vol. 97, Series 1, No. 1, March 1975, CEP74-75JEC7.

Cermak, J. E. and R. L. Petersen, "Atmospheric Transport of Hydrogen Sulfide From Proposed Geothermal Power Plant (Unit 16) Predictions by Physical Modeling in a Wind Tunnel," Colorado State University, CER76-77JEC-RLP47, March 1977.

Deær, D. J. A. and A. G. Robins, "A Technique Used to Study the Dispersion of Gases in the MEL 9.14 m x 2.74 m Wind Tunnel," Central Electric Generating Board Report R/M/N752, United Kingdom, 1974.

Field, J. H. and R. Warden, "A Survey of the Air Currents in the Bay of Gibralter, 1929-1930," Air Ministry, Geophysical Memorandum No. 50, London, 1933.

Halitsky, J., J. Golden, P. Halpern, and P. Wu, "Wind Tunnel Tests of Gas Diffusion From a Leak in the Shell of a Nuclear Power Reactor and From a Nearby Stack," Geophysical Sciences Laboratory Report No. 63-2, New York University, April 1963.

Halitsky, J., "Gas Diffusion Near Buildings," Geophysical Sciences Laboratory Report No. 63-3, New York University, February 1963.

Hino, M., "Maximum Ground-Level Concentration and Sampling Time," Atmospheric Environment, Vol. 2, pp. 149-165, 1968.

Martin, J. E., "The Correlation of Wind Tunnel and Field Measurements of Gas Diffusion Using Kr-85 as a Tracer," Ph.D. Thesis, MMPP 272, University of Michigan, June 1965.

Meroney, R. N. and J. E. Cermak, "Wind Tunnel Modeling of Flow Diffusion Over San Nicolas Island, California," U.S. Navy Contract No. N123(61756)50192 A(PMR), Colorado State University, CER66-67RNM-JEC44, September 1967.

Schlichting, H., Boundary Layer Theory, McGraw-Hill, New York, 1960.

REFERENCES (continued)

Singer, I. A., I. Kazukiko and G. D. Roman, "Peak to Mean Pollutant Concentration Ratios for Various Terrain and Vegetative Cover," Journal of APCA, Vol. 13, No. 1, p. 40, 1963.

Singer, I. A. and M. E. Smith, "The Relation of Gustiness to Other Meteorological Parameters," Journal of Meteorology, Vol. 10, No. 2, 1953.

Turner, P. B., "Workbook of Atmospheric Dispersion Estimates," U.S. Department of Health, Education and Welfare, Public Health Service, Cincinnati, Ohio, 1969.

APPENDIX A

Method for Calculating Prototype Concentrations
From Nondimensional Concentration Coefficient K

- Basic Equation:

$$K = \frac{\chi V_a D^2}{\Lambda Q_s} \quad \text{Prototype}$$

where

$K \equiv$ nondimensional concentration coefficient from wind tunnel study

$\chi \equiv H_2S$ concentration (ppm)

$V_a \equiv$ wind speed at the meteorological station (m/s)

$D \equiv$ cell diameter (equal to 8.5 m)

$\Lambda \equiv$ total volume flow (use 4313 m^3/s)

$Q_s \equiv$ equivalent H_2S concentration in the incoming stack gas [(ppm) (1 - fraction removed)]

- Now solving for $\chi_{prototype}$:

$$\chi_{prototype} = K \frac{\Lambda Q_s}{V_a D^2}$$

$$= 59.7 \frac{K Q_s}{V_a}$$

- Example:

let $K = 20 \times 10^{-5}$

$Q_s = 100$ ppm

$V_a = 9.8$ m/s

then $\chi_{prototype} = \frac{(59.7) \ (20 \times 10^{-5}) \ (100)}{9.8} = 0.12$ ppm

Table 2.1. Model and Prototype Dimensional Parameters for Unit 18
            Sites C and X

	Parameter	Prototype	Model
1.	Building		
	a. length (ℓ)	98.0 m	5.1 cm
	b. width (w)	21.5 m	1.1 cm
	c. height (h)	20.0 m	1.0 cm
2.	Exit Temperature (T_s)	319 °K	293°K
3.	Cell Diameter (D)	8.5 m	0.44 cm
4.	Number of Cells	10	10
5.	Exit Velocity (V_s)	7.6 m/s	0.46 m/s
6.	Volumetric Emission Rate (Λ)	4312.6 m^3/s	71.32 cc/s
7.	Gas Density (ρ_s)	1.07 kg/m^3	0.29 ks/m^3
8.	Ambient Density (ρ_a)	1.20 kg/m^3	1.20 kg/m^3
9.	Wind Speed at Meteorological Tower (V_a)	3.1, 4.5, 8.9 11.6 m/s	0.19, 0.27, 0.55, 0.70 m/s
10.	Ridge Height above Cooling Tower Elevation (H)	122.0 m	0.06 m
11.	Wind Direction	210, 230, 250°	
12.	Surface Roughness (z_o)	0.5 m	0.02 cm

Table 2.2. Model and Prototype Dimensionless Parameters for Unit 18, Sites C and X

Parameter	Prototype	Model
δ_a/H	1.84	2.15
z_o/H	4.1×10^{-3}	3.3×10^{-3}
D/H	0.07	0.07
h/H	0.16	0.16
$R = \dfrac{V_s}{V_a}$	2.5, 1.7, 0.85, 0.66	2.5, 1.7, 0.85, 0.66
$Fr = \dfrac{\rho_a V_a^2}{g(\rho_s - \rho_a)D}$	1.1, 2.2, 8.6, 14.7	1.1, 2.2, 9.2, 15.0
$Dr = \dfrac{\rho_a - \rho_s}{\rho_a}$	0.11	0.76

Table 4.1-1. Summary of Photographs Taken for Unit 18, Site X

Photo or Run No.	Wind Direction	Wind Speed (m/s)
1	250°	11.6
2	250°	4.5
3	250°	8.9
4	250°	3.1
X5	230°	3.1
X6	230°	4.5
X7	230°	8.9
X8	230°	11.6
X9	210°	3.1
X10	210°	4.5
X11	210°	8.9
X12	210°	11.6

Table 4.2-1. Nondimensional Coefficients (x 10^5) for Unit 18, Site X and a Wind Direction of 210°

Location Number	Wind Speed (ms^{-1})			
	3.1	4.47	8.9	11.6
7	0.55	0.04	0.06	0.22
8	0.05	0.05	0.08	0.18
9	0.06	0.00	0.03	0.19
10	0.04	0.00	0.05	0.18
11	0.06	0.01	0.05	0.18
13	0.05	0.01	0.00	0.26
19	0.18	0.04	0.03	0.26
20	0.05	0.02	0.03	0.08
21	0.07	0.02	0.12	0.13
22	0.08	0.02	0.12	0.18
25	0.11	0.01	0.10	0.19
31	0.12	0.03	0.10	0.15
32	0.15	0.05	0.08	0.25
33	0.11	0.03	0.02	0.33
35	0.02	0.03	0.06	0.29
43	0.11	0.03	0.06	0.23
44	0.20	0.04	0.14	0.17
47	0.07	0.01	0.03	0.18
56	0.02	0.05	0.07	0.19
57	0.17	0.08	0.10	0.16
58	0.05	0.02	0.10	0.14
59	0.04	0.04	0.09	0.17
60	0.04	0.16	0.17	0.24
61	0.11	0.07	0.11	0.18
62	0.01	0.08	0.14	0.17
63	0.02	0.19	0.35	0.37
64	0.10	0.07	0.12	0.29
70	0.06	0.07	0.50	0.63
71	0.00	0.54	2.59	2.80
73	0.00	0.49	1.90	0.93
74	0.10	1.11	1.43	1.40
75	0.03	0.06	0.31	0.35
76	0.11	0.16	0.91	0.93
77	0.13	2.21	1.42	1.12

Table 4.2-2. Nondimensional Coefficients (x 10^5) for Unit 18, Site X and a Wind Direction of 230°

Location Number	Wind Speed (ms^{-1})			
	3.1	4.47	8.9	11.6
1	0.02	0.04	0.33	0.33
2	0.00	0.00	0.05	0.01
7	0.06	0.00	4.39	4.04
8	0.07	1.78	2.73	2.80
9	0.00	0.91	1.44	1.28
10	0.02	0.66	1.19	1.17
11	0.01	0.18	0.41	0.31
13	0.03	0.00	0.12	0.10
19	0.02	4.60	6.60	5.63
20	0.03	3.34	5.13	4.49
21	0.03	1.57	3.13	2.47
22	0.04	0.55	1.49	1.08
23	0.02	0.34	0.68	0.74
25	0.03	0.15	0.24	0.13
31	0.00	7.89	7.23	6.02
32	0.07	3.31	2.95	0.93
33	0.07	0.02	2.58	0.87
34	0.06	1.16	1.63	1.37
35	0.00	0.47	0.35	0.71
37	0.06	0.09	0.12	0.31
43	0.05	6.40	5.17	4.25
45	0.02	1.92	--	0.12
46	0.07	1.28	2.02	1.70
47	0.10	0.66	0.81	0.76
49	0.05	0.00	0.12	0.76
56	--	0.03	--	1.48
57	--	1.42	3.04	2.40
58	--	4.59	2.42	2.01
59	0.02	4.64	3.10	2.27
60	0.03	--	0.57	0.51
61	0.03	3.32	1.04	0.82
62	0.08	2.67	0.60	0.57
63	0.16	0.40	0.17	0.20
64	0.04	0.14	0.13	0.27

Table 4.2-3. Nondimensional Coefficients $(\times 10^5)$ for Unit 18, Site X and a Wind Direction of 250°

Location Number	Wind Speed (mg^{-1})			
	3.1	4.47	8.9	11.6
1	0.10	5.46	4.30	0.38
2	--	0.00	--	0.00
7	0.10	0.43	0.08	0.00
8	0.06	0.71	0.08	0.17
9	0.17	1.33	0.19	0.30
10	0.22	0.63	0.58	1.30
11	0.14	2.84	1.51	1.71
12	0.03	3.45	1.31	2.60
13	0.04	2.78	2.62	2.45
14	0.04	1.96	3.16	2.41
19	0.05	0.22	0.08	0.16
20	0.07	0.31	0.05	0.39
21	0.21	0.31	0.16	0.43
22	0.27	0.73	0.39	0.59
23	0.27	1.02	0.55	0.92
24	0.09	1.63	0.91	1.35
25	0.21	2.59	2.18	2.25
26	0.16	3.62	2.40	2.46
31	0.39	0.30	0.38	0.73
32	0.68	1.59	1.23	1.64
33	4.03	10.50	14.60	2.56
34	0.19	0.68	0.38	0.58
35	0.28	0.91	0.59	0.91
36	0.28	1.28	0.71	0.75
37	0.55	2.58	1.40	2.28
38	0.54	--	1.95	2.35
43	--	0.04	0.38	0.00
44	0.33	0.25	0.91	0.00
45	0.11	0.14	0.92	0.42
46	--	--	--	--
47	0.00	0.78	0.16	0.06
48	0.00	1.11	1.02	1.38
49	0.00	1.62	1.10	1.06

Table 4.2-4. Prototype Sampling Location Key* and Site Location Key

Location #	x (m)	y (m)	z (m, MSL)	Location #	x (m)	y (m)	z (m, MSL)
1	-182.88	810.77	597.4	39	2029.97	804.67	402.3
2	195.07	804.67	524.3	40	2103.12	548.64	390.1
3	512.06	640.08	499.9	41	2151.89	292.61	487.7
4	755.09	304.8	609.6	42	2157.98	-201.17	499.9
5	816.86	-30.48	621.8	43	1194.82	2682.24	585.2
6	682.75	420.62	560.8	44	1450.85	2554.	536.4
7	-79.25	1286.26	597.4	45	1694.69	2401.8	499.9
8	109.73	1280.16	548.6	46	1914.14	2218.9	499.9
9	304.8	1255.78	517.44	47	2109.22	2036.1	463.3
10	487.68	1188.72	463.3	48	2304.29	1816.6	426.7
11	664.46	1097.28	451.1	49	2462.78	1591.1	402.3
12	816.86	987.55	426.7	50	2596.9	1353.3	402.3
13	999.74	816.86	438.9	51	2718.82	1060.7	402.3
14	1103.38	646.18	451.1	52	2810.26	780.3	451.1
15	1188.72	475.49	536.4	53	2877.31	530.4	560.8
16	1249.68	280.42	621.8	54	2926.08	-97.5	621.8
17	1280.16	85.34	548.6	56	-97.54	1755.6	597.4
18	1243.58	-298.7	463.3	57	-499.87	1676.4	609.6
19	304.8	1731.26	548.6	58	391.38	2170.2	633.9
20	524.26	1676.4	560.8	59	97.5	2182.4	646.2
21	707.14	1609.34	573	60	-396.2	2158.0	682.8
22	935.74	1493.52	536.4	61	938.8	2779.8	573.0
23	1097.28	137.16	499.9	62	658.4	2865.1	597.4
24	1243.84	1243.58	487.7	63	60.96	2926.1	719.3
25	1402.08	1054.61	426.7	64	670.56	3596.6	670.6
26	1536.19	847.34	390.1	70	-670.56	2072.6	737.6
27	1627.63	646.18	438.9	71	-1798.3	2255.5	722.4
28	1694.69	402.34	438.9	73	-487.68	2804.2	725.4
29	1743.46	170.69	438.9	74	914.4	2804.2	749.8
30	1725.17	-268.22	499.9	75	61.0	4389.1	731.5
31	573.02	2115.31	609.6	76	487.7	4937.8	792.5
32	804.67	2029.97	560.8	77	121.9	3657.6	765.0
33	1024.13	1926.34	524.3	Sites			
34	1243.58	1786.13	512.1	1	402.3	-79.2	719.3
35	1444.75	1633.73	475.5	2	-390.1	-402.3	854.0
36	1597.15	1475.23	463.3	3	-2450.6	182.9	829.1
37	1767.84	1267.97	426.7	Met Station	-2011.7	786.4	1005.8
38	1914.14	1024.13	402.3				

* All locations are with respect to the point represented by the base of the wind direction arrow in Figure 1.1

Table 5.1-1. Summary of Photographs Taken for Unit 18, Site C

Photo or Run No.	Wind Direction	Wind Speed (m/s)
4C	250°	3.1
1C	250°	4.5
2C	250°	8.9
3C	250°	11.6
C5	230°	3.1
C6 (missing)	230°	4.5
C7	230°	8.9
C8	230°	11.6
C9	210°	3.1
C10	210°	4.5
C11	210°	8.9
C12	210°	11.6

Table 5.2-1. Nondimensional Coefficients (x 10^5) for Unit 18, Site C
and a Wind Direction of 210°

Location Number	Wind Speed (ms^{-1})			
	3.1	4.47	8.9	11.6
7	0.09	0.06	0.11	0.06
8	0.04	0.04	0.10	0.04
9	0.04	0.03	0.14	0.00
10	0.04	0.01	0.17	0.00
11	0.02	0.02	0.08	0.02
13	0.01	0.04	0.09	0.03
19	0.01	0.04	0.10	0.05
20	0.03	0.03	0.11	0.04
21	0.02	0.04	0.14	0.03
22	0.02	0.04	0.14	0.12
25	0.02	0.06	0.10	0.06
31	0.04	0.11	0.06	0.10
32	0.06	0.05	0.17	0.10
33	0.03	0.05	0.09	0.19
35	0.03	0.09	0.17	0.08
43	0.04	0.06	0.07	0.14
44	0.08	0.07	0.11	0.18
47	0.03	0.01	0.09	0.00
56	0.04	0.02	0.20	0.00
57	0.05	0.02	0.12	0.14
58	0.05	0.09	0.08	0.08
59	0.06	0.08	0.06	0.01
60	0.06	0.08	0.03	0.03
61	0.06	0.07	0.03	0.04
62	0.05	0.11	0.14	0.05
63	0.04	0.14	0.23	0.02
64	0.04	0.09	0.16	0.00
70	0.01	0.18	0.18	0.04
71	0.06	1.28	1.21	0.91
73	0.02	0.49	0.43	0.30
74	0.00	1.59	1.02	0.79
75	0.01	0.38	0.18	0.11
76	0.04	1.11	0.75	0.33
77	0.06	1.07	1.14	0.83

Table 5.2-2. Nondimensional Coefficient (x 10^5) for Unit 18, Site C
and a Wind Direction of 230°

Location Number	Wind Speed (ms^{-1})			
	3.1	4.47	8.9	11.6
1	--	0.03	0.04	0.09
2	0.05	0.02	0.00	0.09
7	0.01	0.77	1.02	0.94
8	0.03	0.63	0.80	0.66
9	0.04	0.60	0.70	0.31
10	0.03	0.32	0.66	0.24
11	0.68	0.16	0.71	0.12
13	0.04	0.13	0.02	0.07
19	0.03	3.18	3.13	2.96
20	0.02	2.88	2.00	2.00
21	0.02	1.21	0.73	0.86
22	0.04	0.38	0.28	0.23
23	0.05	0.13	0.18	0.21
25	0.04	0.05	0.11	0.09
31	0.07	4.49	3.56	4.11
32	0.04	2.52	2.26	2.19
33	0.19	1.53	1.95	2.17
34	0.05	0.85	0.58	0.45
35	0.10	0.47	0.19	0.23
37	0.13	0.07	0.22	0.10
43	0.01	5.72	3.35	3.46
45	0.01	0.91	0.97	1.03
46	0.02	1.42	0.67	0.46
47	0.12	0.69	0.42	0.07
49	0.04	0.00	0.26	0.36
56	--	0.69	0.12	0.05
57	--	4.94	4.77	5.09
58	0.07	6.28	3.69	3.58
59	0.07	5.26	3.81	3.66
60	0.06	4.33	3.26	1.88
61	0.13	3.48	2.31	1.63
62	0.06	3.00	2.17	1.26
63	0.16	0.72	0.67	0.30
64	0.09	0.69	0.76	0.39

Table 5.2-3. Nondimensional Coefficients (x 10^5) for Unit 18, Site C
and a Wind Direction of 250°

| Location Number | Wind Speed (ms^{-1}) | | | |
	3.1	4.47	8.9	11.6
1	0.40	5.12	4.05	2.97
2	--	--	0.74	0.00
7	0.32	0.56	0.46	0.12
8	1.02	0.70	1.26	0.16
9	0.26	1.43	1.25	0.00
10	0.69	0.95	1.17	0.46
11	0.09	2.82	1.23	0.81
12	0.16	3.34	2.35	1.58
13	0.55	3.18	2.85	1.89
14	0.56	2.50	3.45	2.24
19	0.34	0.05	0.09	0.00
20	0.43	0.00	0.01	0.00
21	0.51	0.19	0.47	0.00
22	0.53	0.61	0.96	0.00
23	0.72	1.24	1.15	0.20
24	0.27	2.01	1.15	0.45
25	--	1.99	2.29	0.48
26	0.58	2.61	3.34	2.15
31	0.00	--	0.00	0.00
32	1.81	1.02	3.62	2.39
33	2.18	2.53	3.54	3.09
34	0.73	0.56	1.14	0.31
35	1.26	0.90	2.02	0.89
36	0.81	2.11	1.67	0.53
37	0.62	2.36	2.18	1.15
38	--	0.02	1.33	0.00
43	--	0.10	0.00	0.00
44	0.35	0.00	0.63	0.00
45	0.47	--	0.47	0.19
46	--	0.01	--	--
47	0.64	0.37	0.25	0.00
48	1.49	0.00	1.60	0.00
49	0.98	0.74	1.51	0.18
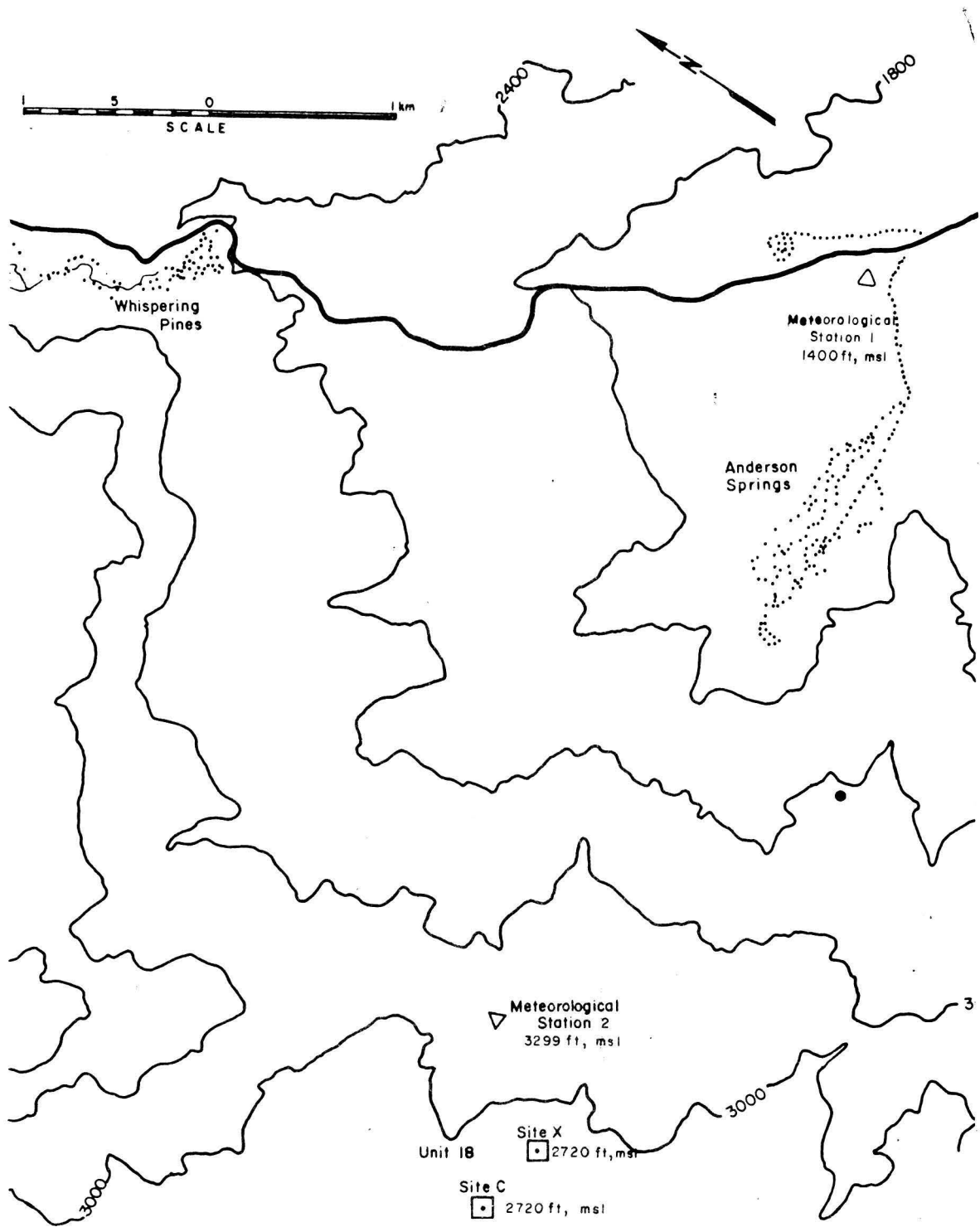
Figure 1.1. Map showing geyser geothermal area and location of proposed
geothermal plant sites C and X for Unit 18.
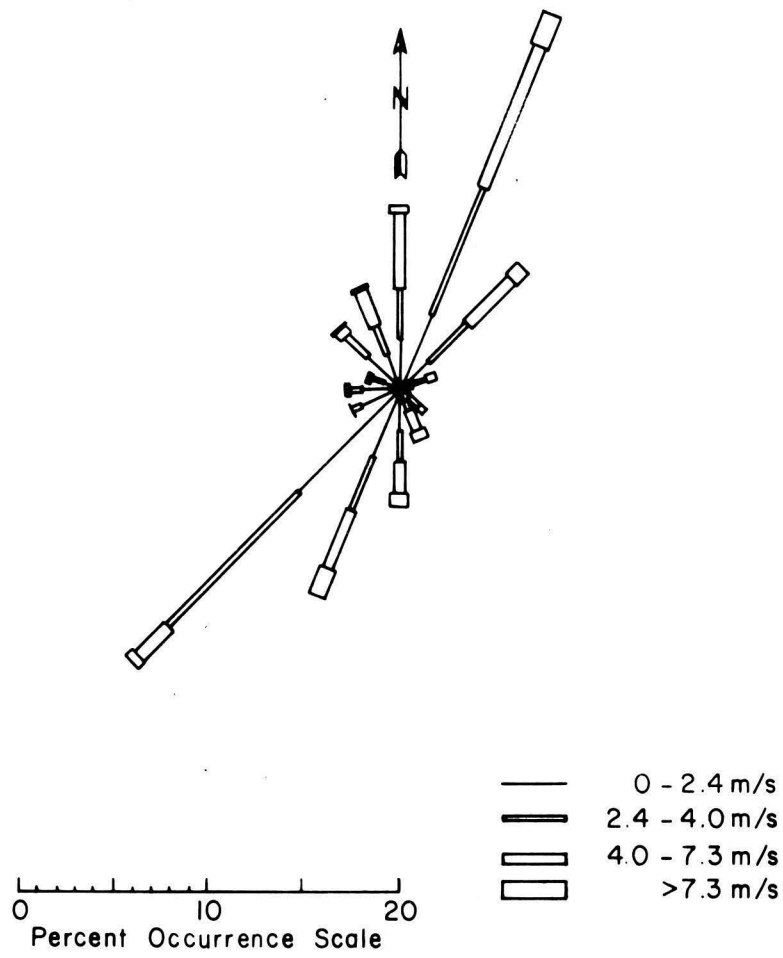
Figure 1.2a. Wind rose from meteorological station #1.
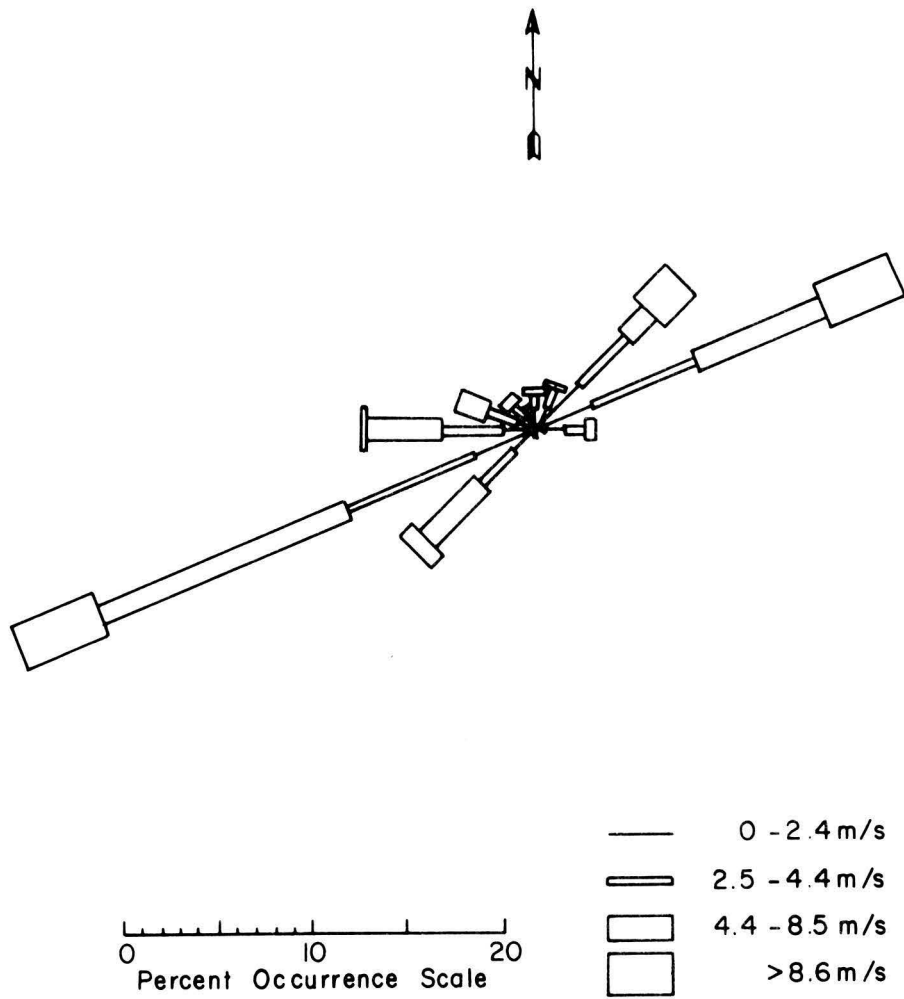
Figure 1.2b. Wind rose from meteorological station #2.
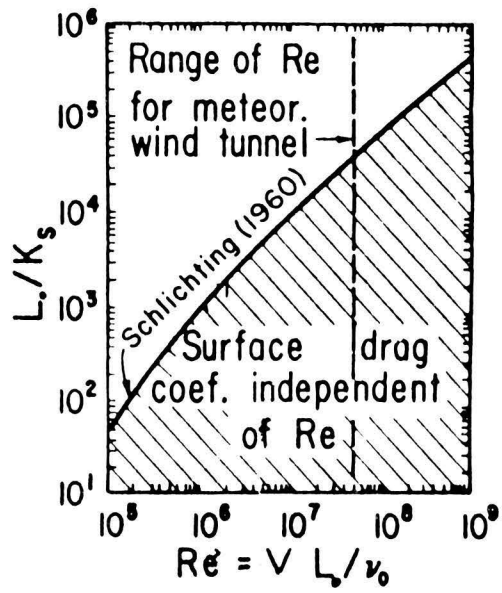
Figure 2.1.   Reynolds Number at Which Flow Becomes Independent
of Reynolds Number for Prescribed Relative Roughness
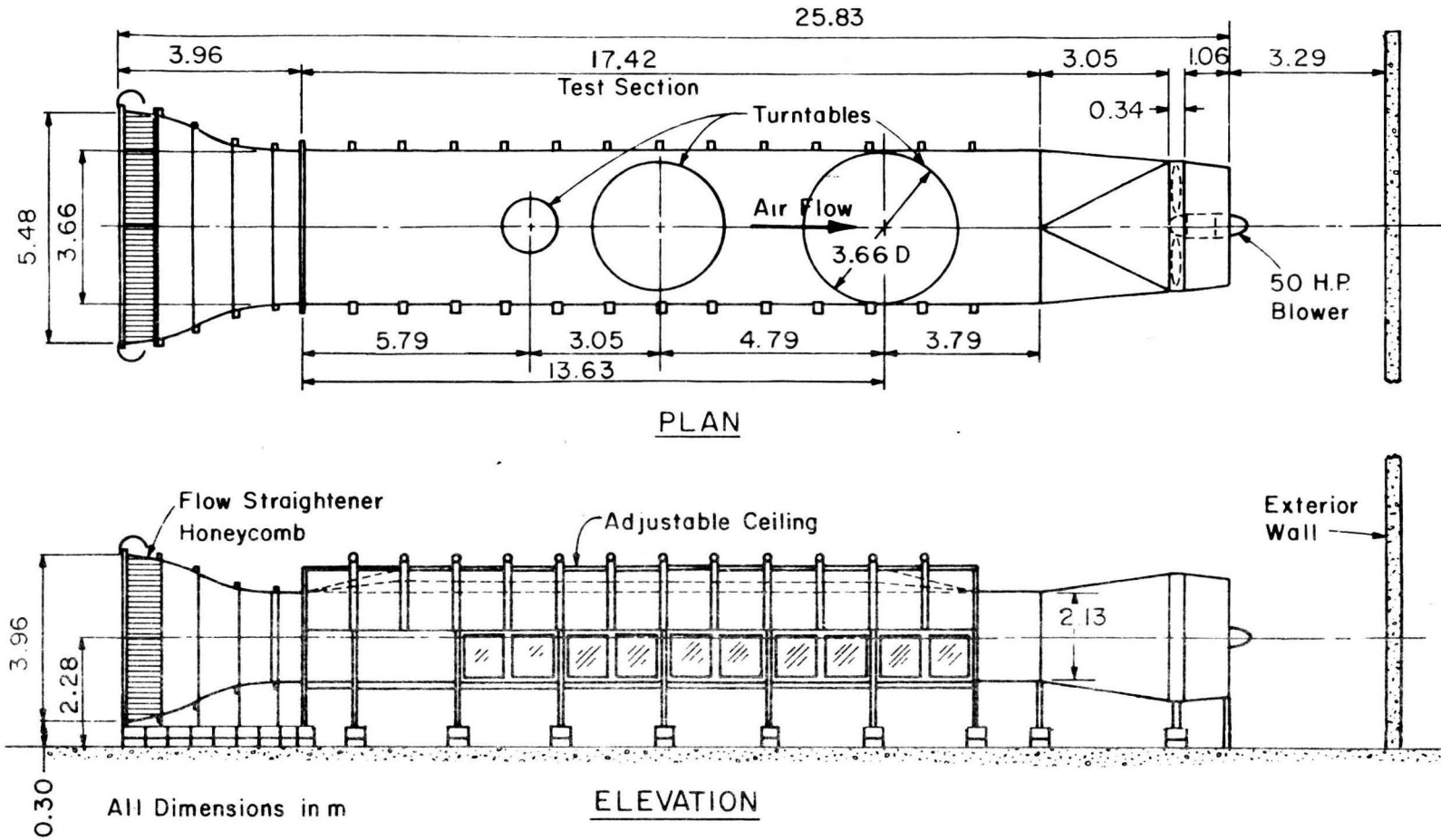
Figure 3.1. Environmental Wind Tunnel

FLUID DYNAMICS & DIFFUSION LABORATORY
COLORADO STATE UNIVERSITY

45
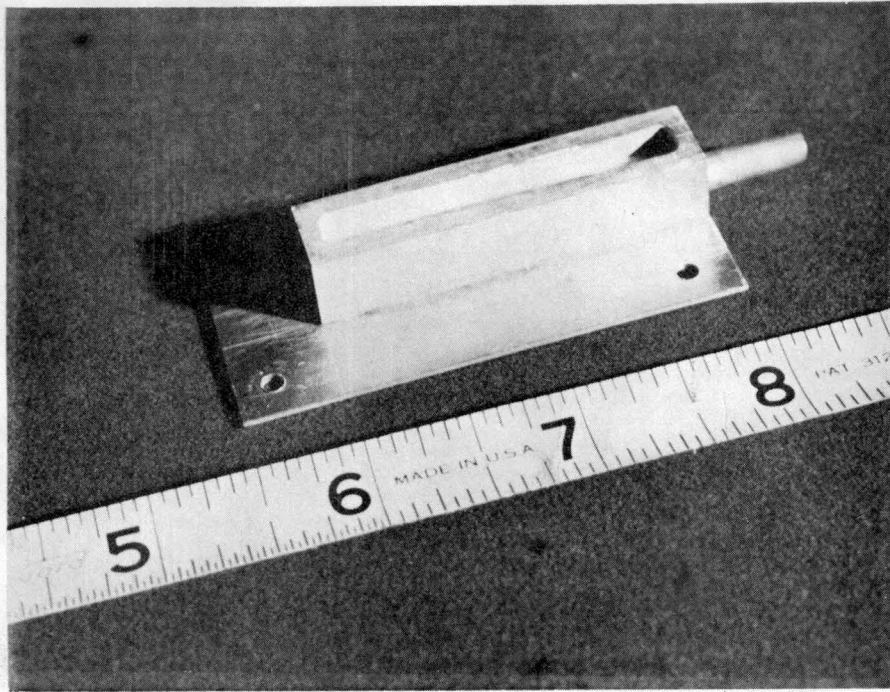
Figure 3.2-1 Photograph of Cooling Tower Model (Scale 1:1920)

Figure 3.2-2 Photograph of Terrain Model in the Environmental
Wind Tunnel

Cooling Tower

Wind Tunnel Floor

Flow meter

Valve

Pump

TiCl$_4$

Mixing Chamber

Block Diagram for
Smoke Visualization Technique
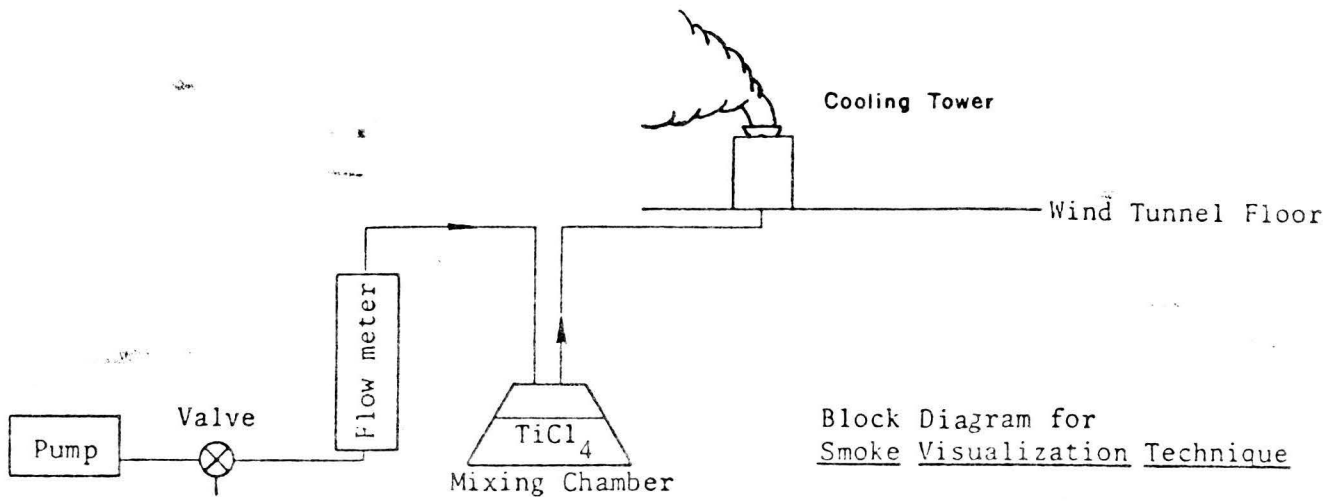
Figure 3.3-1.   Schematic of plume visualization equipment.

Samples from Wind Tunnel

Gas
Chromatograph
with
FID

Sample

Collapsable
Polyethylene
Partitions

Collector
Bottles

Air

Connector

⊗ Valves
—— Tubing
——▶ Flow Direction During Sampling
--▶- Flow Direction During Transfer

Vacuum
Pump
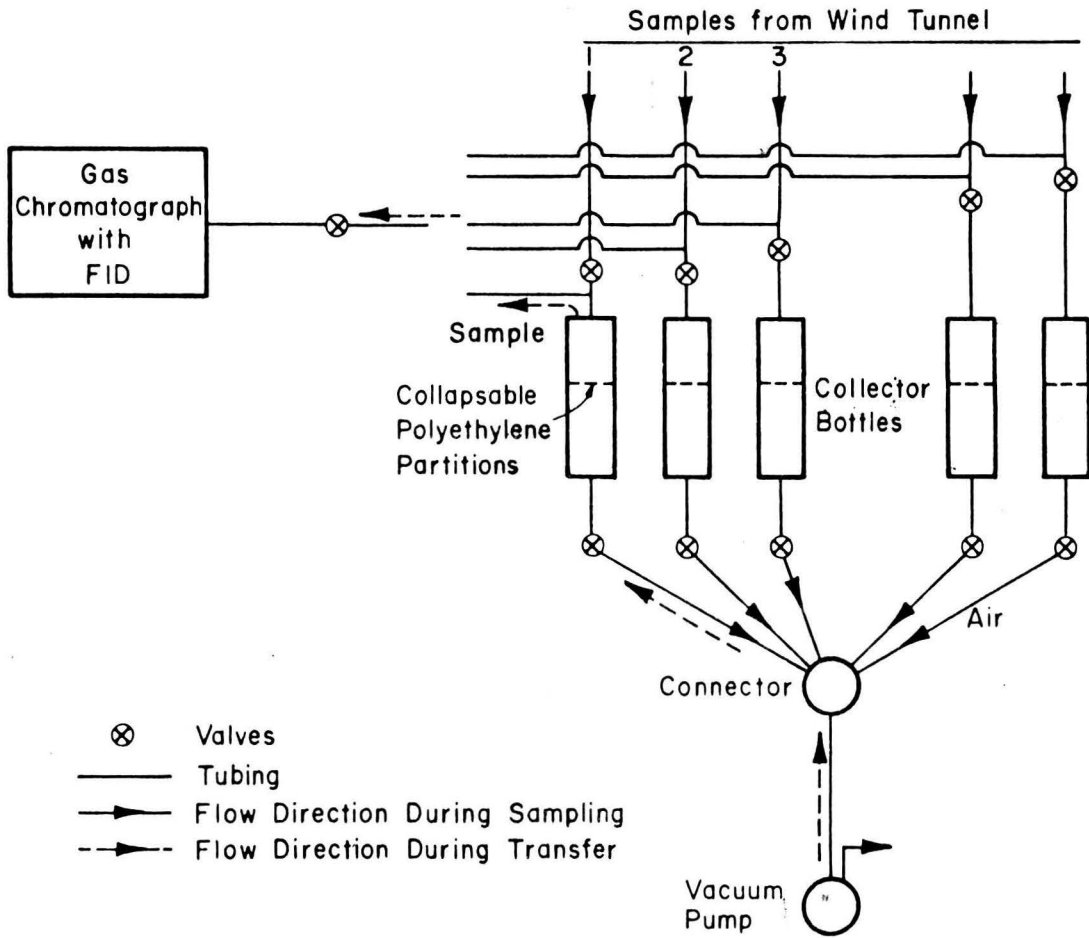
Figure 3.4-1. Schematic of tracer gas sampling system.

$$V\,[m/s] = 0.536\ E\,[V] + 0.064$$
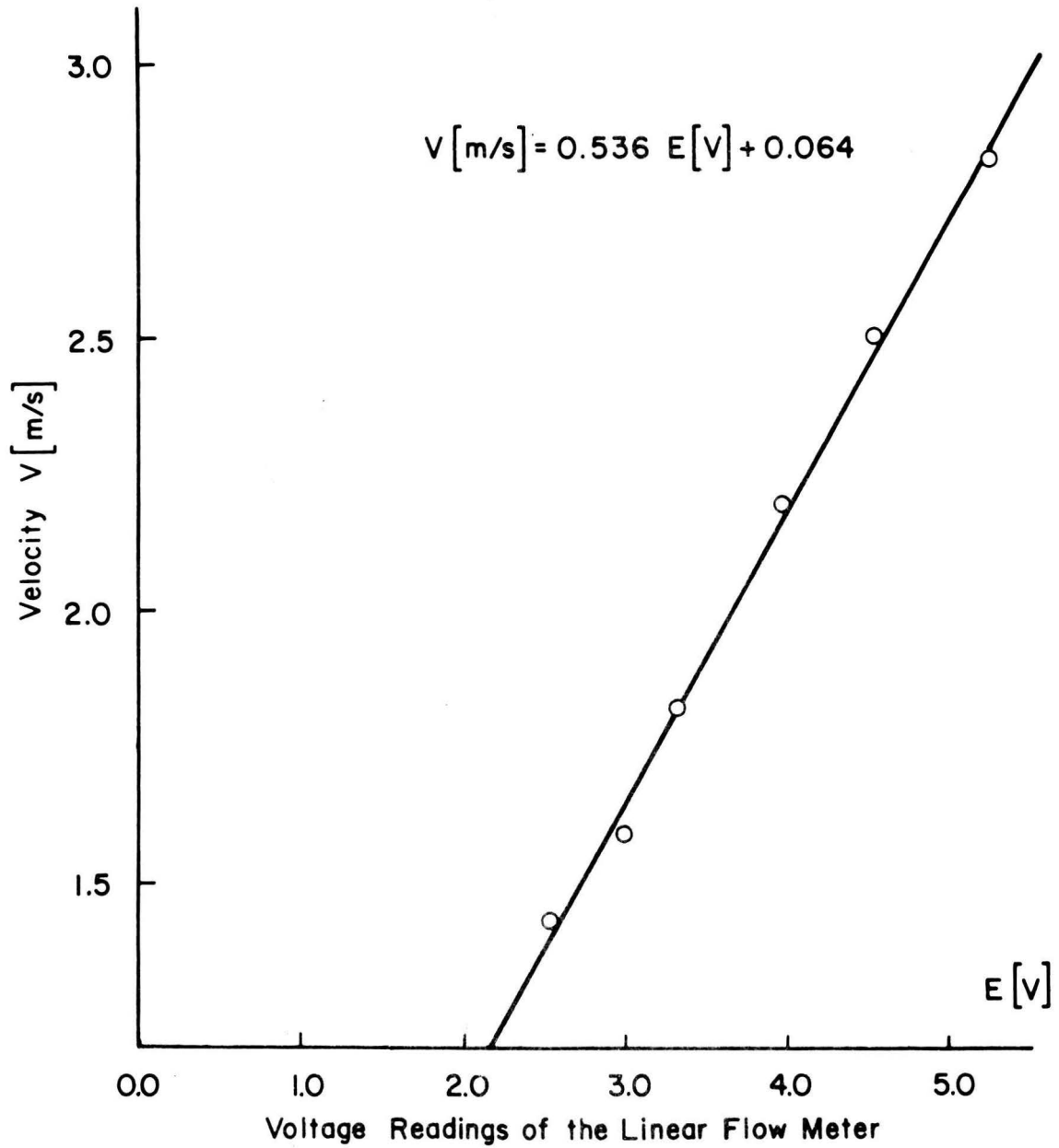
Figure 3.5-1.   Calibration Curve for Datametrics Linear Flow Meter
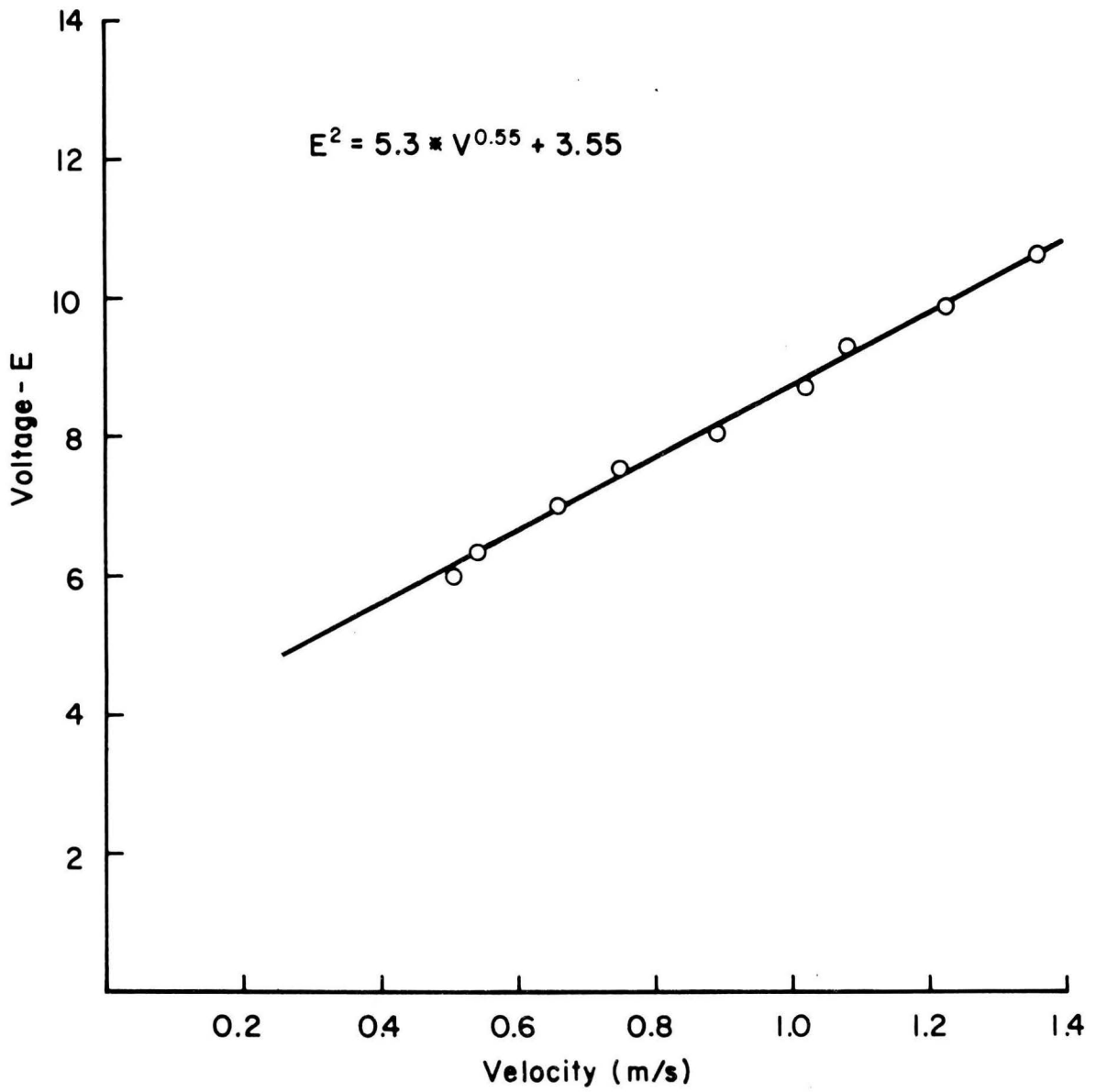
Figure 3.5-2.   Calibration Curve for the TSI Hot-Wire Anemometer

(a)

(b)

(c)
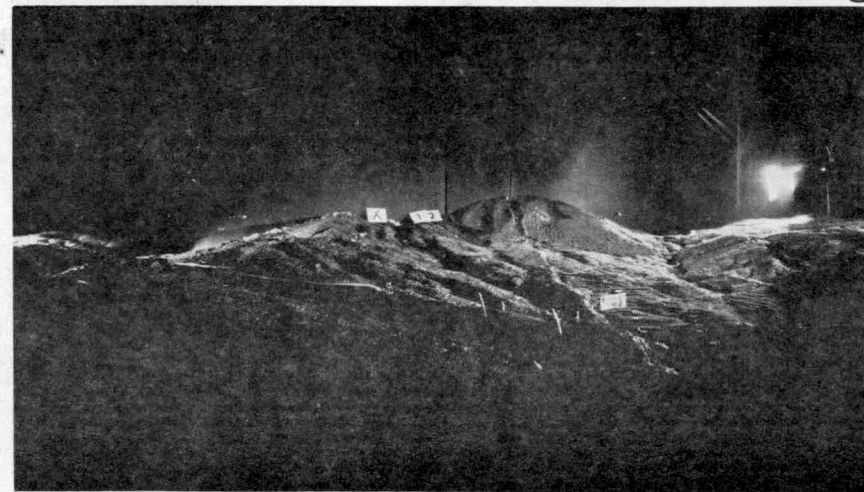
(d)

Figure 4.1-1. Plume visualization for Unit 18, Site X for 210° wind direction and wind speeds of a) 3.1, b) 4.5, c) 8.9 and d) 11.6 m/s.
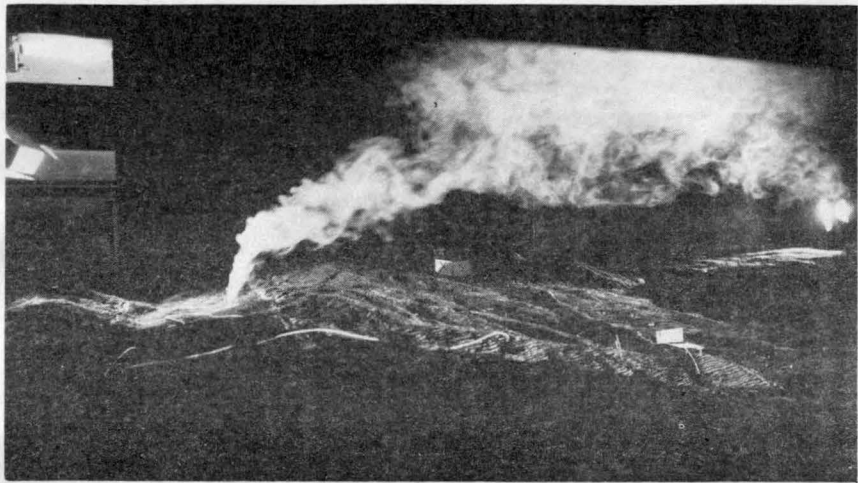
(a)
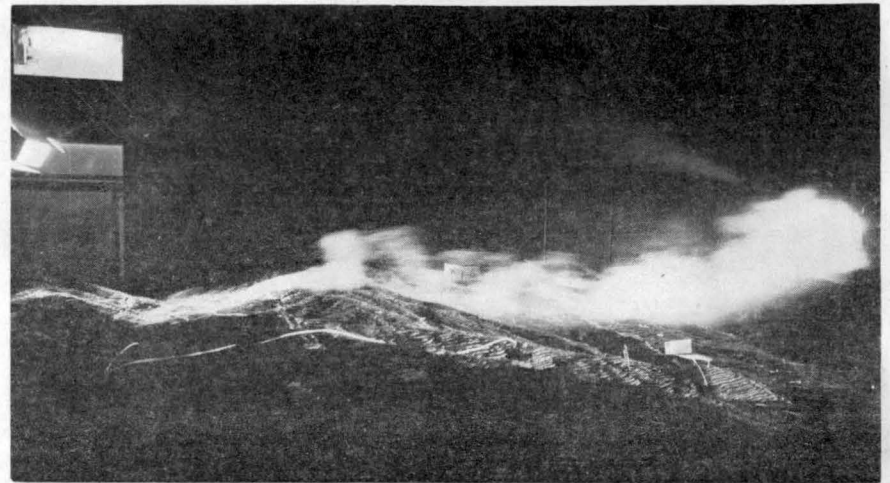
(b)
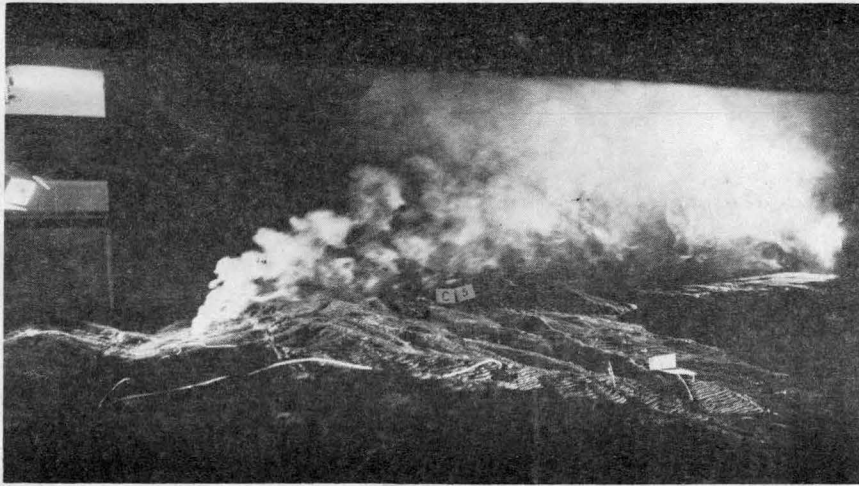
(c)
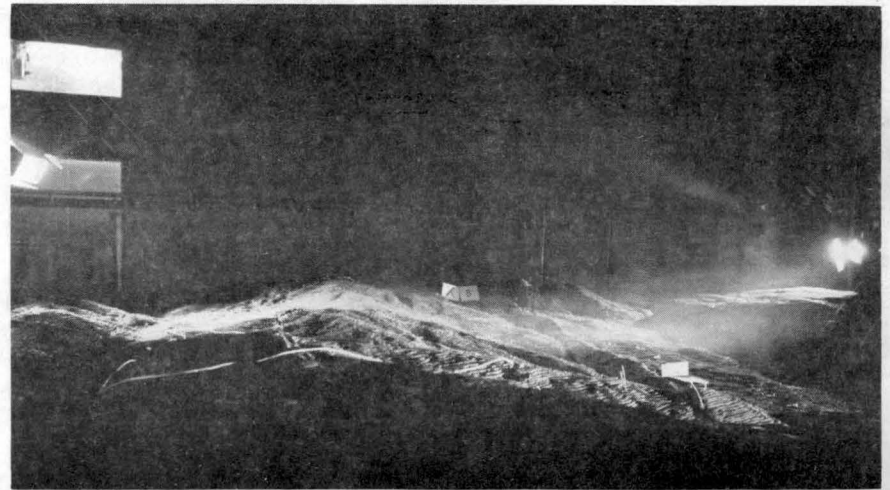
(d)

Figure 4.1-2. Plume visualization for Unit 18, Site X for 230° wind direction and wind speeds of
a) 3.1, b) 4.5, c) 8.9 and d) 11.6 m/s.
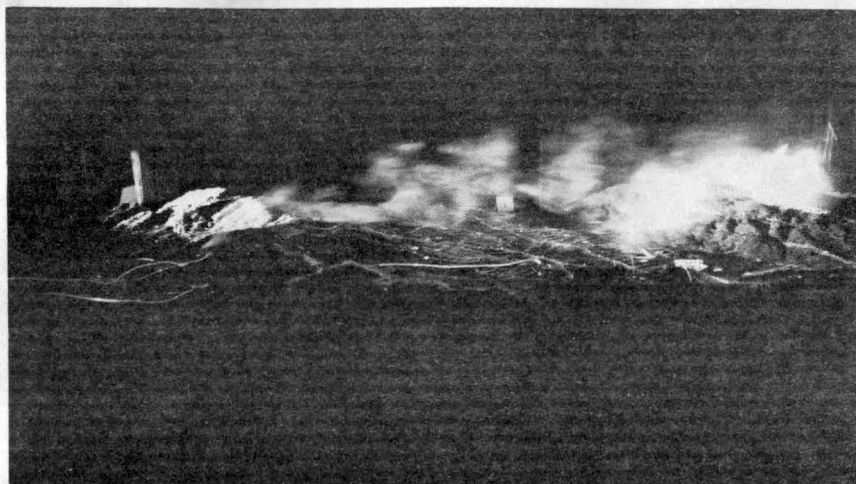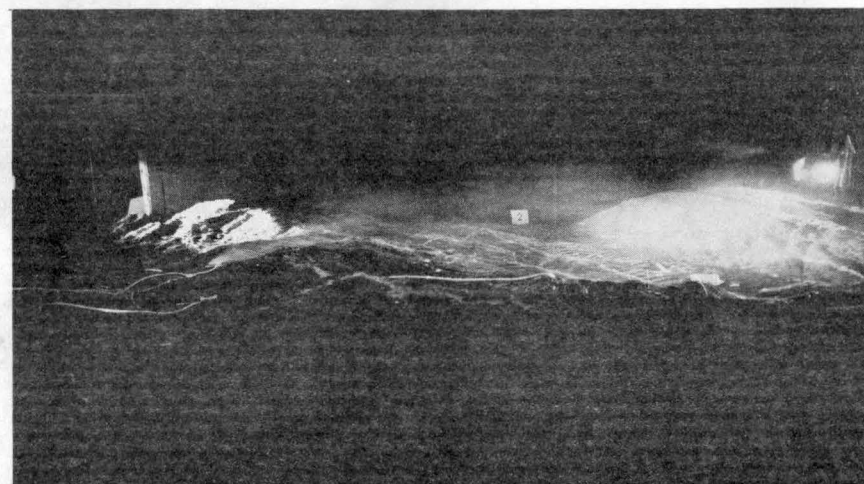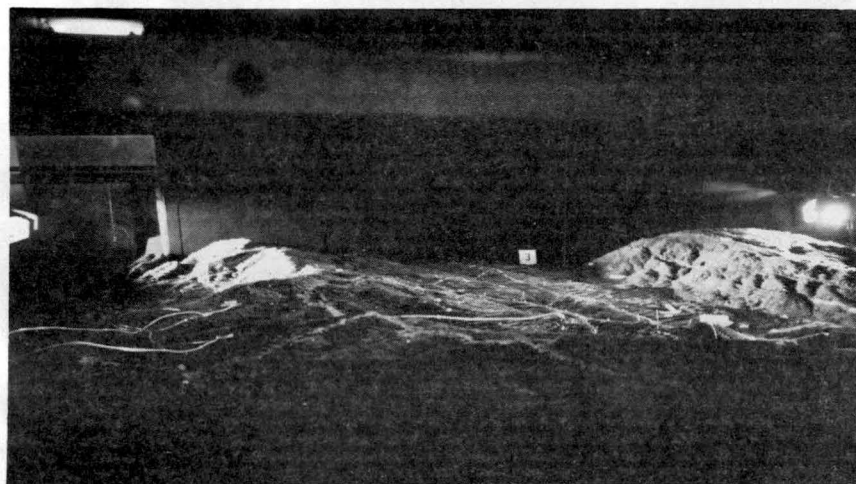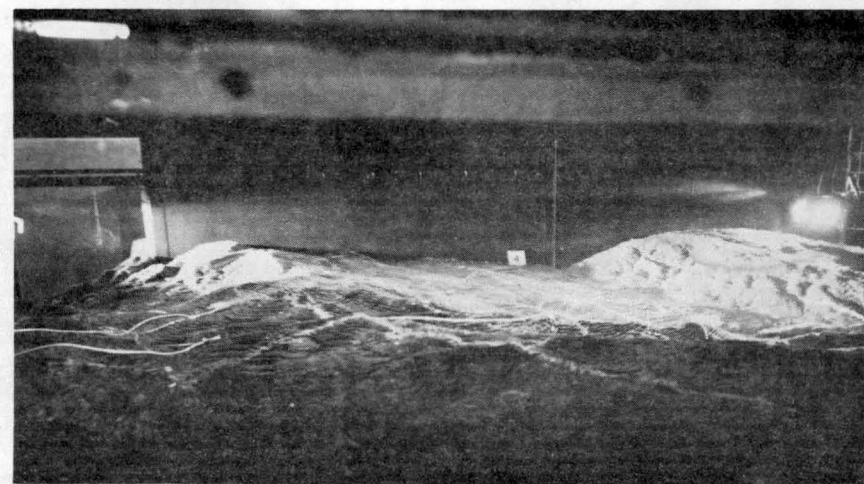
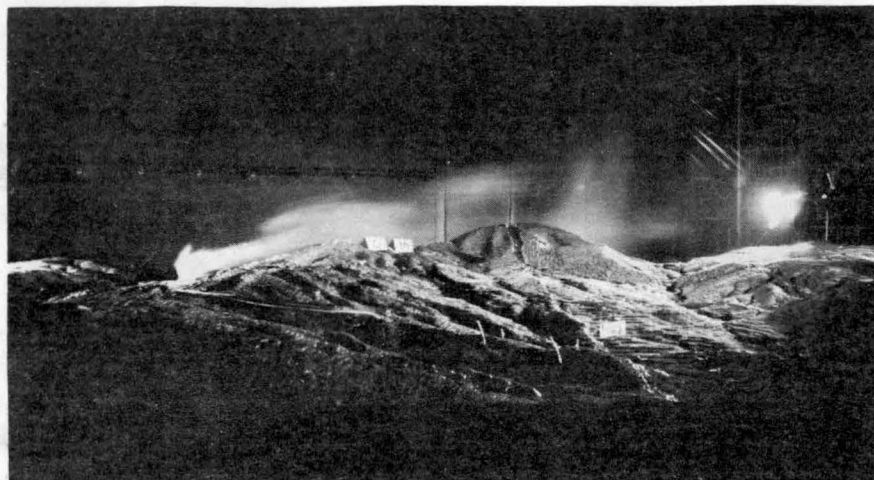Figure 4.1-3. Plume visualization for Unit 18, Site X for 250° wind direction and wind speeds of a) 3.1, b) 4.5, c) 8.9 and d) 11.6 m/s.
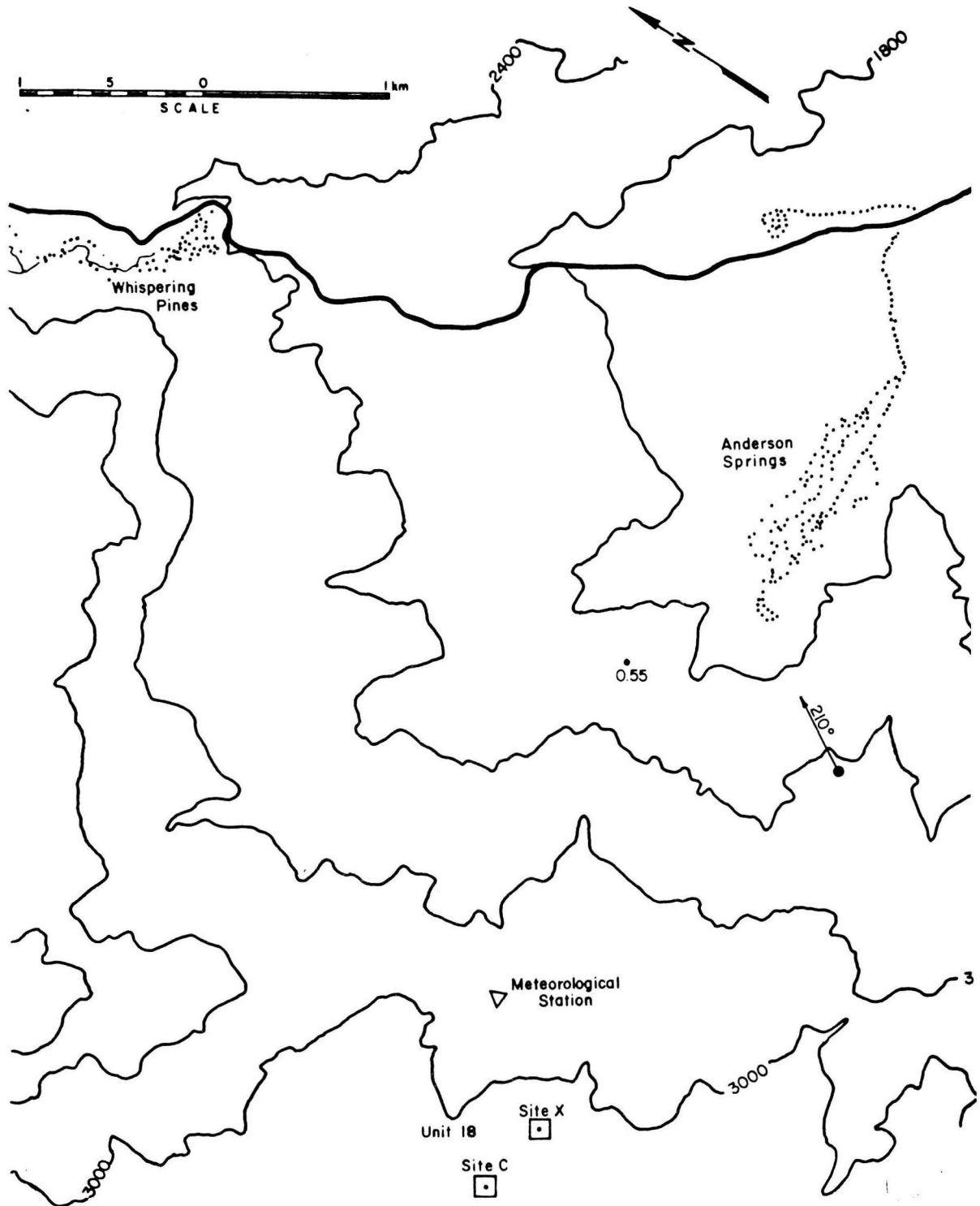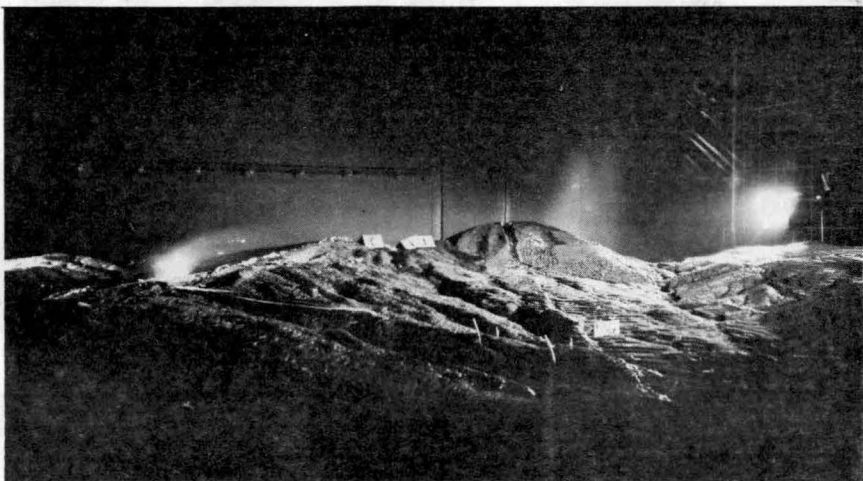
Figure 4.2-1a. Isopleths (x 10^5) of nondimensional concentration coefficient K for Unit 18, Site X, a 210° wind direction, and wind speeds of a) 3.1, b) 4.5, c) 8.9 and d) 11.6 m/s.
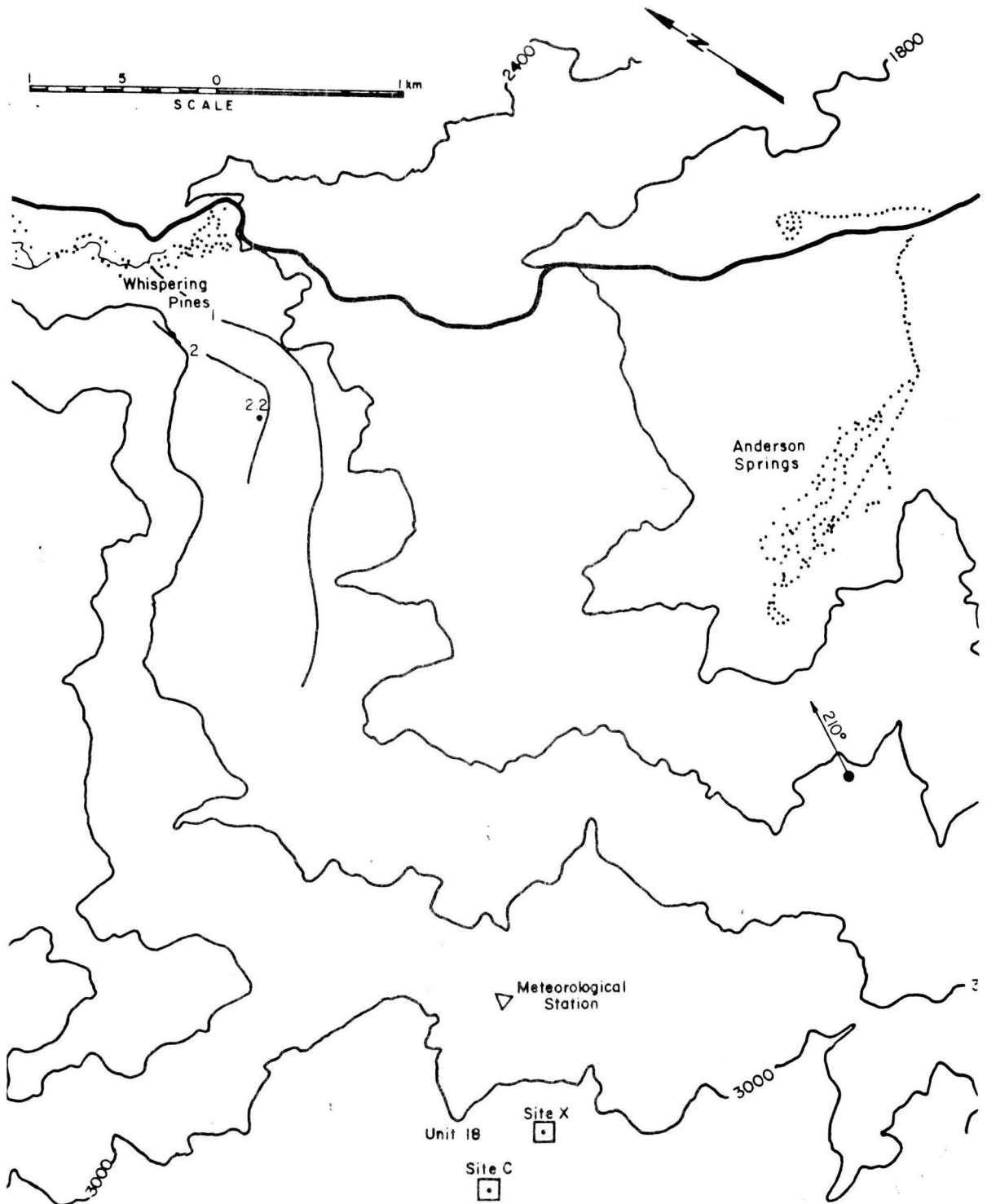
Figure 4.2-1b. Isopleths (x 10^5) of nondimensional concentration coefficient K for Unit 18, Site X, a 210° wind direction and wind speeds of a) 3.1, b) 4.5, c) 8.9 and d) 11.6 m/s.
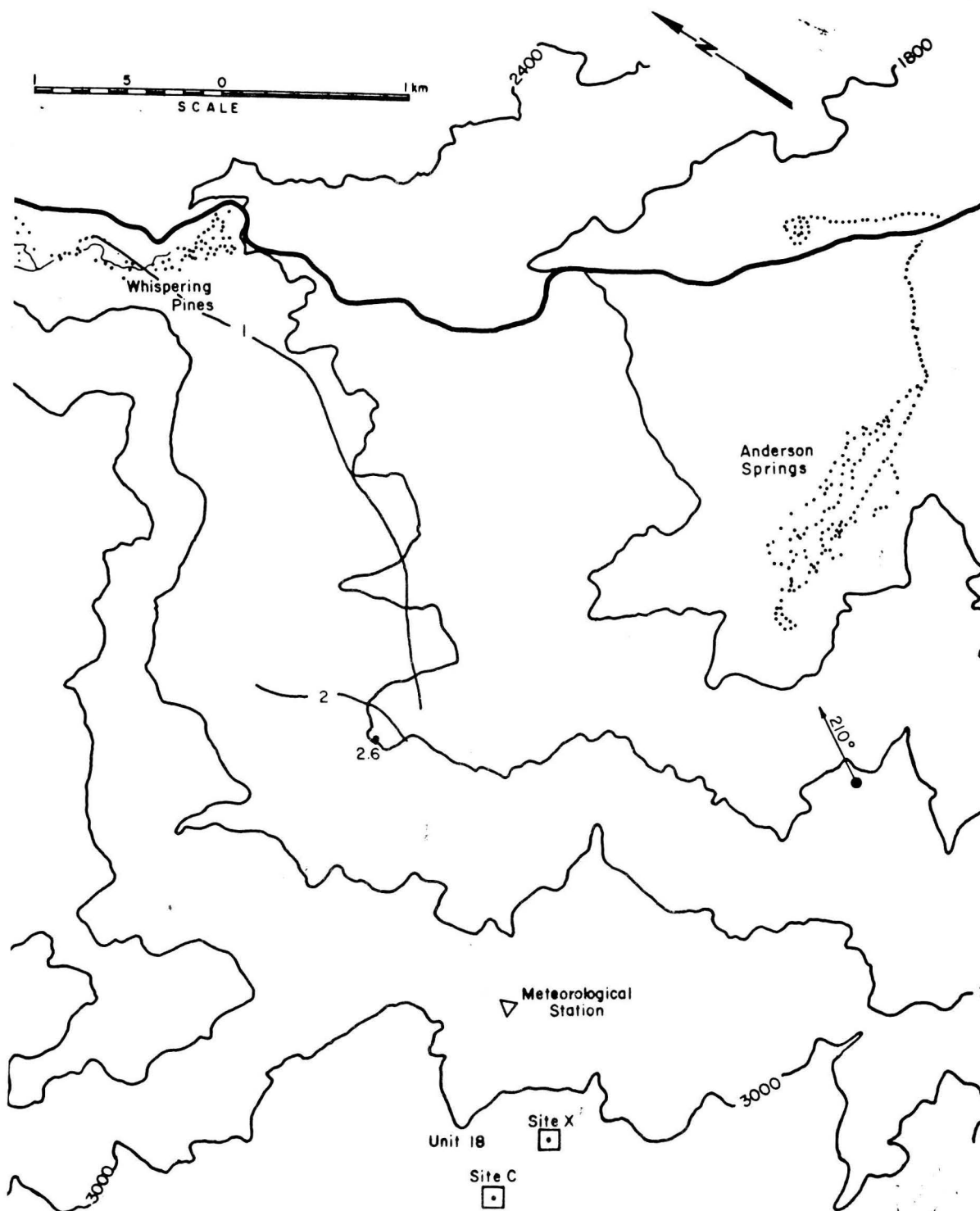
Figure 4.2-1c. Isopleths (x 10^5) of nondimensional concentration coefficient K for Unit 18, Site X, a 210° wind direction and wind speeds of a) 3.1, b) 4.5, c) 8.9 and d) 11.6 m/s.
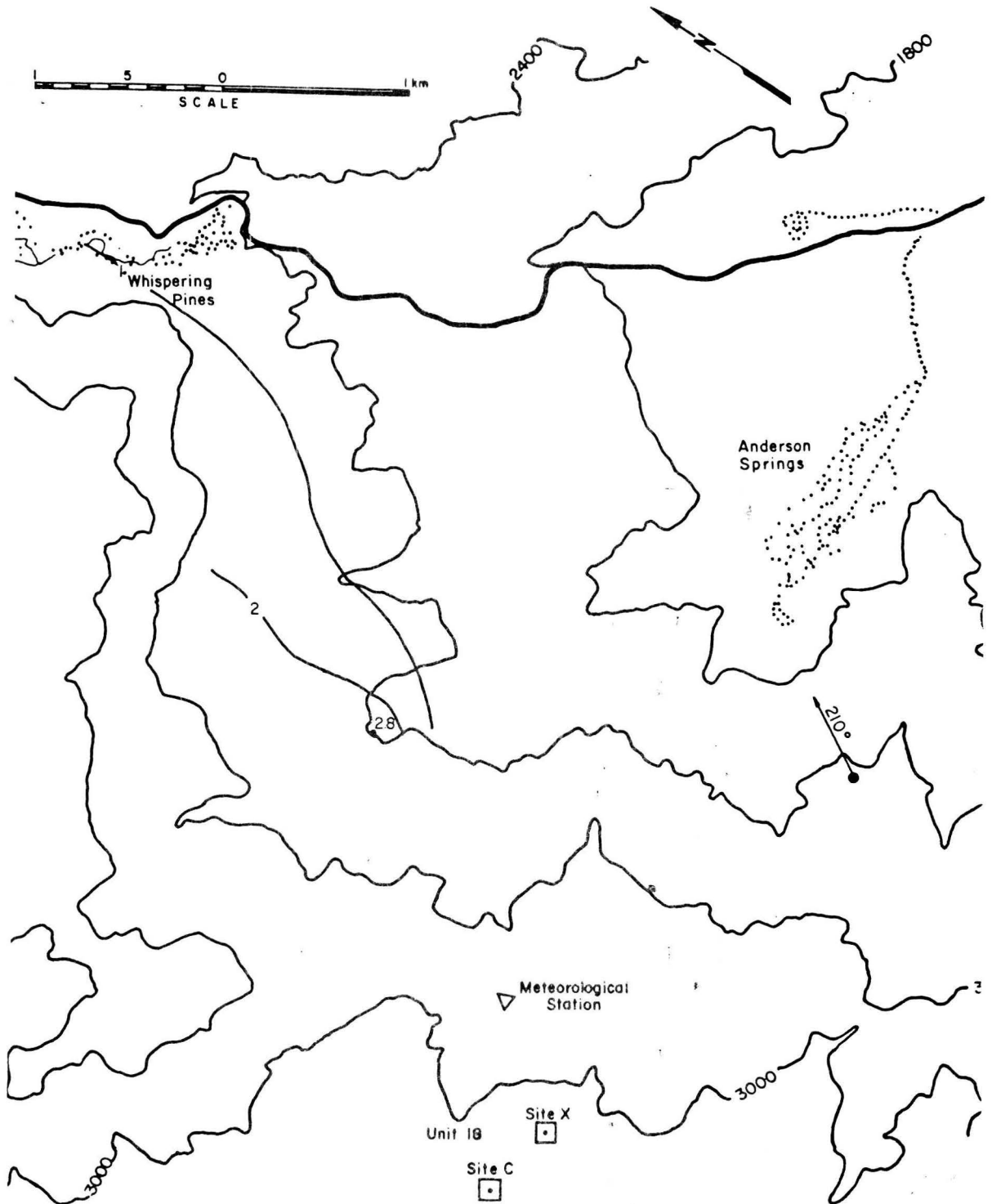
Figure 4.2-1d. Isopleths (x 10^5) of nondimensional concentration coefficient K for Unit 18, Site X, a 210° wind direction and wind speeds of a) 3.1, b) 4.5, c) 8.9 and d) 11.6 m/s.
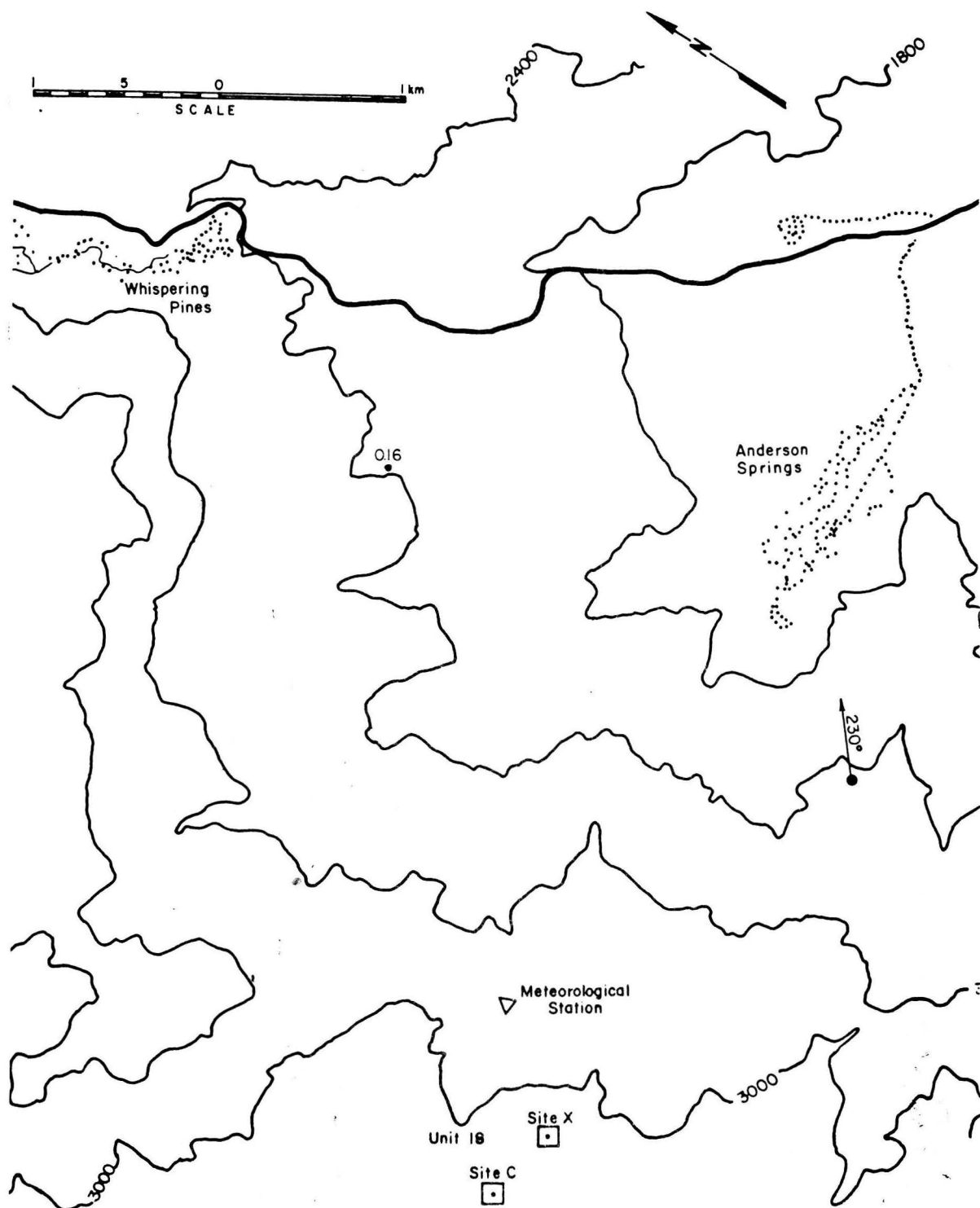
Figure 4.2-2a. Isopleths (x 10^5) of nondimensional concentration coefficient K for Unit 18, Site X, a 230° wind direction and wind speeds of a) 3.1, b) 4.5, c) 8.9 and d) 11.6 m/s.
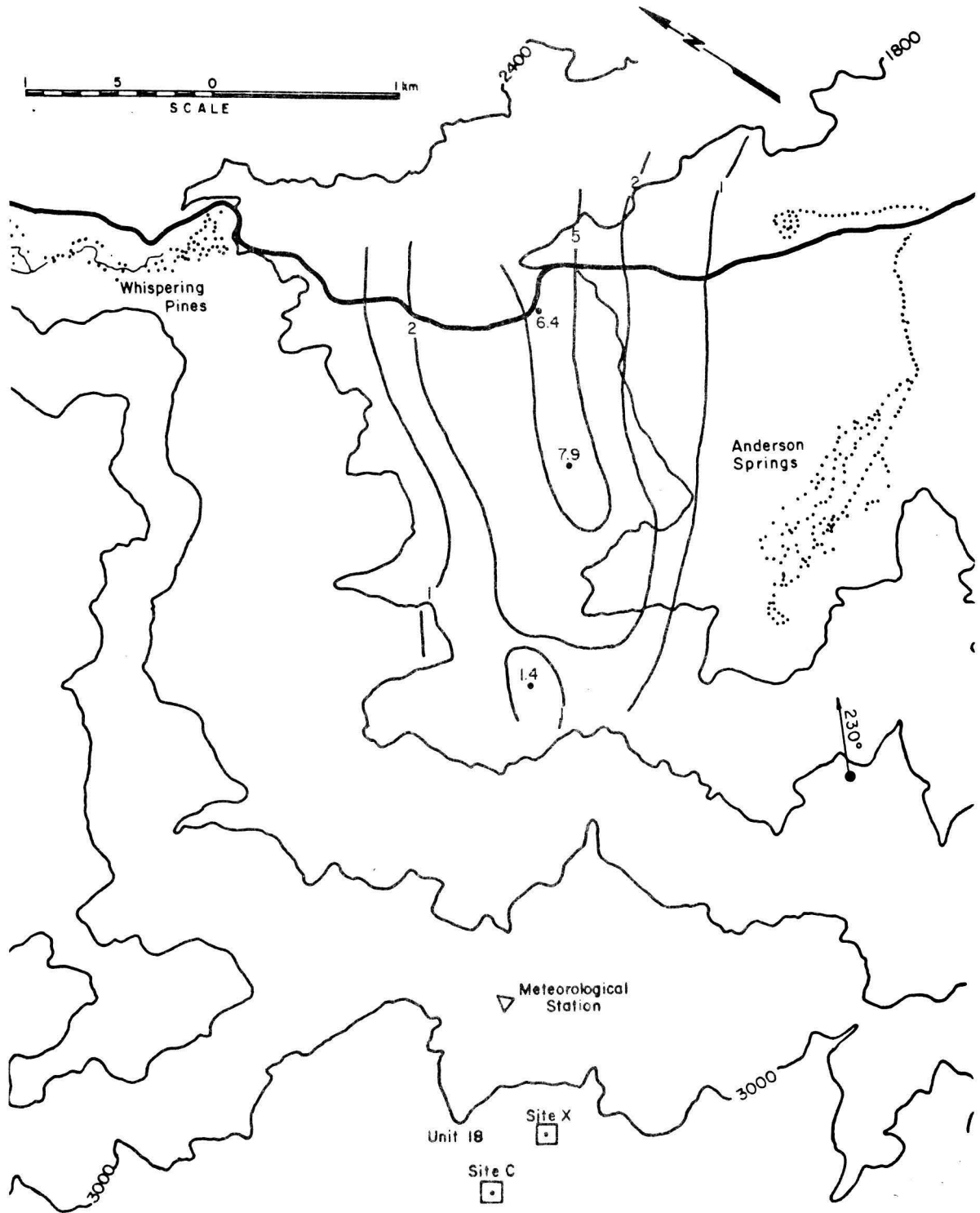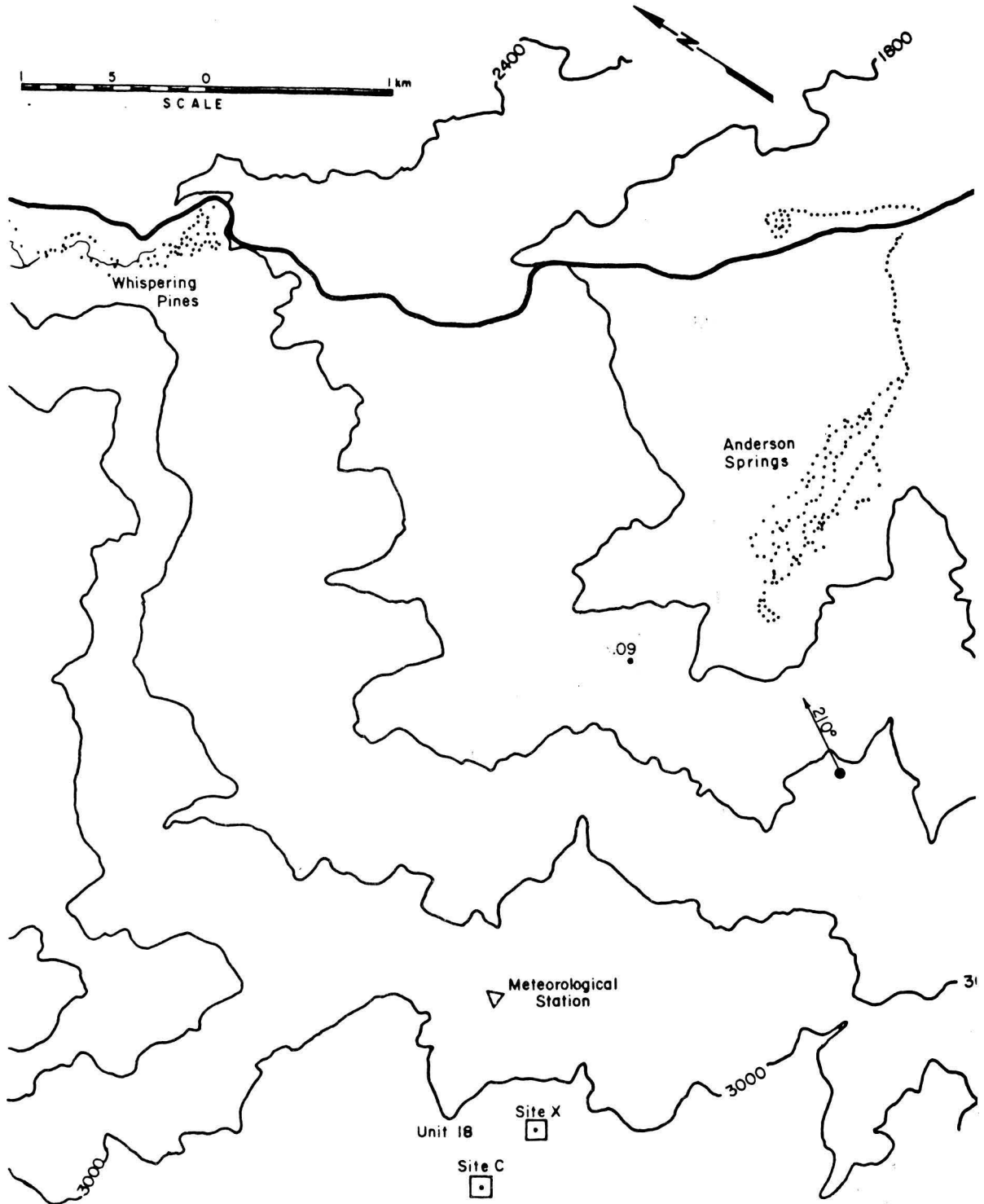
Figure 4.2-2b. Isopleths (x 10^5) of nondimensional concentration coefficient K for Unit 18, Site X, a 230° wind direction and wind speeds of a) 3.1, b) 4.5, c) 8.9 and d) 11.6 m/s.
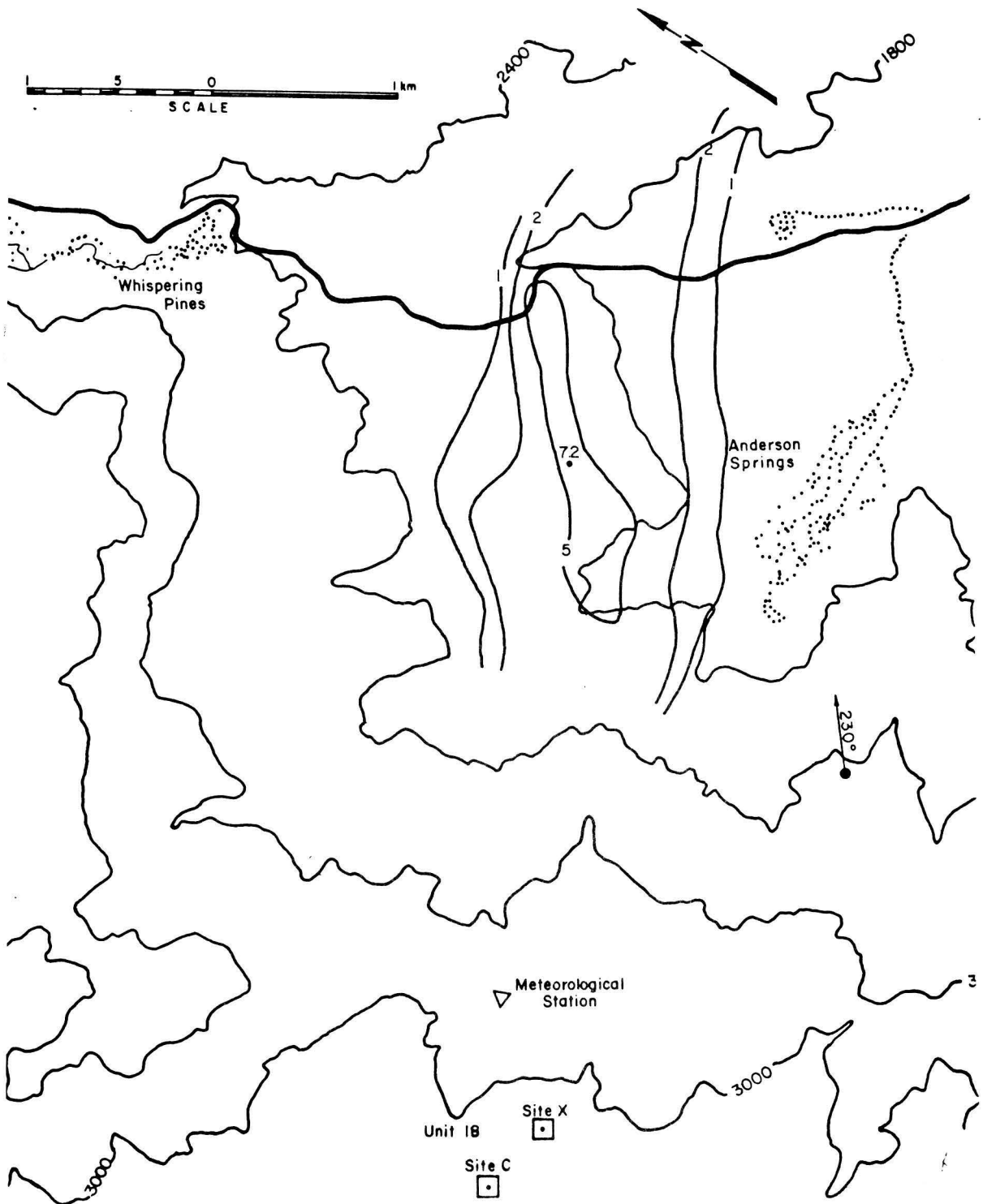
Figure 4.2-2c. Isopleths (x 10^5) of nondimensional concentration coefficient K for Unit 18, Site X, a 230° wind direction and wind speeds of a) 3.1, b) 4.5, c) 8.9 and d) 11.6 m/s.
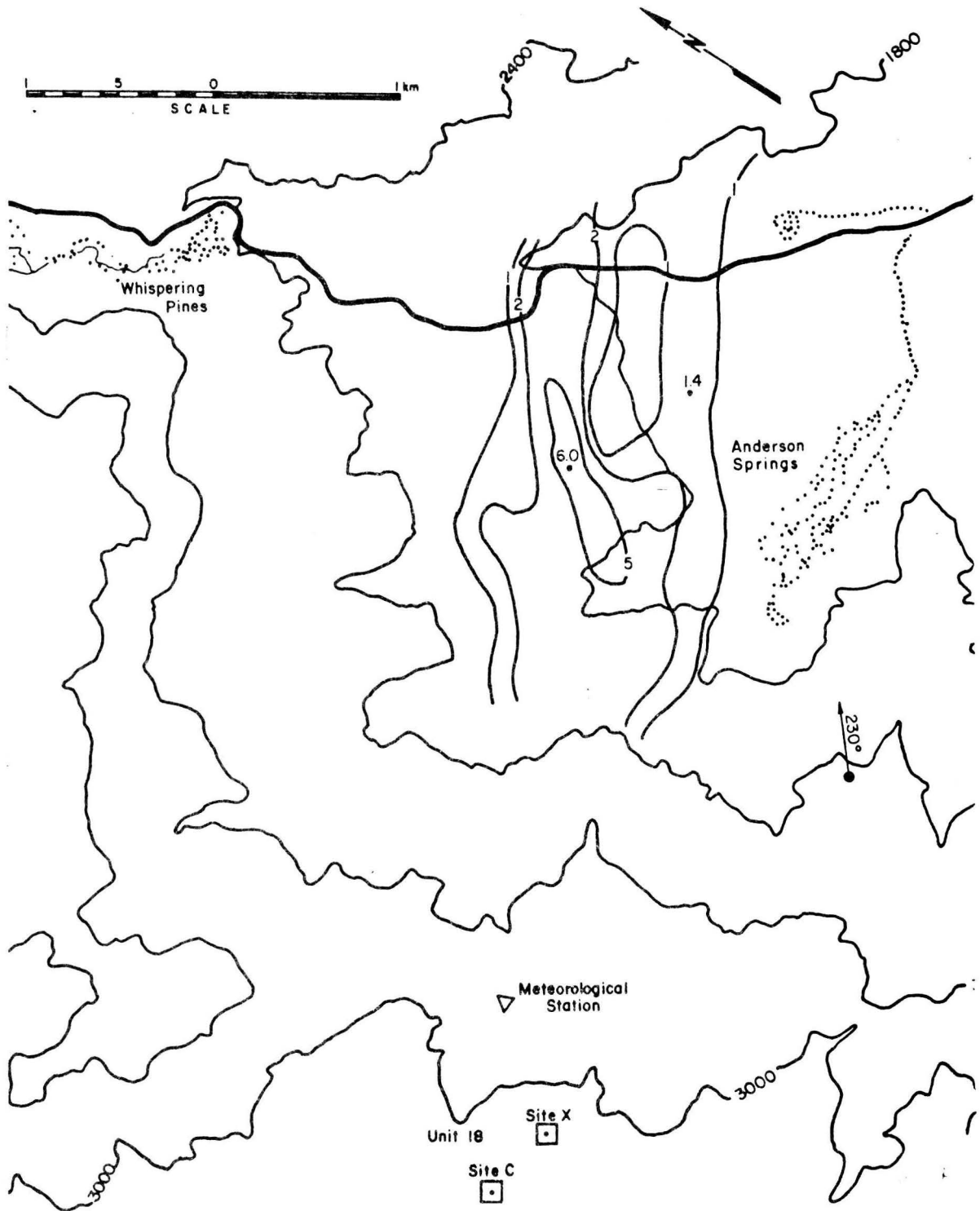
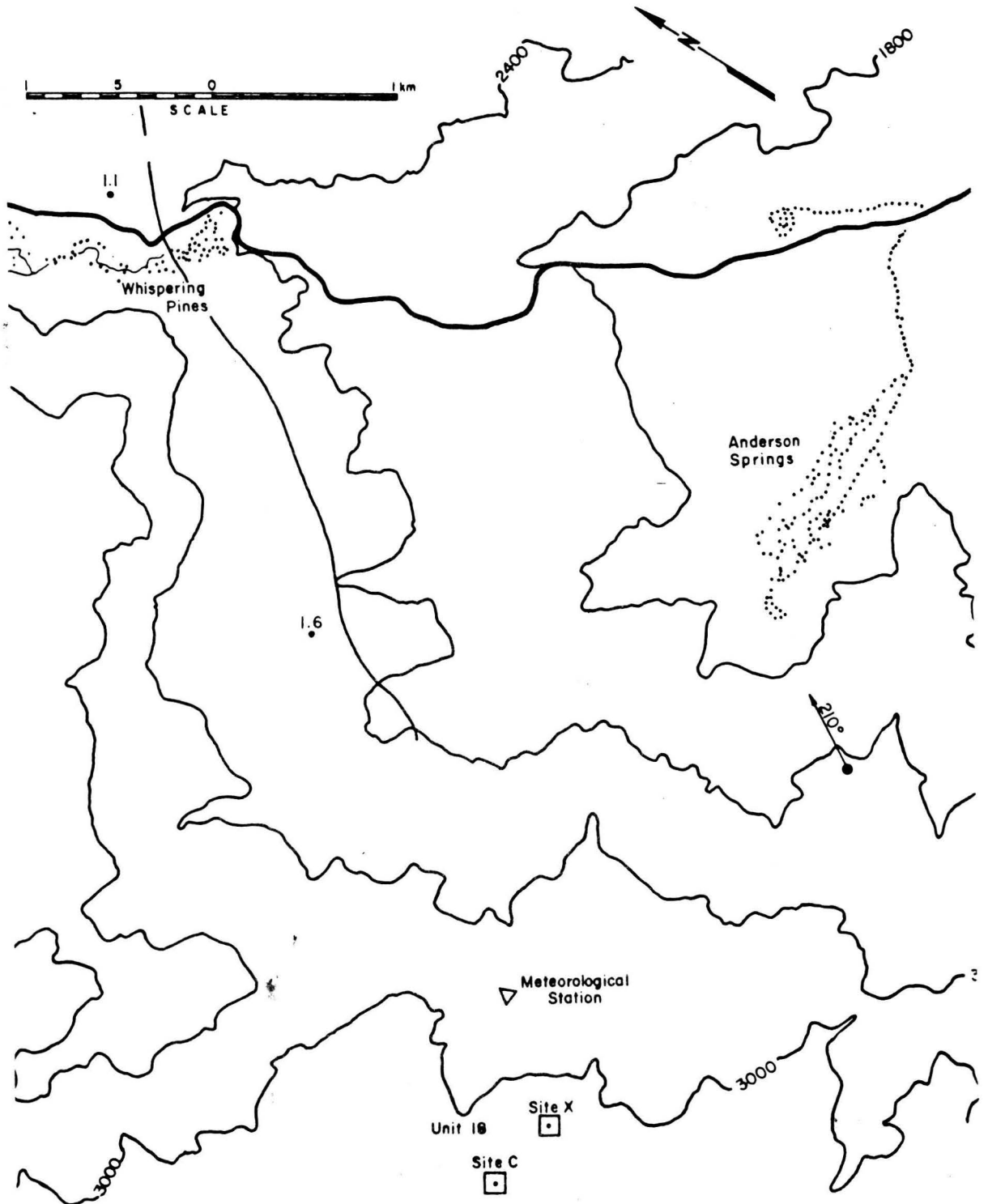Figure 4.2-2d. Isopleths (x 10^5) of nondimensional concentration
coefficient K for Unit 18, Site X, a 230° wind
direction and wind speeds of a) 3.1, b) 4.5, c) 8.9
and d) 11.6 m/s.
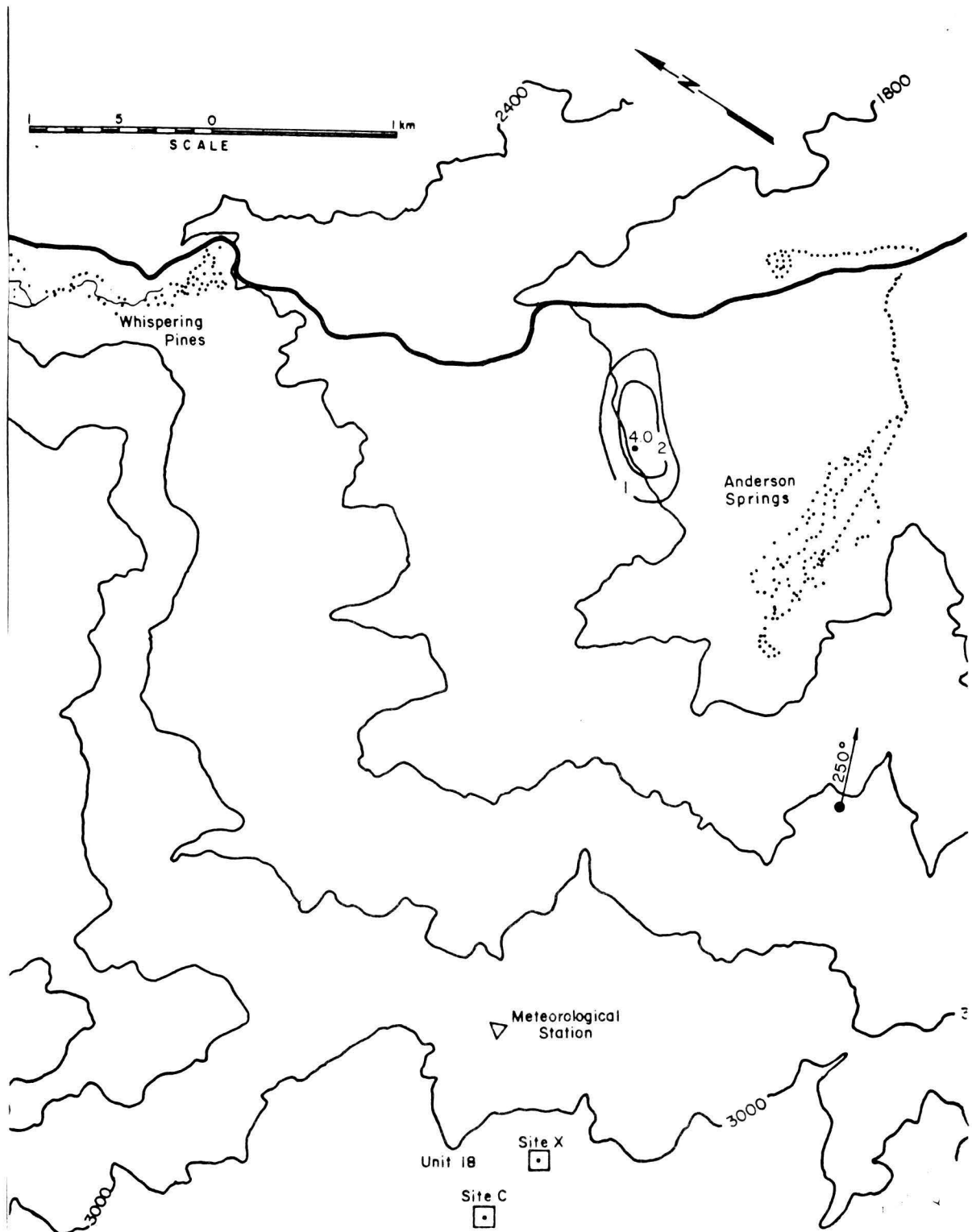
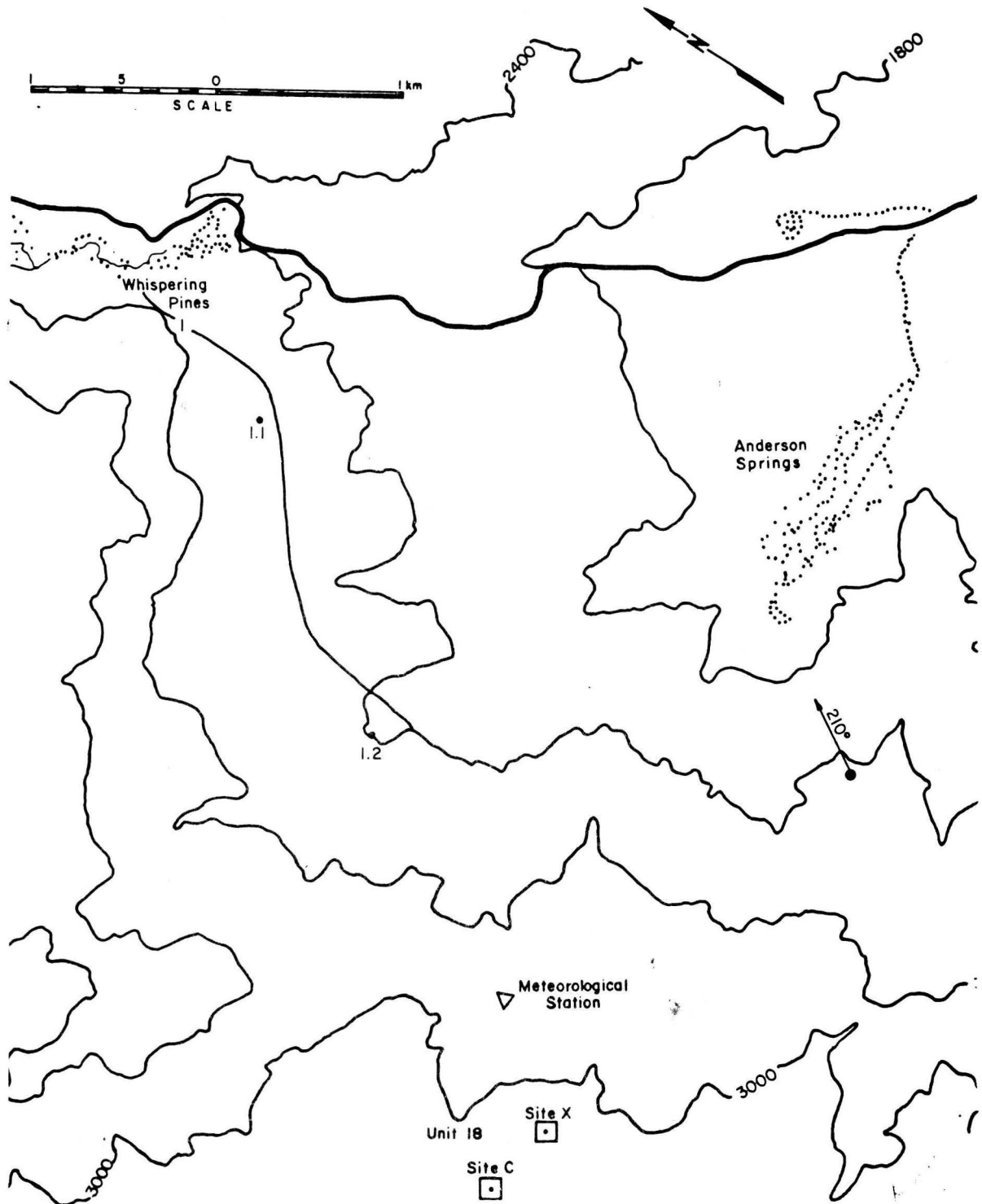Figure 4.2-3a. Isopleths (x 10^5) of nondimensional concentration coefficient K for Unit 18, Site X, a 250° wind direction and wind speeds of a) 3.1, b) 4.5, c) 8.9 and d) 11.6 m/s.
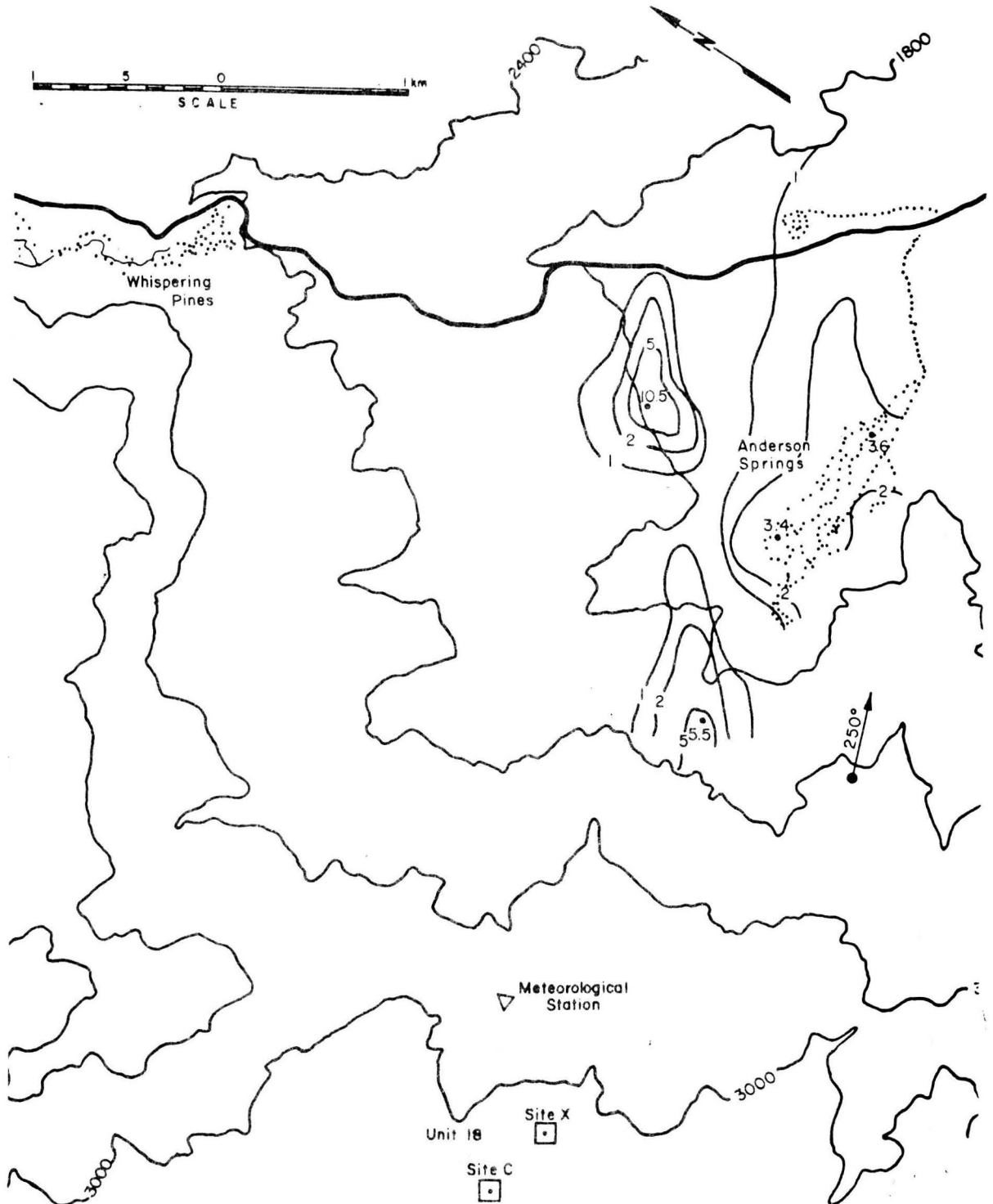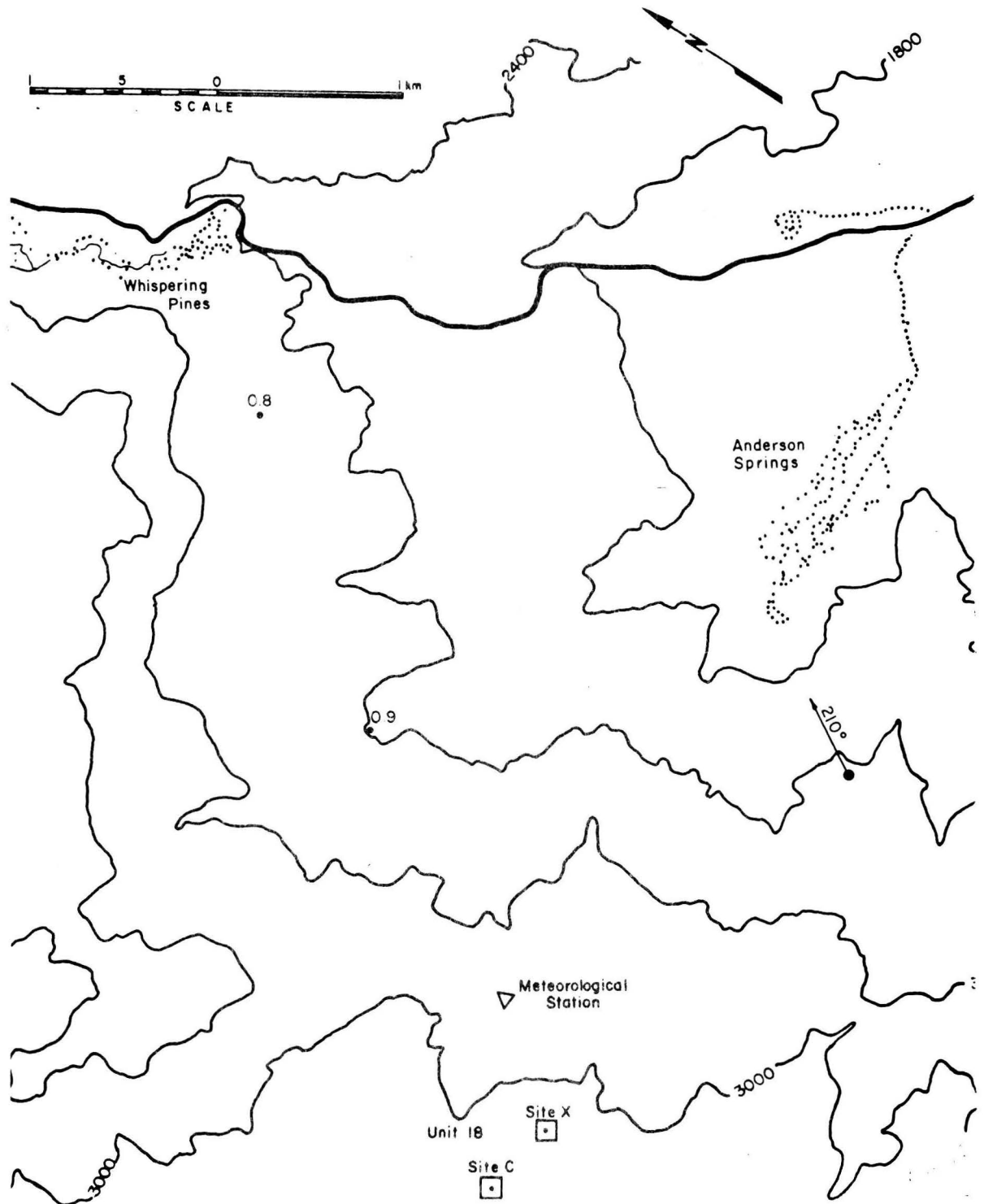
Figure 4.2-3b. Isopleths (x 10^5) of nondimensional concentration coefficient K for Unit 18, Site X, a 250° wind direction and wind speeds of a) 3.1, b) 4.5, c) 8.9 and d) 11.6 m/s.
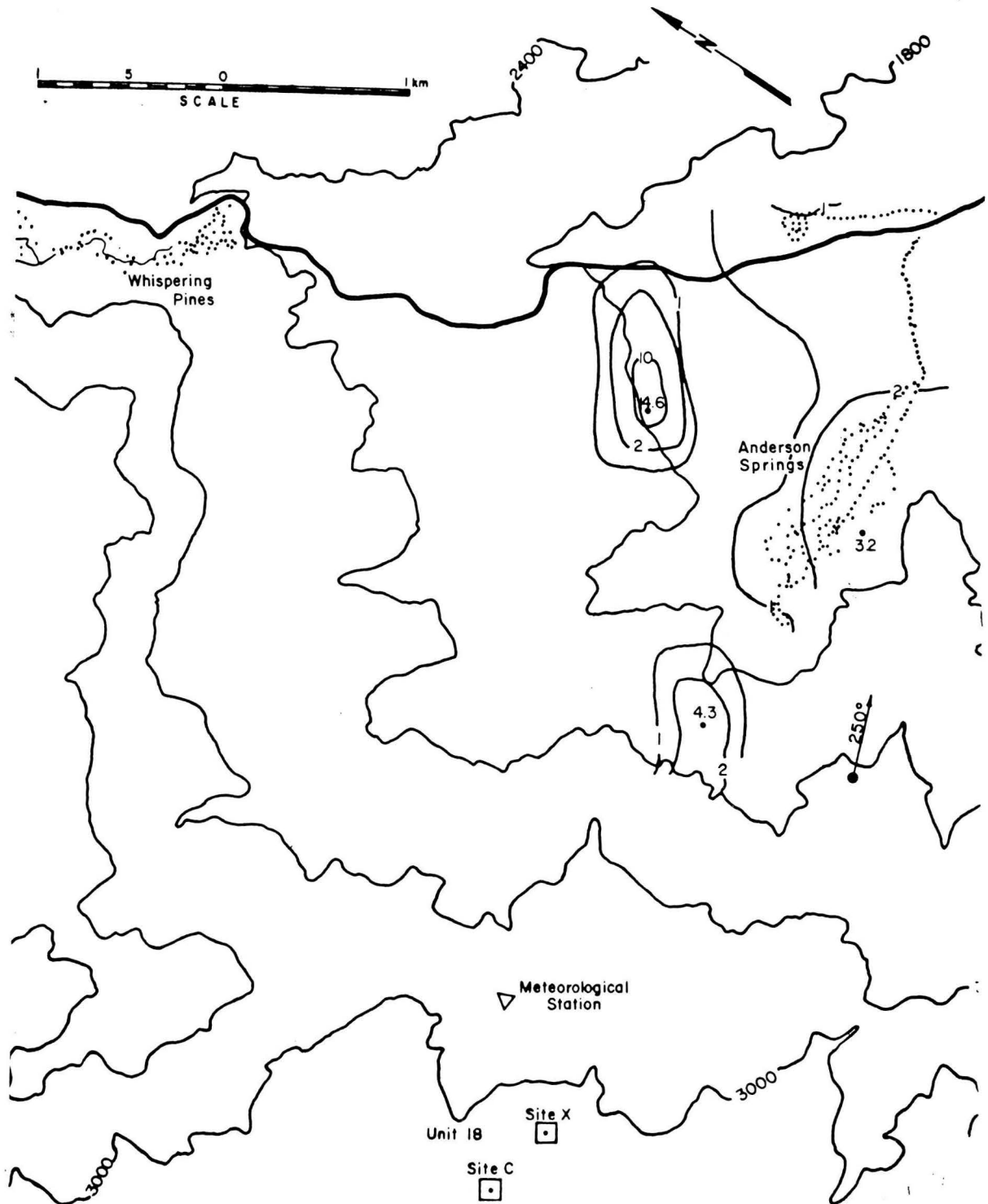
Figure 4.2-3c. Isopleths (x 10^5) of nondimensional concentration coefficient K for Unit 18, Site X, a 250° wind direction and wind speeds of a) 3.1, b) 4.5, c) 8.9 and d) 11.6 m/s.

64
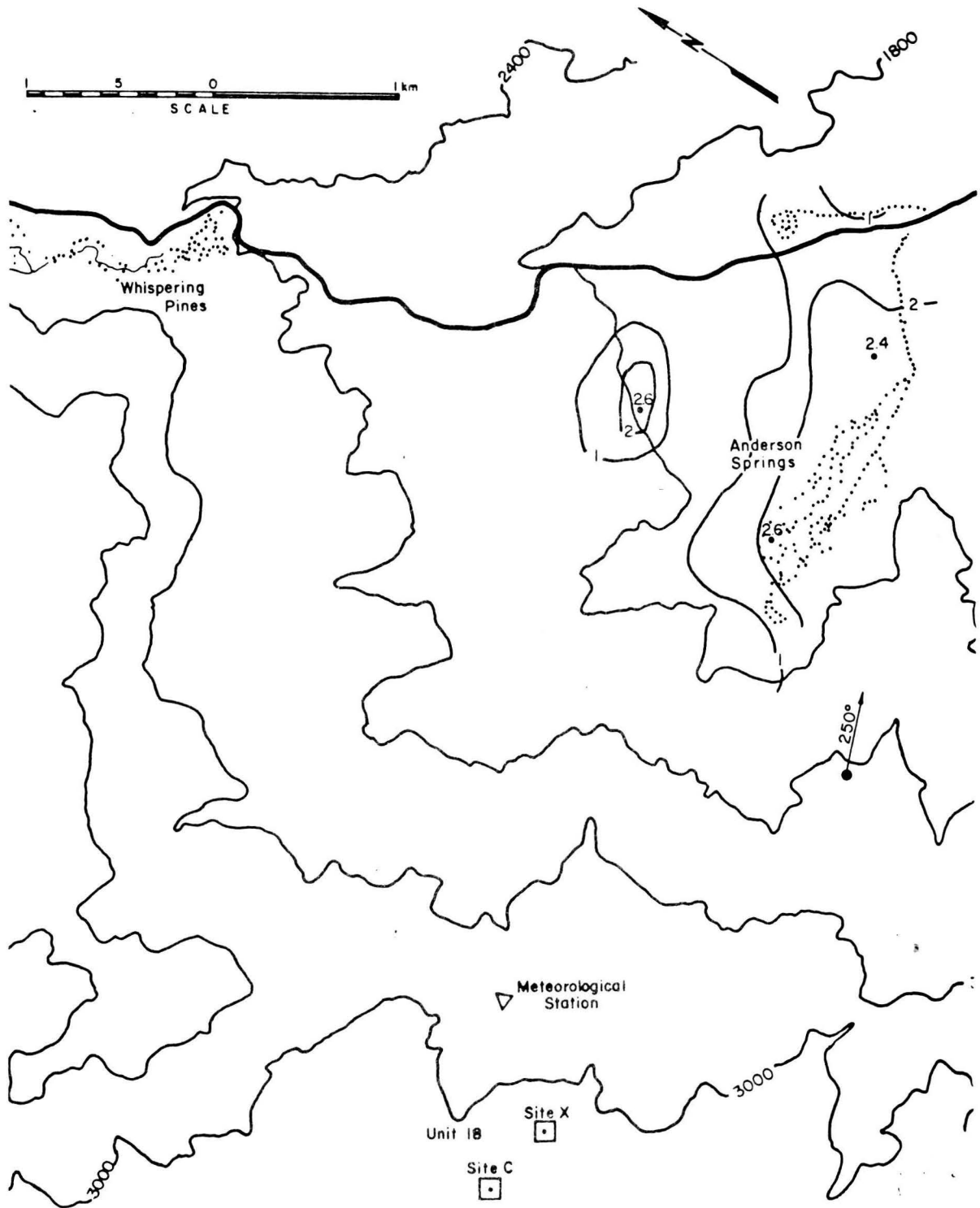
Figure 4.2-3d. Isopleths (x 10^5) of nondimensional concentration
coefficient K for Unit 18, Site X, a 250° wind
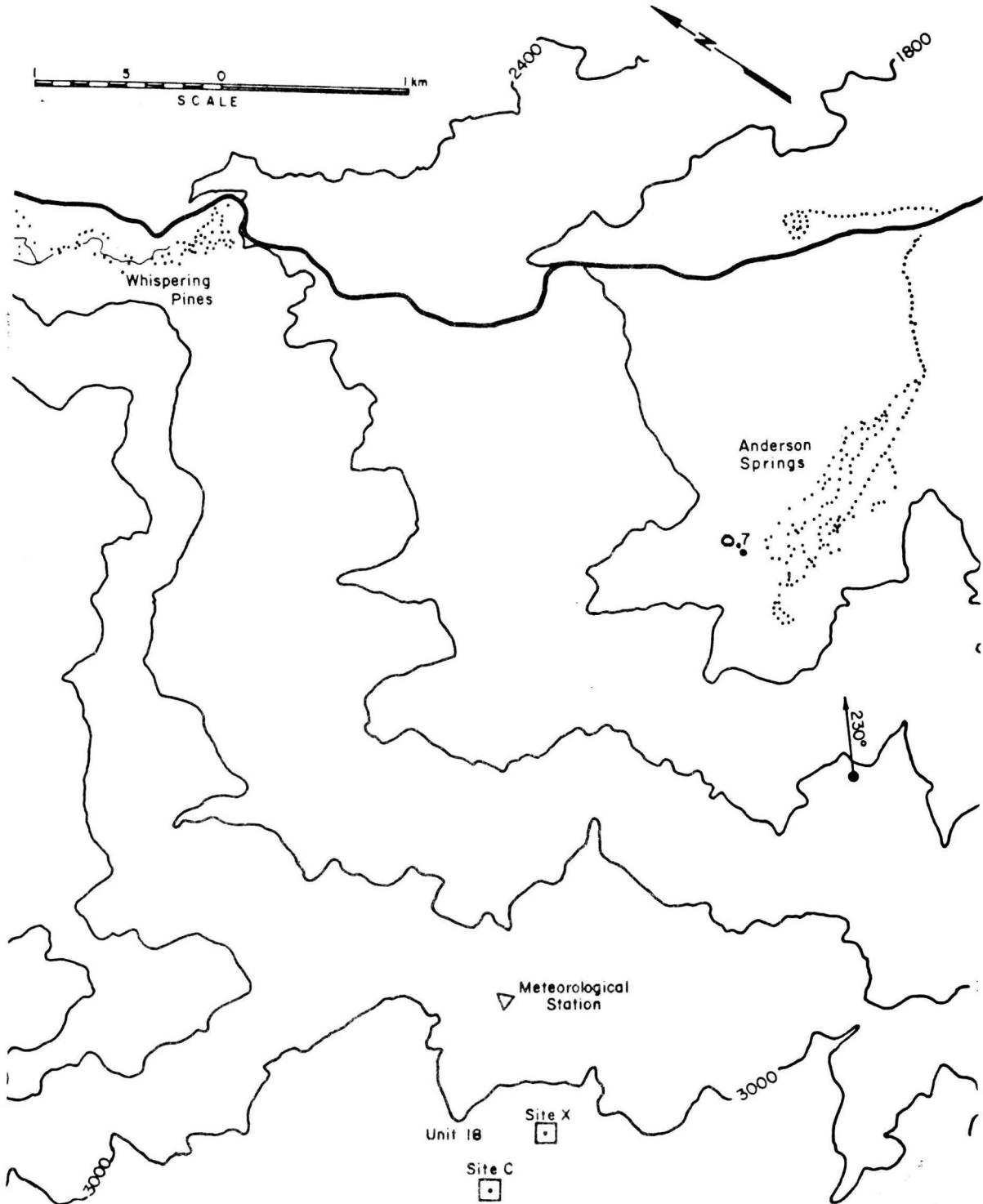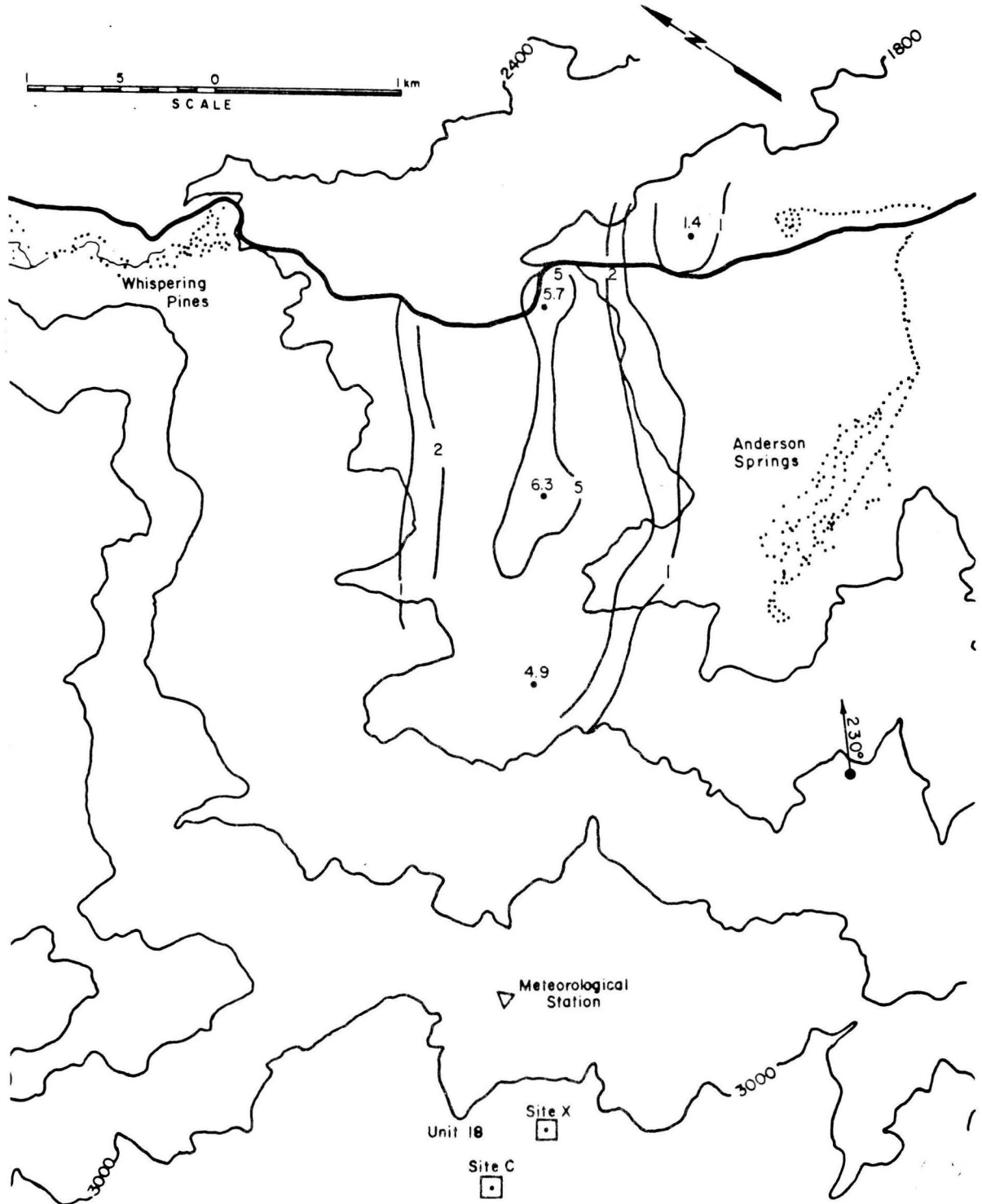direction and wind speeds of a) 3.1, b) 4.5, c) 8.9
and d) 11.6 m/s.
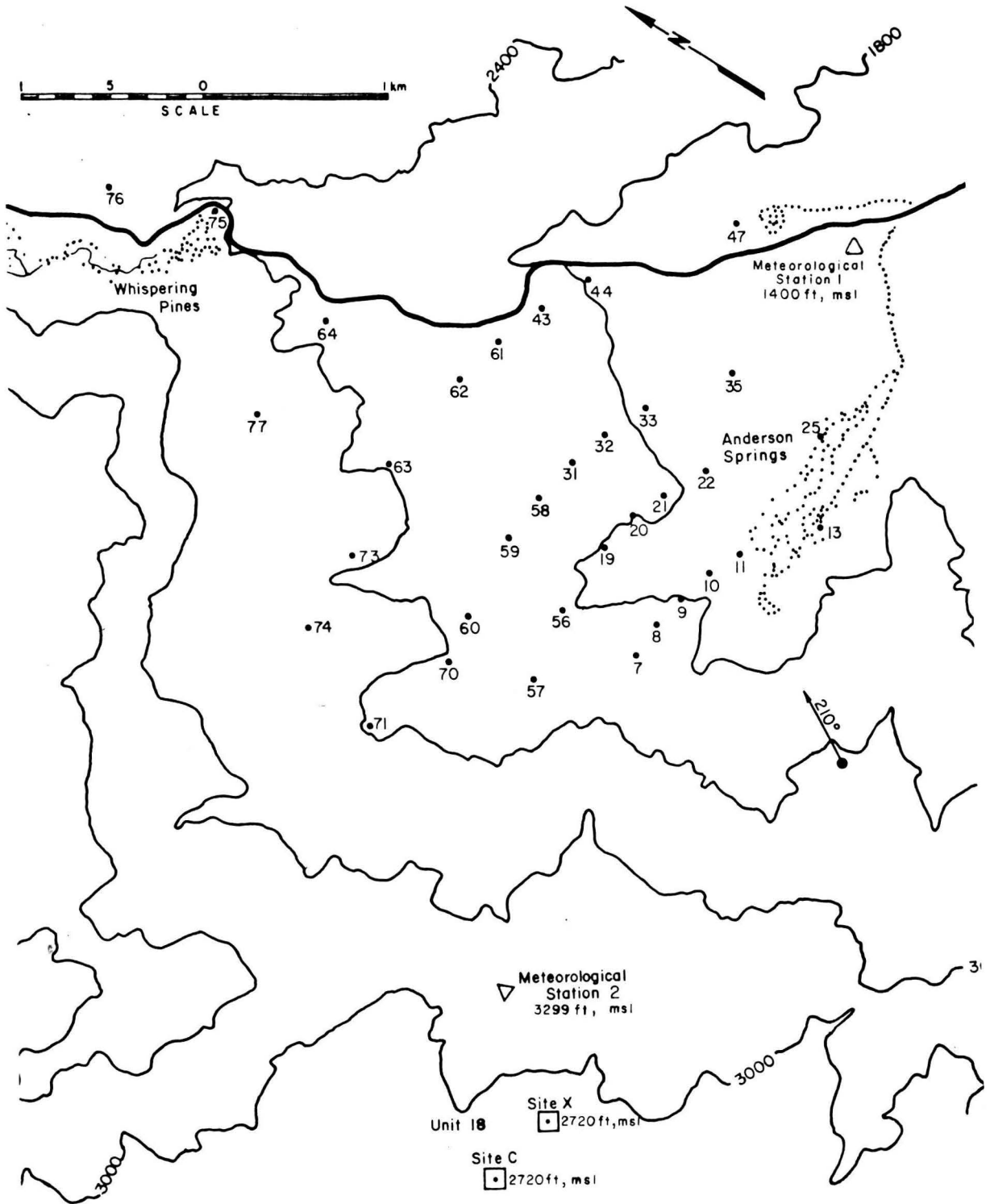
Figure 4.2-4. Sampling location for a wind direction of 210°.
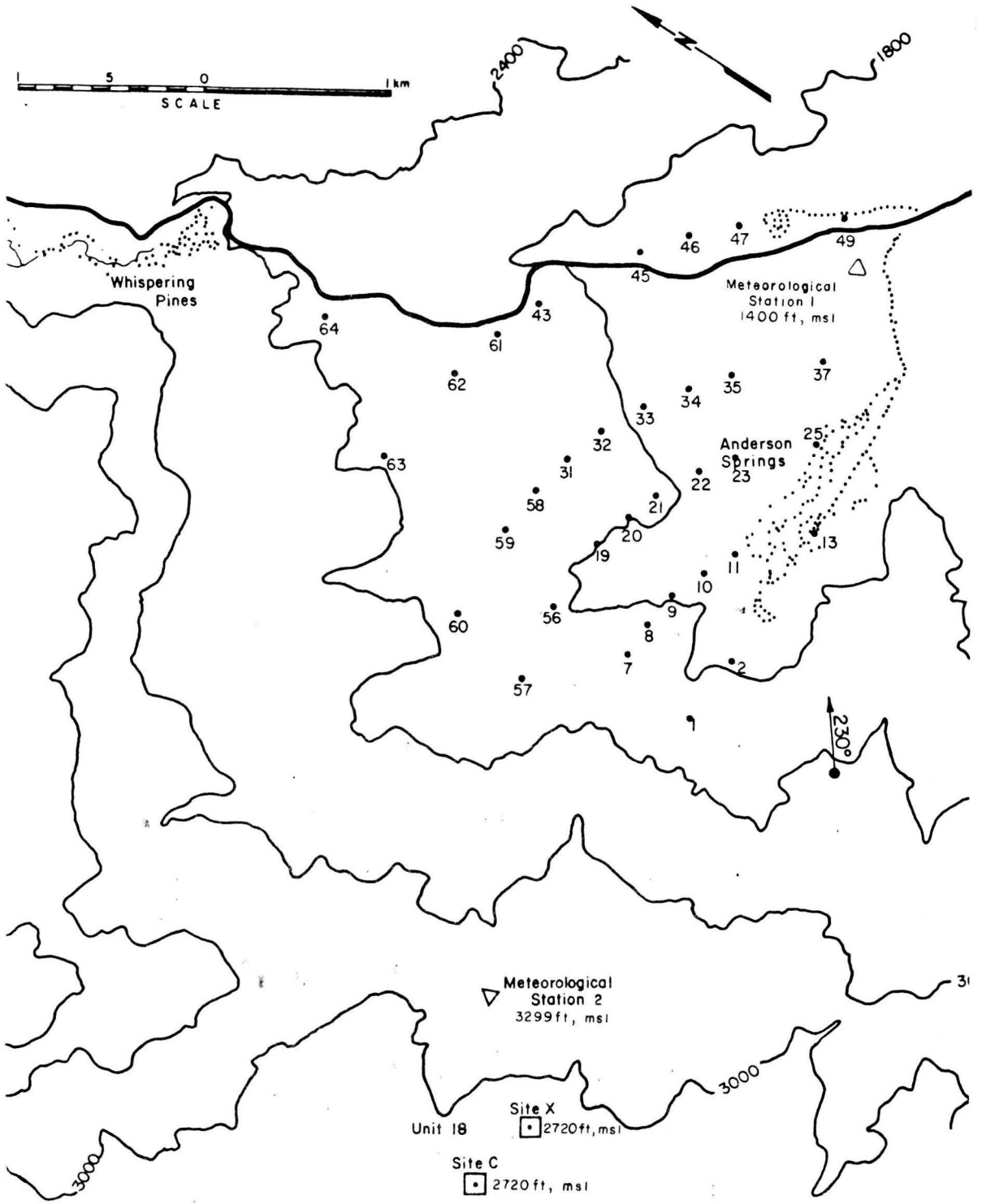
Figure 4.2-5. Sampling location for a wind direction of 230°.
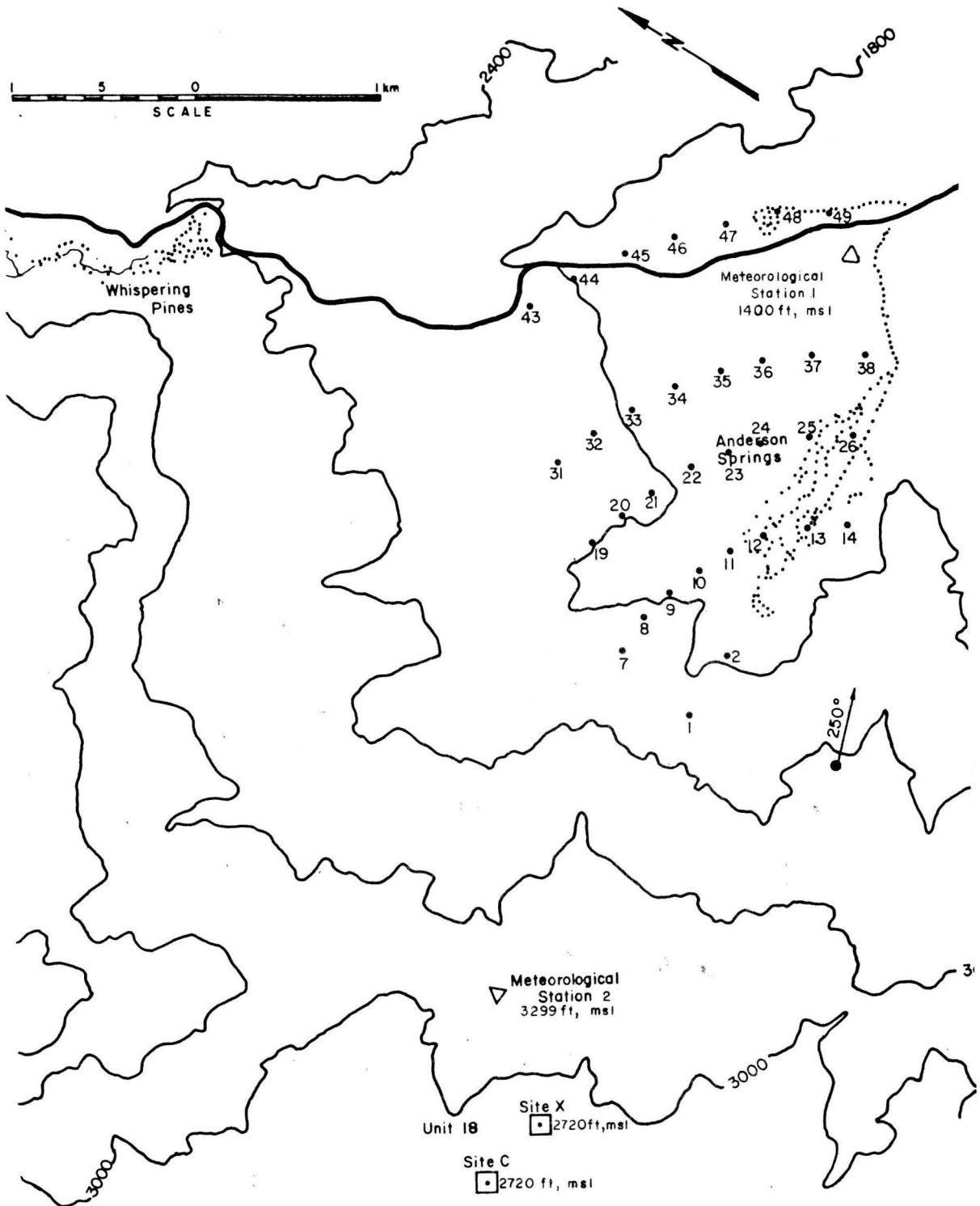
Figure 4.2-6. Sampling location for a wind direction of 250°.
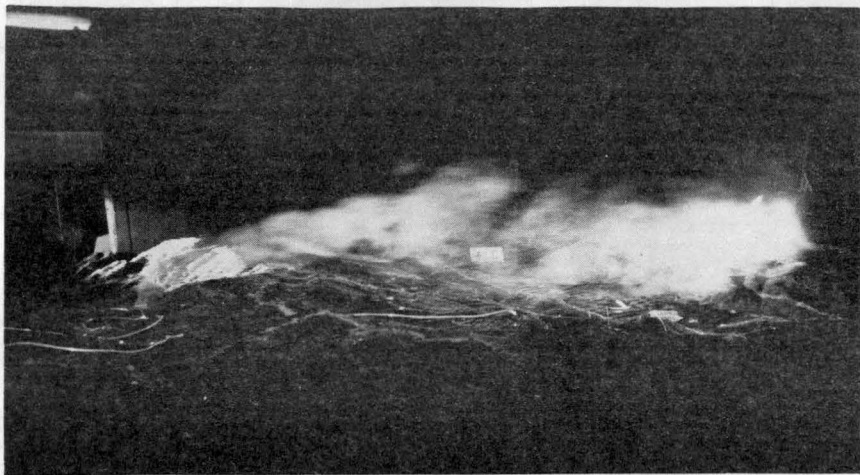
(a)
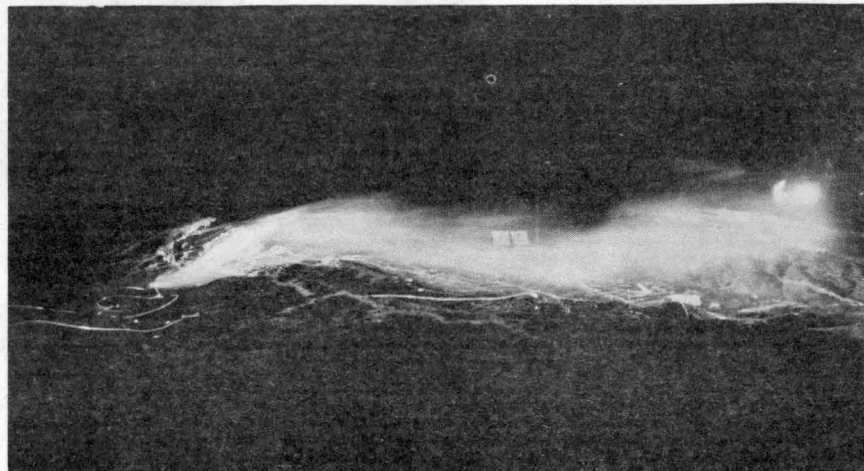
(b)
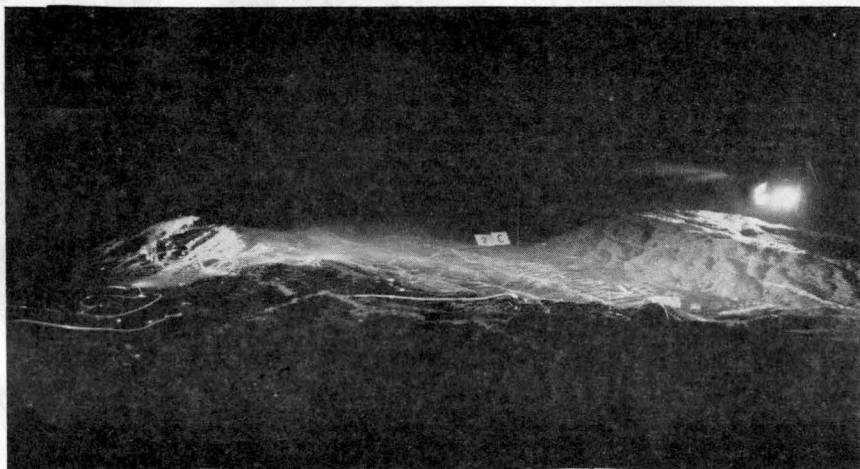
(c)

(d)

Figure 5.1-1. Plume visualizations for Unit 18, Site C, a 250° wind direction and wind speeds of a) 3.1, b) 4.5, c) 8.9, and d) 11.6 m/s.

(a)

(b)

(c)

Figure 5.1-2. Plume visualizations for Unit 18, Site C, a 230° wind direction and wind speeds of a) 3.1, b) 8.9, and c) 11.6 m/s.

(a)

(b)

(c)
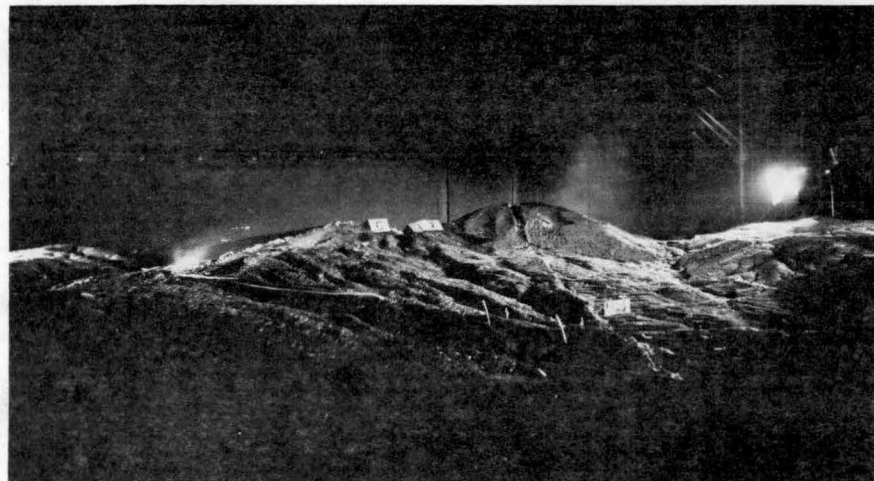
(d)

Figure 5.1-3. Plume visualizations for Unit 18, Site C, a 210° wind direction and wind speeds of
a) 3.1, b) 4.5, c) 8.9, and d) 11.6 m/s.

Figure 5.2-1a. Isopleths (x 10^5) of nondimensional concentration
coefficient K for Unit 18, Site C, a 210° wind
direction and wind speeds of a) 3.1, b) 4.5, c) 8.9
and d) 11.6 m/s.

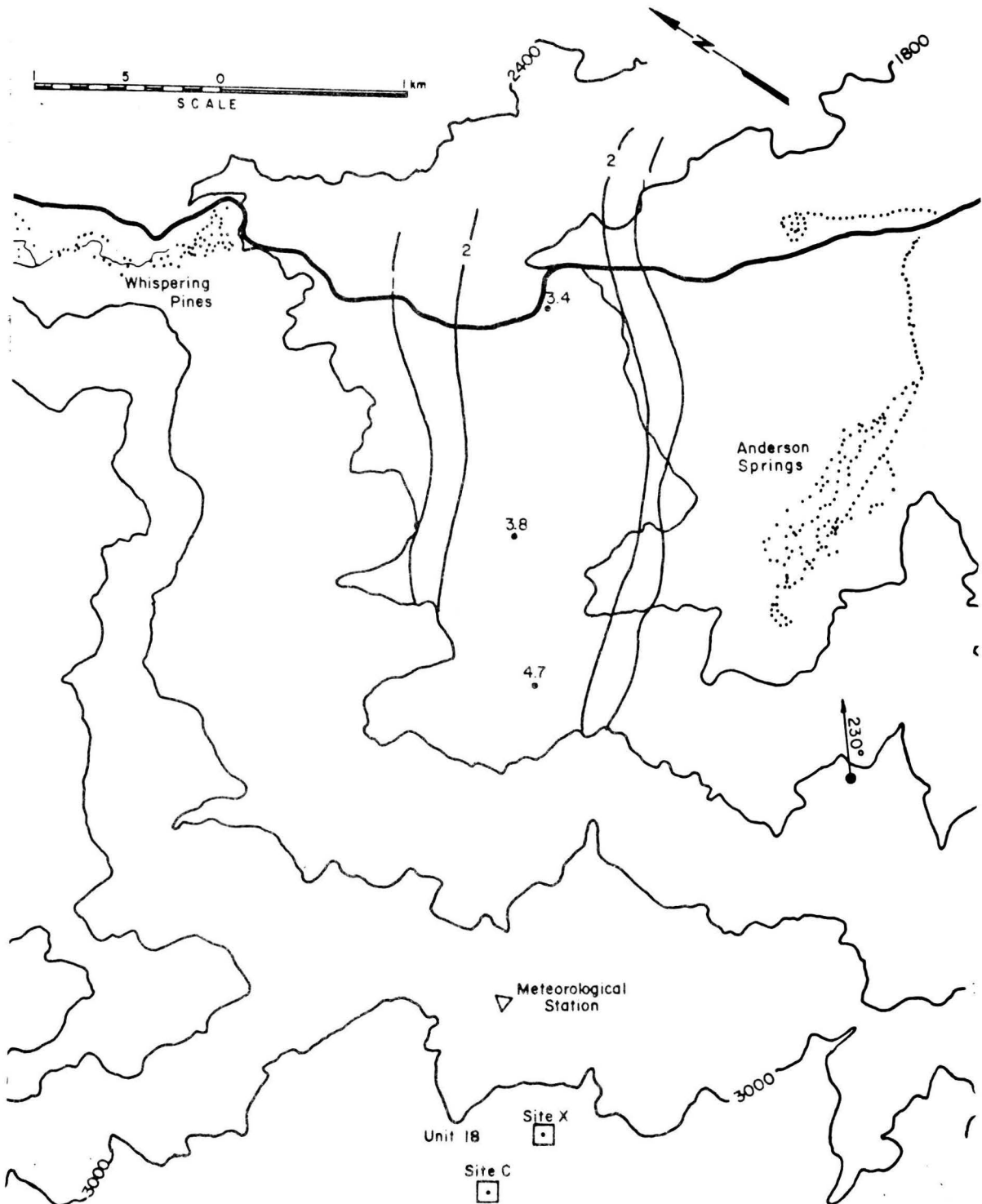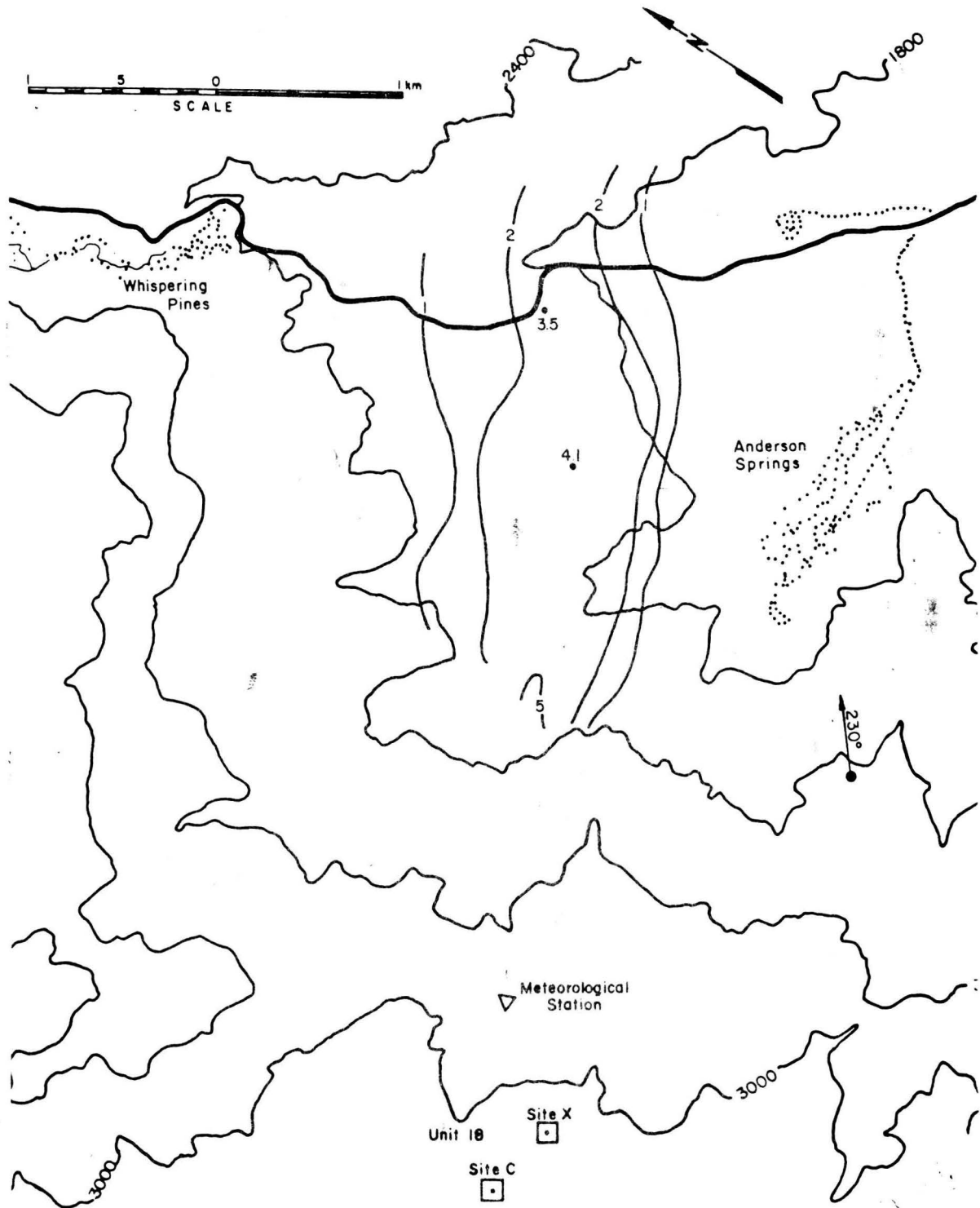Figure 5.2-1b. Isopleths (x 10^5) of nondimensional concentration coefficient K for Unit 18, Site C, a 210° wind direction and wind speeds of a) 3.1, b) 4.5, c) 8.9 and d) 11.6 m/s.

Figure 5.2-1c. Isopleths (x 10^5) of nondimensional concentration coefficient K for Unit 18, Site C, a 210° wind direction and wind speeds of a) 3.1, b) 4.5, c) 8.9 and d) 11.6 m/s.

Figure 5.2-1d. Isopleths (x 10^5) of nondimensional concentration
coefficient K   for Unit 18, Site C, a 210° wind
direction and wind speeds of a) 3.1, b) 4.5, c) 8.9
and d) 11.6 m/s.

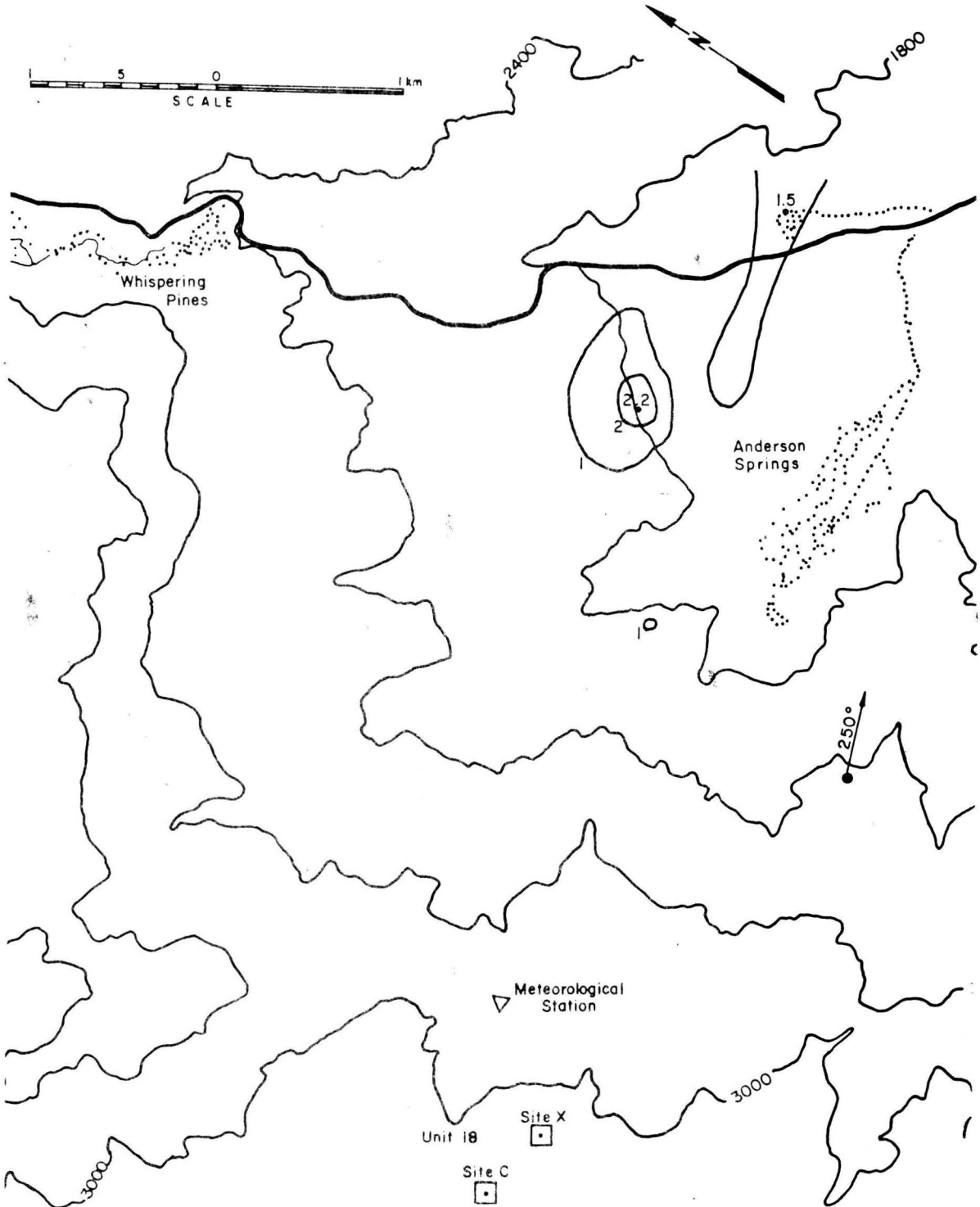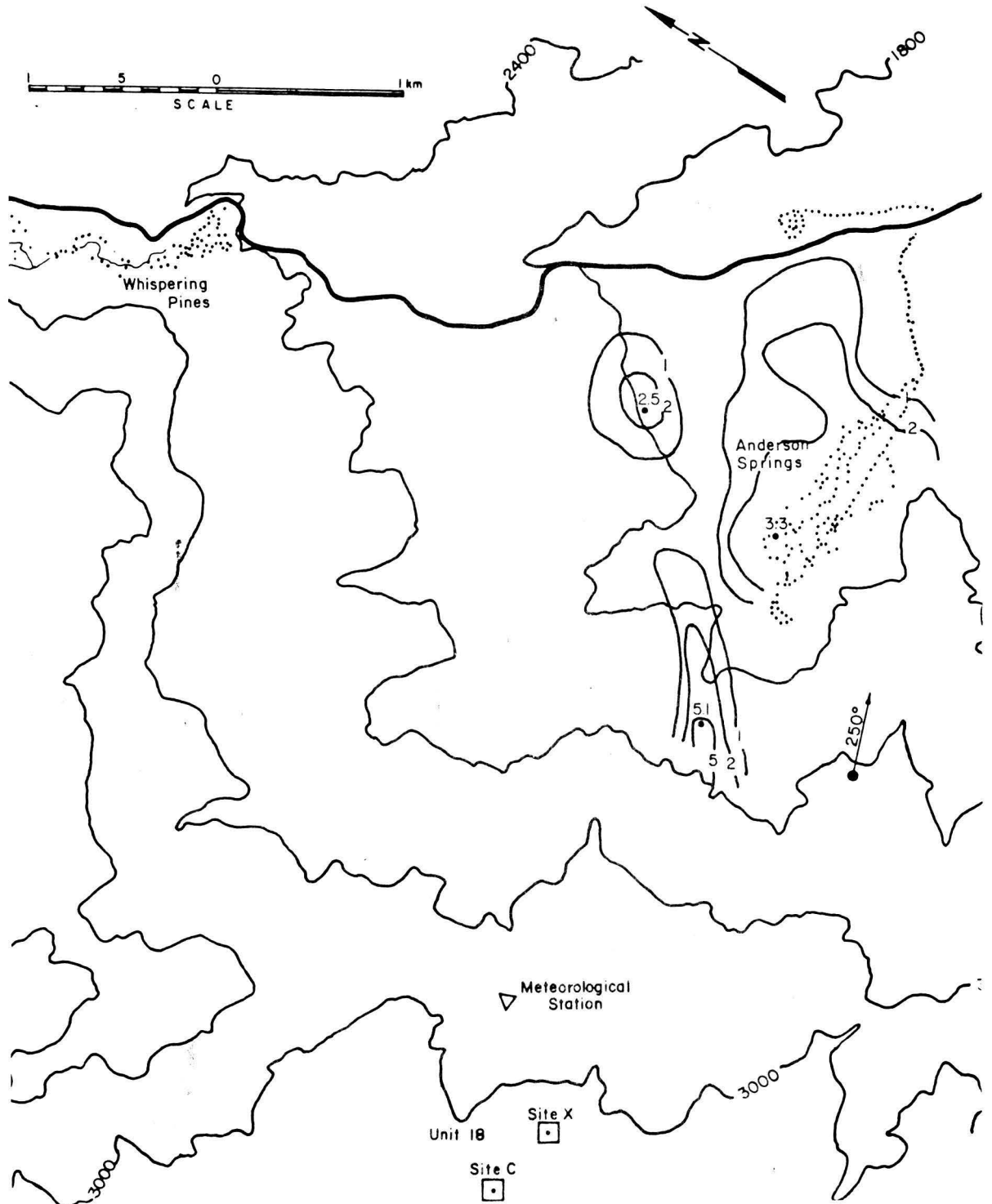Figure 5.2-2a. Isopleths (x 10^5) of nondimensional concentration
coefficient K for Unit 18, Site C, a 230° wind
direction and wind speeds of a) 3.1, b) 4.5, c) 8.9
and d) 11.6 m/s.

Figure 5.2-2b. Isopleths (x 10^5) of nondimensional concentration coefficient K for Unit 18, Site C, a 230° wind direction and wind speeds of a) 3.1, b) 4.5, c) 8.9 and d) 11.6 m/s.

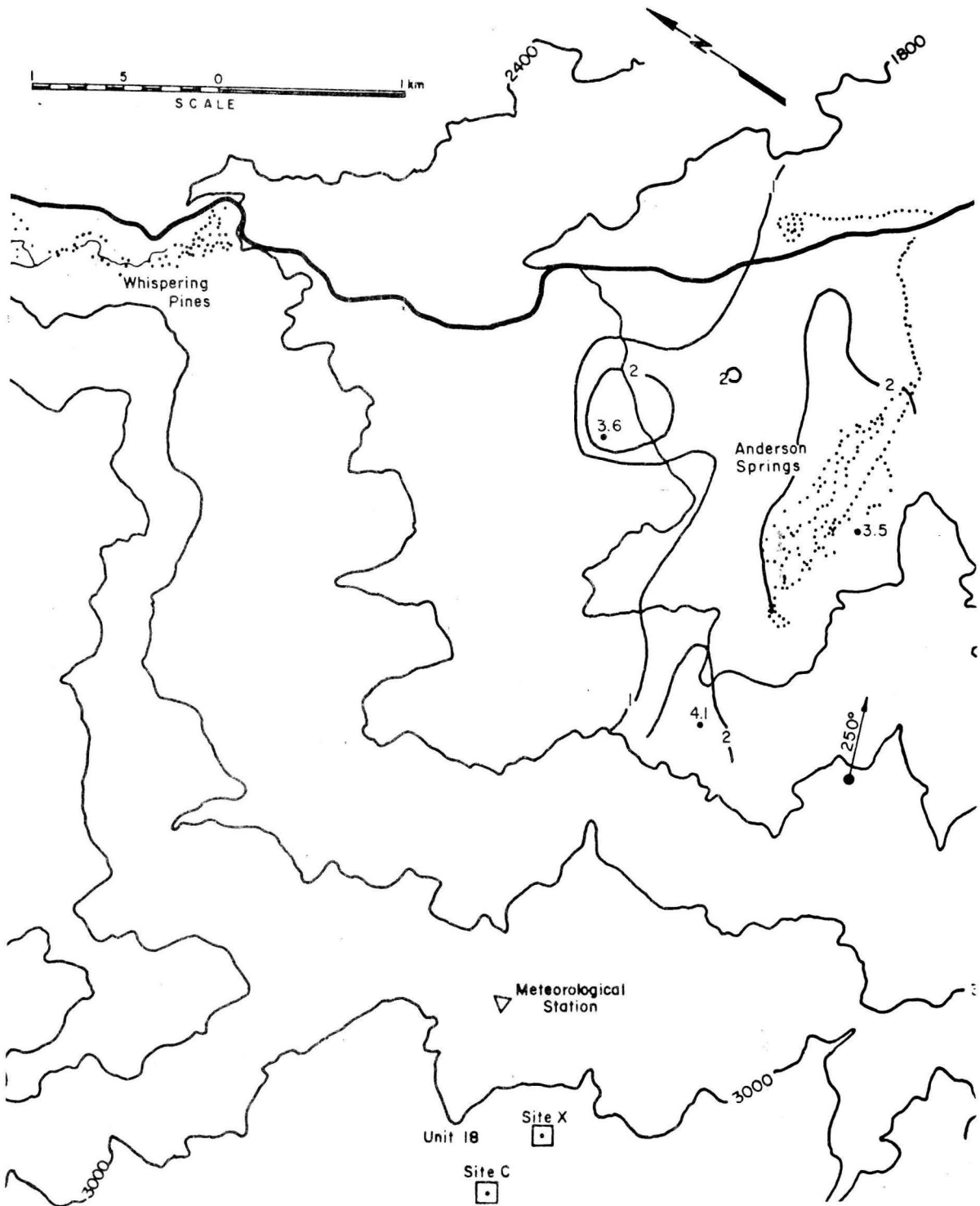Figure 5.2-2c. Isopleths (x 10^5) of nondimensional concentration coefficient K for Unit 18, Site C, a 230° wind direction and wind speeds of a) 3.1, b) 4.5, c) 8.9 and d) 11.6 m/s.

Figure 5.2-2d. Isopleths (x 10^5) of nondimensional concentration
coefficient K for Unit 18, Site C, a 230° wind
direction and wind speeds of a) 3.1, b) 4.5, c) 8.9
and d) 11.6 m/s.

Figure 5.2-3a. Isopleths (x 10^5) of nondimensional concentration coefficient K for Unit 18, Site C, a 250° wind direction and wind speeds of a) 3.1, b) 4.5, c) 8.9 and d) 11.6 m/s.

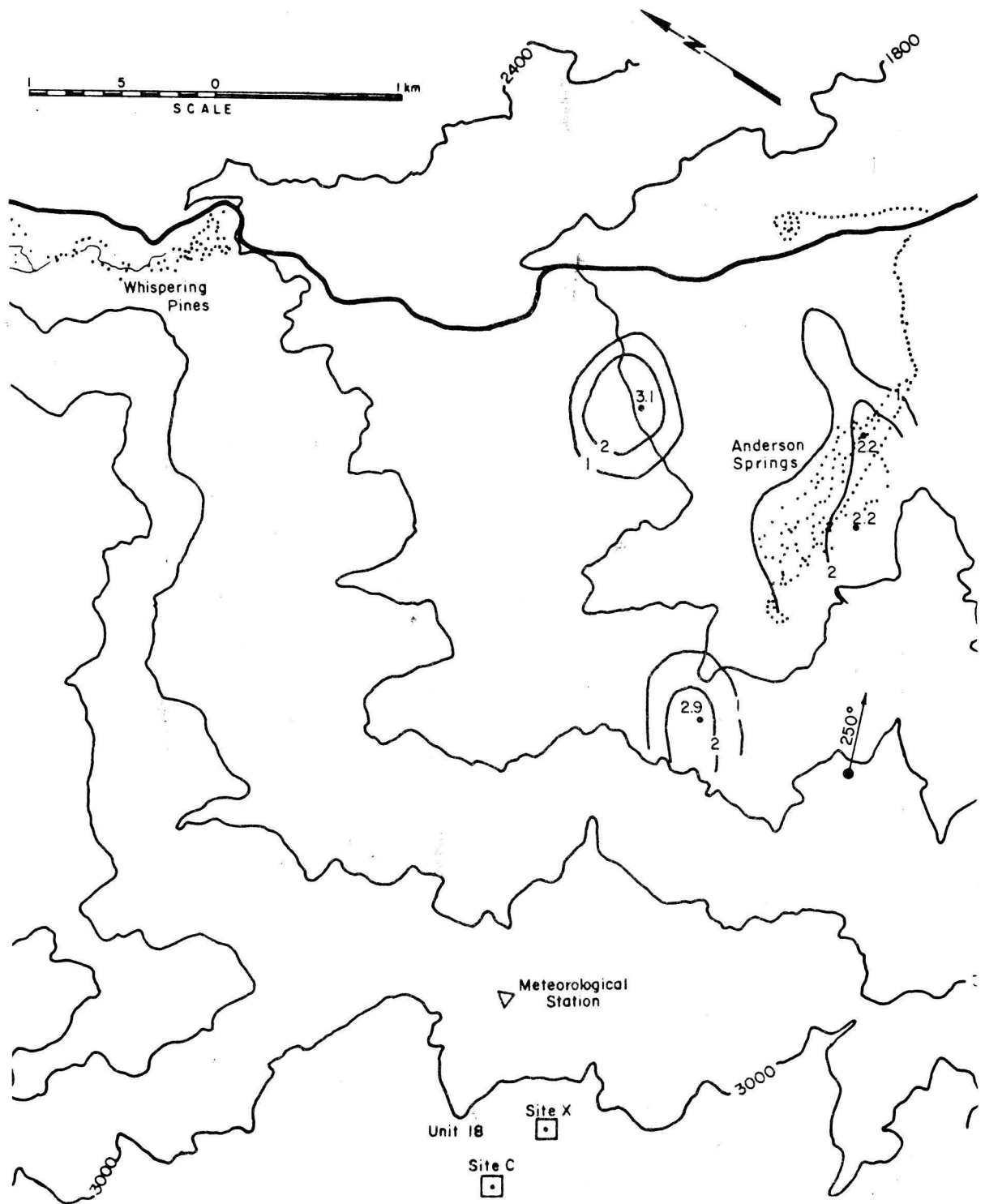Figure 5.2-3b. Isopleths (x 10^5) of nondimensional concentration coefficient K for Unit 18, Site C, a 250° wind direction and wind speeds of a) 3.1, b) 4.5, c) 8.9 and d) 11.6 m/s.

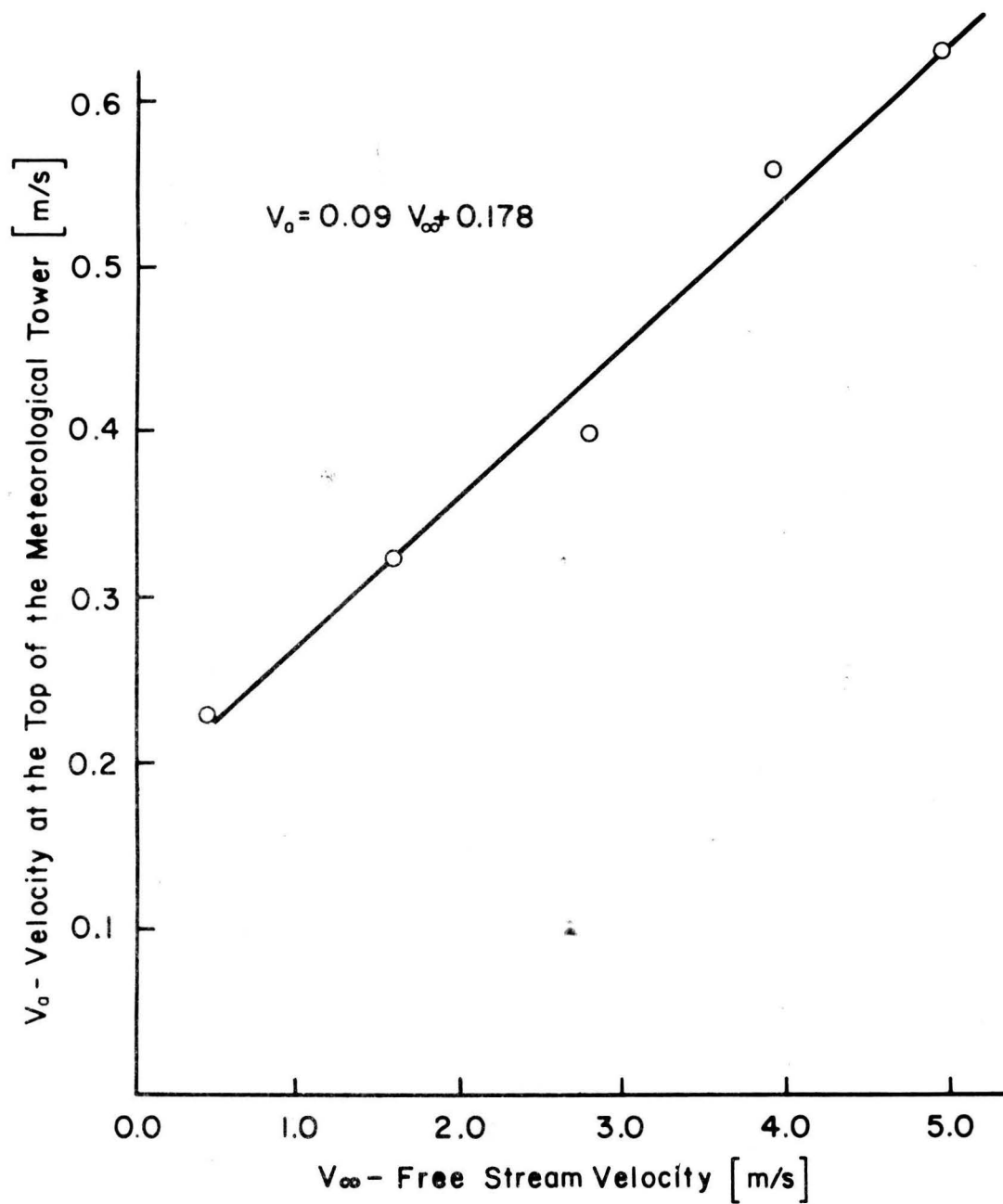Figure 5.2-3c. Isopleths (x 10^5) of nondimensional concentration coefficient K for Unit 18, Site C, a 250° wind direction and wind speeds of a) 3.1, b) 4.5, c) 8.9 and d) 11.6 m/s.

Figure 5.2-3d. Isopleths (x 10^5) of nondimensional concentration
coefficient K   for Unit 18, Site C, a 250° wind
direction and wind speeds of a) 3.1, b) 4.5, c) 8.9
and d) 11.6 m/s.

$$V_a = 0.09\, V_\infty + 0.178$$

Figure 6-1. Free Stream Velocity Versus the Velocity at the Top of the Meteorological Tower (model) for the 210° Wind Direction

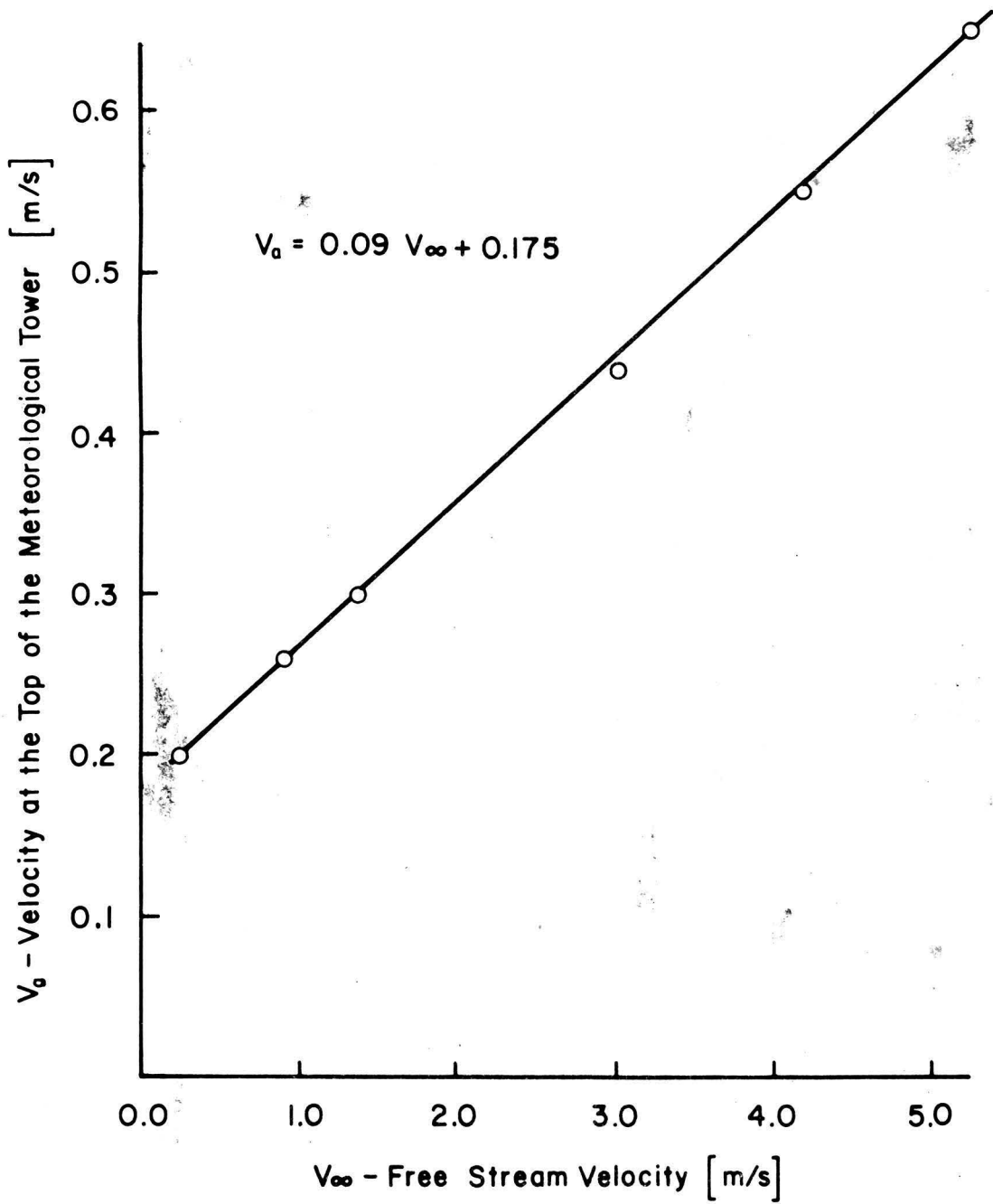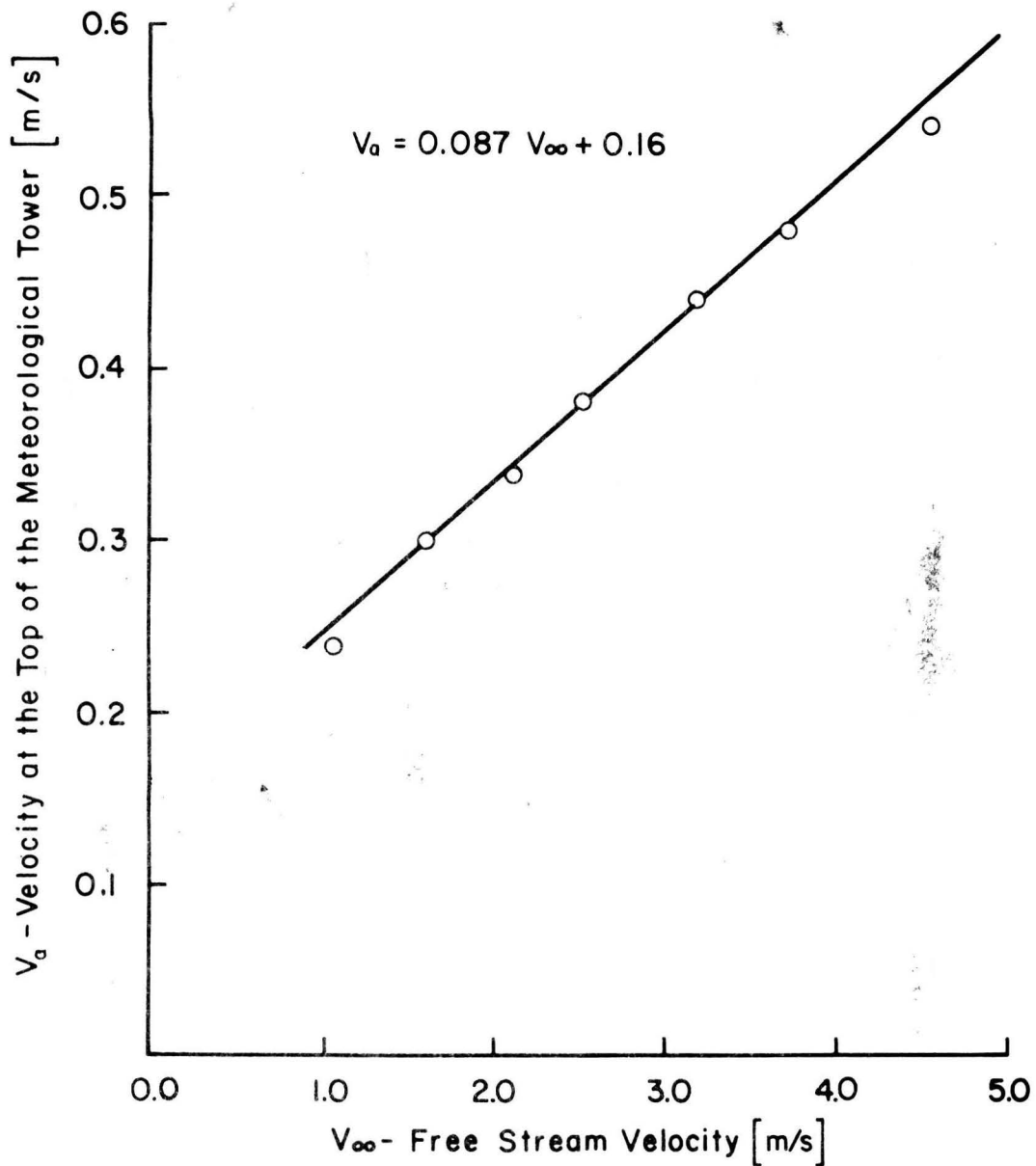$$V_a = 0.09\ V_\infty + 0.175$$

Figure 6-2.   Free Stream Velocity Versus the Velocity at the Top
of the Meteorological Tower (model) for the 230° Wind
Direction

Figure 6-3. Free Stream Velocity Versus the Velocity at the Top of the Meteorological Tower (model) for the 250° Wind Direction
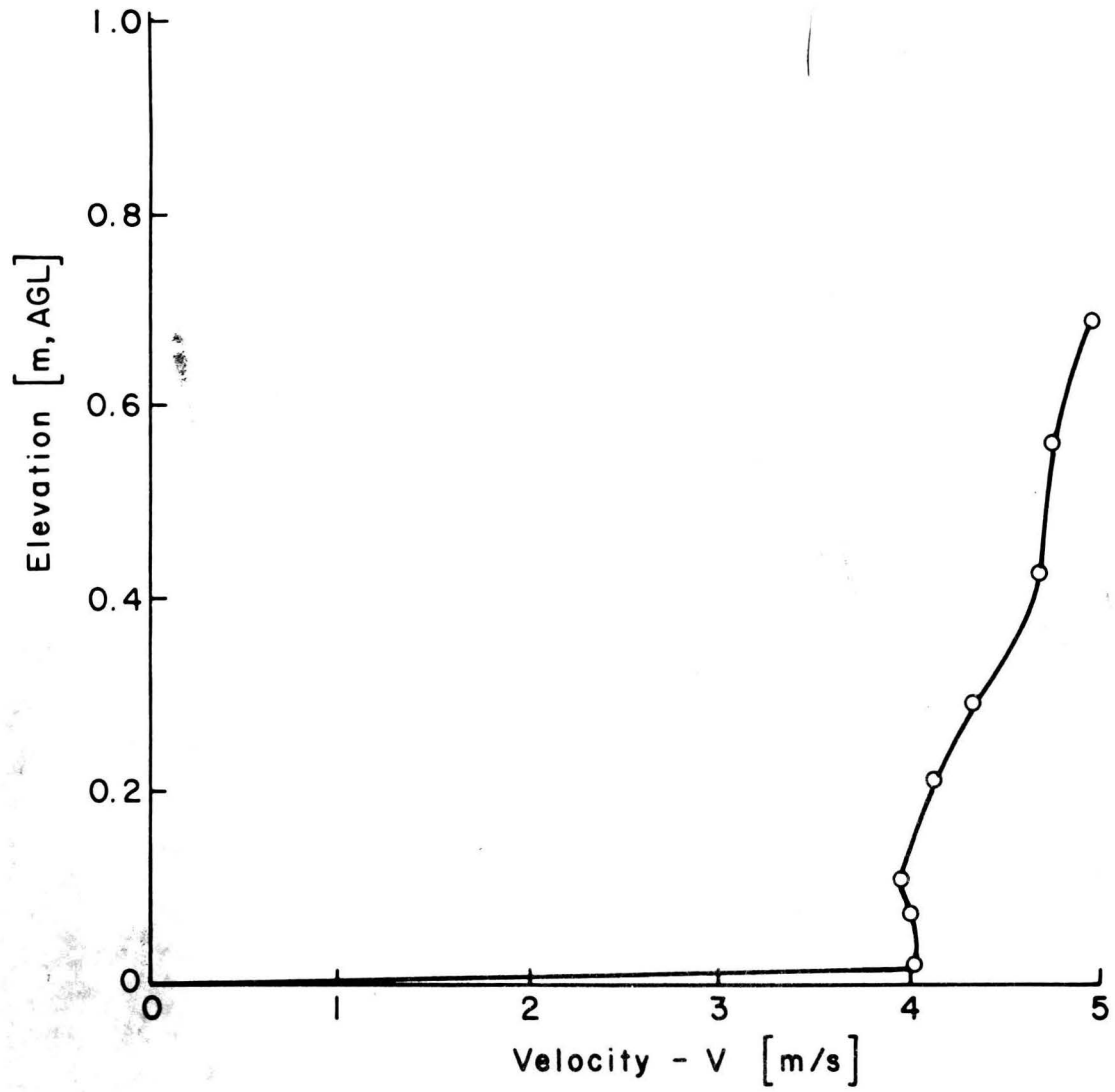
Figure 6-4. Velocity Profile above the Meteorological Tower for
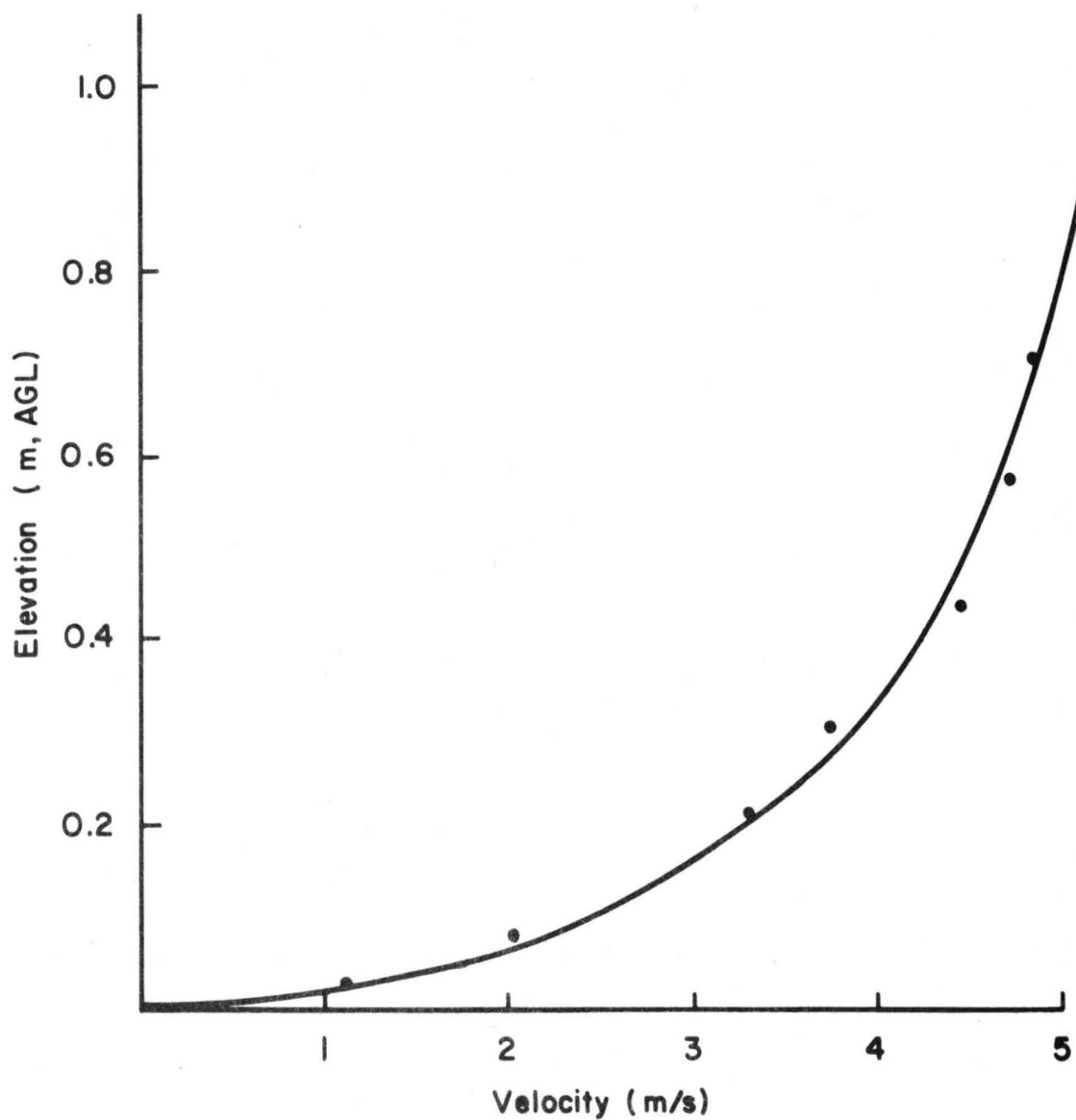the 250° Wind Direction (site elevation--1006 m, MSL)

Figure 6-5. Velocity Profile above Site C for the 250° Wind Direction
(site elevation--830 m, MSL)